An Engineering Trade Space Analysis for a
Space-Based Hyperspectral
Chromotomographic Scanner

THESIS

Phillip Sheirich, Major, USAF

AFIT/GA/ENY/09-M08

DEPARTMENT OF THE AIR FORCE
AIR UNIVERSITY

AIR FORCE INSTITUTE OF TECHNOLOGY

Wright-Patterson Air Force Base, Ohio

AFIT/GA/ENY/09-M08

An Engineering Trade Space Analysis for a Space-Based Hyperspectral Chromotomographic Scanner

THESIS

Presented to the Faculty
Department of Aeronautical and Astronautical Engineering
Graduate School of Engineering and Management
Air Force Institute of Technology
Air University
Air Education and Training Command
In Partial Fulfillment of the Requirements for the
Degree of Master of Science in Astronautical Engineering

Phillip Sheirich
Major, USAF

March 2009

APPROVED FOR PUBLIC RELEASE; DISTRIBUTION UNLIMITED.

AFIT/GA/ENY/09-M08

An Engineering Trade Space Analysis for a Space-Based Hyperspectral Chromotomographic Scanner

Phillip Sheirich
Major, USAF

Approved:

/signed/	17 March 2009
Dr. Jonathan Black PhD (Chairman)	Date
/signed/	17 March 2009
Dr. Richard Cobb PhD (Member)	Date
/signed/	17 March 2009
Lt Col Eric Swenson PhD (Member)	Date
/signed/	17 March 2009
Dr. Glen Perram PhD (Member)	Date

AFIT/GA/ENY/09-M08

Abstract

Hyperspectroscopy for fast transient events such as battlefield explosions is an undeveloped area of spectral imaging. This thesis is an examination and analysis of issues involved with taking a laboratory design for a rotating prism hyperspectral chromotomographic (CT) instrument and producing a first approximation satellite payload design, operating scheme and orbit to demonstrate this technology in low-earth orbit. This instrument promises the capability of adding a time dimension to the normal spatial and spectral data produced by most hyperspectral imagers. The ultimate goal is to conduct experiments showing spectral definition of transient combustion events on the ground from space.

This thesis examines the overall design requirements for operation of this instrument in a space environment. It begins with a discussion of spectroscopy, the current literature on the topic of hyperspectral imagers, and a review of some representative hyperspectral imagers currently in operation. This is followed by an examination of the laboratory instrument, identifying key components and operating principles of that instrument. Then a definition of some general instrument requirements to conduct the experiment is presented. This continues with a trade-space analysis of major instrument components to include: front-end optics, the rotating prism, focal plane array, on-orbit calibration, and data production, storage and downlink. An operational analysis of a notional test event encompasses Chapter IV. The thesis concludes with a summary of the major issues presented and recommendations for further work leading towards the actual construction and employment of the proposed space-based instrument.

Acknowledgements

I would like to acknowledge the great debt I owe to my committee, Dr. Richard Cobb, Lt Col Eric Swenson, Dr. Glen Perram and especially Dr. Jonathan Black my committee chair. In addition I received invaluable help from Lt Cols Michael Hawks and Jeremy Holtgrave who exhibited enormous patience in discussing numerous areas of Optics with me.

Phillip Sheirich

Table of Contents

Page

Abstract iv

Acknowledgements v

List of Figures viii

List of Tables xi

I. Introduction 1
  1.1 Spectroscopy 2
  1.2 Example Spectrographic Imagers 4
    1.2.1 Thematic Mapper 4
    1.2.2 AVIRIS 8
  1.3 Temporal Dimension 12
  1.4 Problem Statement and Organization 14

II. Hyperspectral Imaging Background Review 16
  2.1 Collection Techniques 16
  2.2 Literature Review 19
  2.3 Operational Instrument Review 27
  2.4 CTHIS prototype 38
    2.4.1 Geometric Optics 42

III. CTEx Design and Trade Space 48
  3.1 Requirements and Assumptions 48
  3.2 Front-end Optics 51
    3.2.1 Reflection vs Refraction 52
    3.2.2 Telescope Design 55
  3.3 Prism 56
  3.4 Focal Plane Array and Camera 63
    3.4.1 Cameras 75
  3.5 Data Handling 77
    3.5.1 Data Generation 77
    3.5.2 Data Storage 79
    3.5.3 CPU 81
  3.6 On-orbit Calibration 82
  3.7 Overall Design Space 84
    3.7.1 Materials and Structure 86

Page

IV. Concept of Operations 89
4.1 Platform and Orbit 89
4.2 System Check 89
4.3 Collection Event 91
4.3.1 Test Plan 93
4.3.2 CTEx Data Collection 94
4.4 Space Environment Considerations 99

V. Conclusions 103
5.1 Thesis Summary 103
5.2 Issues 104
5.3 Further Study Needed 105
5.4 Testing 107
5.5 Conclusion 109

Appendix A. Operational Hyperspectral Imagers [45] 111

Appendix B. Prism Specifications 115

Appendix C. Fast Frame-Rate Camera Specifications 117

Appendix D. ISS Orbital Data 127

Appendix E. RC Telescope Optical Collimation Procedures 128

Appendix F. Newport Rotation Table 135

Appendix G. Computer Optical Products CM-5000 137

Appendix H. International Space Station 140

Appendix I. BAE Systems [11] 142

Bibliography 144

List of Figures

Figure		Page
1.1	Visible Spectrum	3
1.2	Camouflaged tent	4
1.3	Camouflaged tent in three spectral views	5
1.4	Thematic Mapper Design	7
1.5	Thematic Mapper Spectral Bands	7
1.6	Atmospheric Spectral Absorption	9
1.7	AVIRIS	10
1.8	Pixel Spatial-Spectral Illustration	11
1.9	3-D Hyperspectral Data Cube	13
2.1	Whiskbroom and Pushbroom Collection Techniques	18
2.2	Offner interferometer	21
2.3	Chowdhury Lens	23
2.4	Curved Prism Design	24
2.5	EnMap Optical System	25
2.6	CTIS layour	26
2.7	Offner Spectrometer	27
2.8	Offner CTIS Lab Results	28
2.9	IR Photodiode Ranges	30
2.10	CRISM Optical Design	33
2.11	CRISM Slewing Strategy	35
2.12	CRISM Subassemblies	36
2.13	CRISM Key Components	37
2.14	CRISM Assemblies	37
2.15	CTHIS laboratory design	39
2.16	CT Image Reconstruction	40
2.17	CTHIS lab instrument front-end optics	43

Figure | Page

2.18 Thin lens optics for light collimation 44
2.19 Chromatic Aberration 45
2.20 Achromatic Doublet 45
2.21 Dispersing prism 46
2.22 Direct vision prism in rotator 47
3.1 CRISM Requirements 51
3.2 Law of Reflection 53
3.3 Proposed Mersenne Telescope Design. 56
3.4 Spectral dispersion illustration 58
3.5 Thermal Expansion of Prism 61
3.6 CCD Bucket Analogy 64
3.7 CCD Function 65
3.8 CCD/CMOS quantum efficiency 66
3.9 Monolithic and Hybrid CMOS 67
3.10 CCD vs CMOS at pixel level 68
3.11 Monolithic CMOS Chip 68
3.12 CMOS scanning techniques 69
3.13 Windowing concept illustration 71
3.14 HICO design 73
3.15 Thematic Mapper Scan Mirror Design 74
3.16 Hard Disk/Solid State Drive illustration 79
3.17 HDD vs SSD performance 80
3.18 LED data 85
3.19 Instrument Configuration Space 86
3.20 Hubble day/night pointing disturbance 88
4.1 Japanese Experimental Module (JEM) 90
4.2 JEM Resources 91
4.3 CTEx Coverage Report 93

Figure Page

4.4 Test Equipment List 97

4.5 Example Transient Event Tests 98

4.6 South Atlantic Anomaly 101

4.7 ISS Orbit Through South Atlantic Anomaly 102

List of Tables

Table Page

2.1 Hyperion design parameters and on-orbit performance 31

3.1 CTEx Driving Requirements 52

4.1 CTEx Systems Check 92

5.1 Trade-Space Summary 110

An Engineering Trade Space Analysis for a Space-Based Hyperspectral Chromotomographic Scanner

I. Introduction

This thesis will present a trade-space analysis for an engineering design of an experimental chromotomography-based hyperspectral imager (Chromotomographic Imaging Experiment - CTEx). The basis for this instrument is a current laboratory instrument, the Chromotomographic Hyperspectral Imaging System (CTHIS), which, as the name implies, employs chromotomographic techniques for data extraction from images. The objective of this study is to provide a first-order engineering trade-space analysis for such an instrument. The design will address issues involved in launching and operating this instrument in space. It will take into account the stresses of launch, the challenges of the space environment such as heating, cooling and solar radiation, and the much greater distances between the target and the instrument Focal Plane Array (FPA) for example. In the end, the instrument will be designed, built, launched and operated in low-earth orbit. It will provide proof-of-concept validation of the practicality and effectiveness of hyperspectral chromotomographic remote sensing of the Earth's surface from space.

Spectral data analysis is already widely used in both military and civilian applications. Examples include defeating camouflage, categorizing mineral deposits, tracking climate change and analyzing the growth and health of vegetation for agricultural or forestry use. CTEx promises to add additional capabilities for analyzing fast changing events such as battlefield explosions, rocket engine tests, or the smoke plume resulting from industrial fires. Measuring spectral changes from imagery of these types of situations will enhance users' ability to determine the chemical content of the explosive, smoke plume or any other transient event.

1.1 Spectroscopy

Spectroscopy is the use of variations in the spectral signature of an observed geometric space, object or event to extract data about that target which is not apparent in traditional electro-optical imagery. In remote sensing an image may be analyzed within a single spectral band (monochromatic), several spectral bands (multispectral) or many spectral bands (hyperspectral). Although there is no authoritative differentiation between multi- and hyperspectral imaging, there is a general consensus that image analysis in more than about a dozen spectral bands qualifies as "hyperspectral". In addition, multispectral instruments, such as the LandSat Thematic Mapper, which is discussed below, usually do not use contiguous bands, rather using selected specific bands and bandwidths at various points in the electro-magnetic spectrum for particular applications. In other words, if the entire spectral area of interest is from 400 - 1000 nm, a hyperspectral imager will collect data over that entire spectral bandwidth and break up that width into a dozen or more smaller bands. By contrast, a multispectral imager will collect data on only a few specific parts of the entire band, and those parts will not necessarily lie next to each other; there will be large gaps over the entire bandwidth where no data is taken at all. For reference, the EM spectrum with the visible light portion highlighted is presented in Figure 1.1.

The advantages of using spectral imaging data as opposed to more familiar, visible light images (panchromatic), i.e. photography, is that many objects can be distinguished from their surroundings by strong reflection, or lack thereof, in specific parts of the spectrum but are washed out in a panchromatic view. The distinguishing reflectance (or emittance) in a small portion of the EM spectrum may be undetectable when an entire portion of the spectrum, such as the visible light portion, is observed as a whole. Further, hyperspectral imagery provides much more data, with finer resolution, than can be gathered through multispectral or panchromatic imaging.

As pointed out above, an example of the use of hyperspectroscopy is in the detection and identification of camouflaged equipment. This application is illustrated

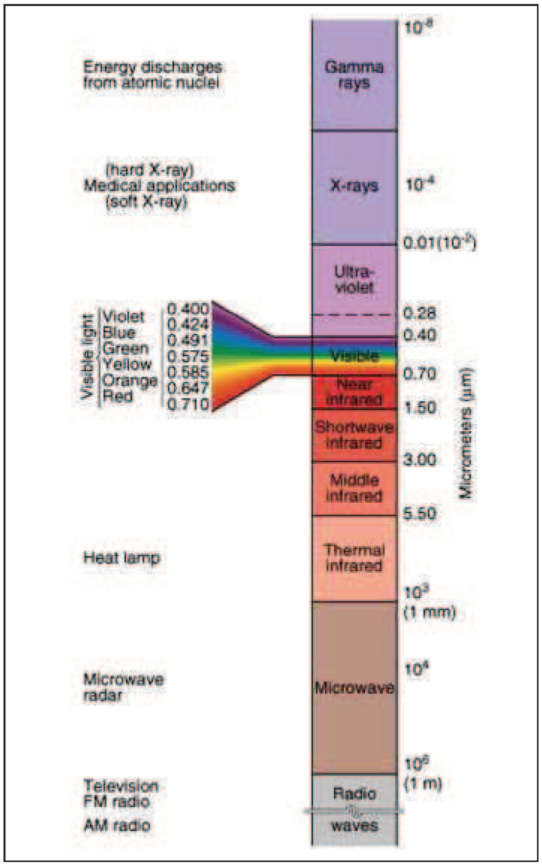

Figure 1.1: The EM spectrum [41]

below in Figure 1.2. This is a side-on, close-up view of a camouflaged tent. Camouflage generally works on the principle of masking an object's color (visible light reflectance) and shape by matching it to the background. However, when the same camouflaged object is observed in many narrow spectral bands, the differences in signature between it and that background become much more apparent. Observe the same tent in an overhead panchromatic and then in multispectral and hyperspectral imagery (Figure 1.3). In the multispectral image more detail is apparent, but the tent is still not noticeable. The hyperspectral image clearly shows an anomalous feature that can be further investigated. Note that the color in these images is not true color but is a processing technique that contrasts parts of the spectral signature with others to highlight differences. This is another advantage of hyperspectroscopy. Post-image processing can be used to focus on different spectral wavelengths in order to distin-

guish particular features of interest. This is especially advantageous where the analyst knows the areas of the spectrum where a particular type of material has the strongest reflectance, i.e. a tank may be most strongly reflectant in the near infrared band. An analyst looking for tanks in an image can highlight that area of the spectrum to see if anything stands out in stark contrast to the background.

Figure 1.2: Camouflaged tent [4]

1.2 Example Spectrographic Imagers

In order to better illustrate the concepts introduced here a brief examination of two representative imagers is presented. Although several space-borne hyperspectral imagers are discussed in detail in the next chapter, it will be advantageous to use the Thematic Mapper and the Airborne Visible/Infrared Imaging Spectrometer (AVIRIS) instruments to clarify some of the basic terminology at this point.

1.2.1 Thematic Mapper. Remote sensing of the Earth's surface using multi- and hyperspectral instruments is not a new concept. Examples of both air and space borne instruments are readily available. These include the Thematic Mapper (TM), which is a Landsat satellite-based multispectral instrument using seven different spectral bands to analyze the same geography or to maximize the information that can be collected on a particular area. The TM uses seven spectral bands from the visible to the mid-IR regions.

> The Thematic Mapper (TM) is a seven channel sensor mounted on the Landsat platform which is maintained in a sun-synchronous, near-polar

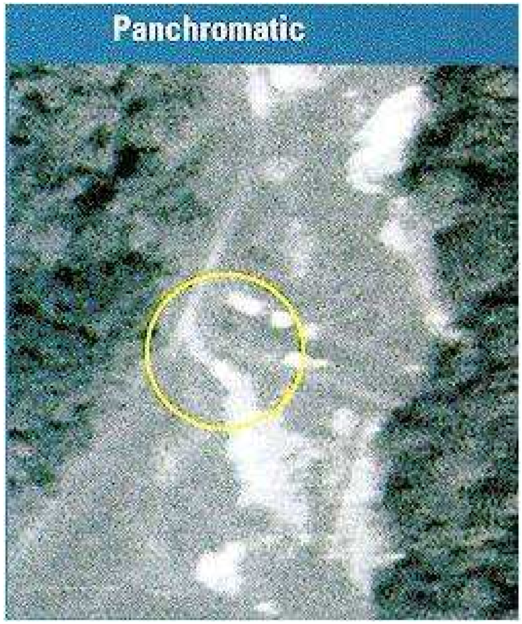

(a) Panchromatic image of camouflaged tent

(b) Multispectral image of camouflaged tent

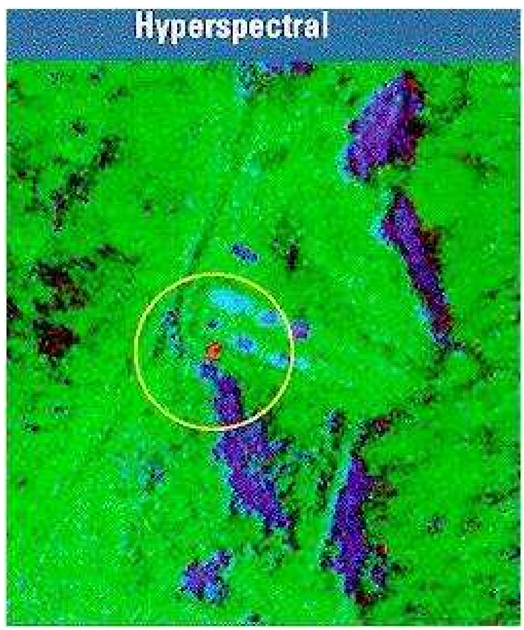

(c) Hyperspectral image of camouflaged tent

Figure 1.3: Camouflaged tent in three spectral views [4].

orbit at an altitude of 705 km. This provides for global repeat coverage every 16 days. TM data are recorded at 30-m ground resolution across a swath of 185 km, except for the thermal data that are recorded at 120-m ground resolution.

Band description:

1. BLUE (0.45-0.52 m): Designed for water body penetration, making it useful for coastal water mapping. Also useful for soil/vegetation discrimination, forest type mapping and cultural feature identification.
2. GREEN (0.52-0.60 m): Designed to measure green reflectance peak of vegetation for vegetation discrimination and vigor assessment. Also useful for cultural feature identification.
3. RED (0.63-0.69 m): Designed to sense in a chlorophyll absorption region aiding in plant species differentiation. Also useful for cultural feature identification.
4. NEAR INFRARED (0.76-0.90 m): Useful for determining vegetation types, vigor, and biomass content, for delineating water bodies, and for soil moisture discrimination.
5. MID-INFRARED (1.55-1.75 m): Indicative of vegetation moisture content and soil moisture. Also useful for differentiation of snow from clouds.
6. THERMAL INFRARED (10.4-12.5 m): Useful in vegetation stress analysis, soil moisture discrimination, and thermal mapping applications.
7. MID-INFRARED (2.08-2.35 m): Useful for discrimination of mineral and rock types. Also sensitive to vegetation moisture content.
[10]

This particular instrument uses a diffraction grating and bandpass filters to separate light reflected from the Earth's surface into several spectral bands and then pass those specific bands of electromagnetic radiation onto a focal plane array (FPA) which is sensitive to light in that band (or bands). The FPA(s) form part of an instrument cluster for collecting, storing and transmitting (with possibly some processing as well) images in electronic form.

As can be seen from the band descriptions, the Thematic Mapper uses rather broad spectral bands. This is well illustrated in Figure 1.5 where the TM bands and spectrum are shown graphically:

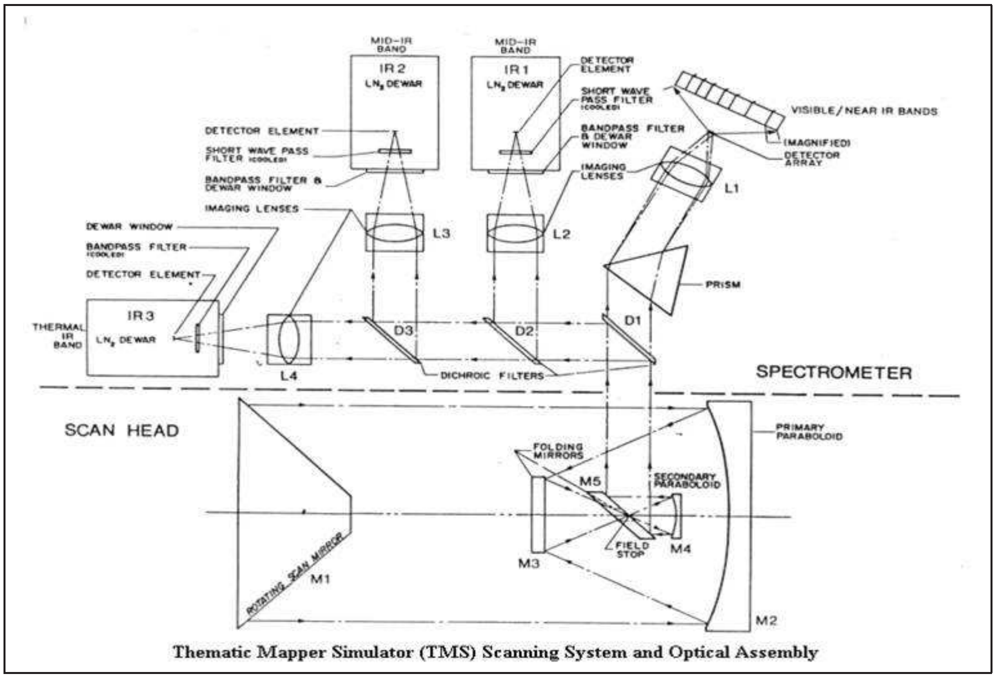

Figure 1.4: Thematic Mapper design [41]

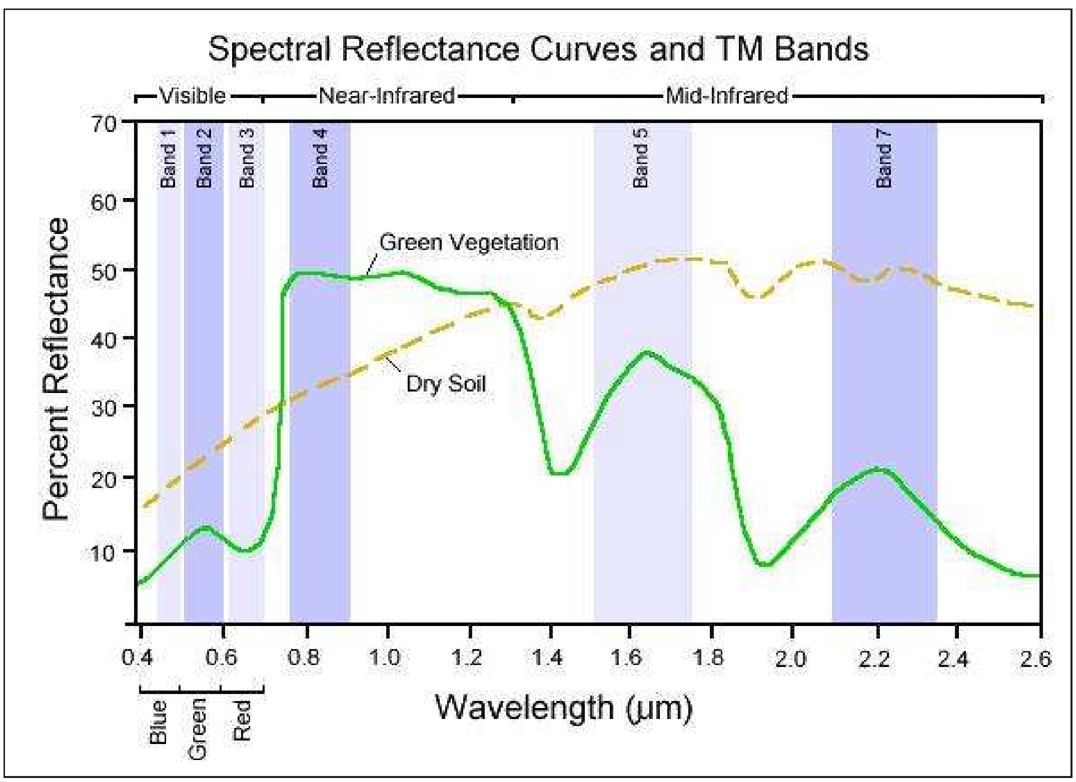

Figure 1.5: Thematic Mapper spectral bands illustration [41]

The purpose of the Thematic Mapper is to provide data for the study of vegetation, soil, geography and climate on the Earth. As such, these broad bands work relatively well. Of course the TM was also a relatively early operational employment of spectroscopy in space-based remote sensing.

Since Landsat TM first became operational in the 1970s there have been many air- and space-based applications of multi- and hyperspectral imaging instruments used in the private and public sectors. Chapter II will provide background on some of these instruments to help illustrate their design and capabilities. However, AVIRIS will be briefly discussed here as an aide in clarifying important basic concepts associated with hyperspectral imaging.

1.2.2 AVIRIS. AVIRIS is a true hyperspectral imager. It produces imagery in 224 contiguous bands from 400 to 2500 nanometers, thereby offering spectral resolution of 9.375 nm or .0094 μm. This resolution is good enough to identify various surface and atmospheric constituents at the particle or molecular level, but not good enough to separate molecular isotopes of the same compounds or elements in most cases. Nevertheless, as the AVIRIS mission is to study processes of global environmental and climate change, this resolution is certainly sufficient [5]. In relation to the spectral resolution and bandwidth, it is important to note the relationship that exists and the tradeoffs presented. A wide bandwidth, in this case covering from the beginning of visible light all the way through short wave infrared (SWIR), .400 - 2.5 μm, covers a greater portion of the EM spectrum and thereby provides more data. This is particularly important when imaging through the Earth's atmosphere as radiation absorption, especially by water and carbon dioxide, create gaps in the imagers ability to collect target data. This is illustrated in Figure 1.6. Broad spectrum coverage helps to mitigate the effects of these gaps in data analysis.

Conversely, the larger the spectral bandwidth, the more spectral bands are required to achieve the same spectral resolution. For AVIRIS, with 224 bands over 2100 nm of bandwidth, spectral resolution is about 10 nm. If the entire bandwidth

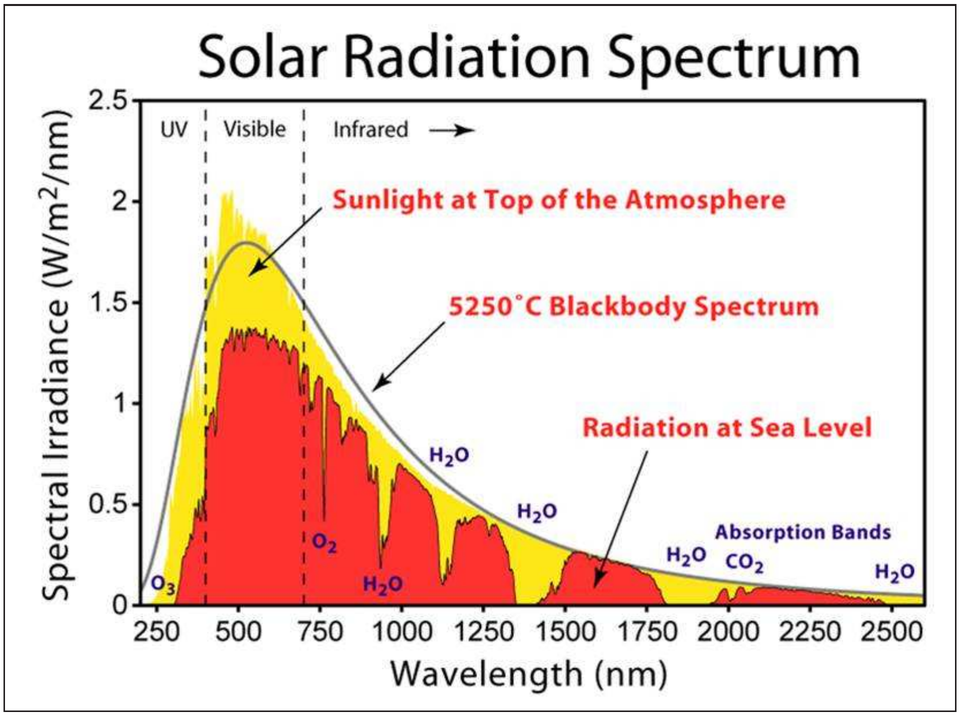

Figure 1.6: Absorption of reflected solar radiation by atmospheric components such as water create gaps in an imagers ability to collect spectral data. [39]

was only in the visible portion of the spectrum the instrument would require 30 bands to achieve the same spectral resolution. Spectral resolution requirements drive requirements for the size, sensitivity and data throughput of the instrument's light detecting focal plane array. The size of the target bandwidth as a whole determines the materials required for the FPA and whether more than one FPA will be required. This is due to the limits on EM sensitivity for various materials. For example, silicon based photoelectric FPA elements can be used for the visible light and some near infrared (NIR) parts of the spectrum. While longer wavelengths from NIR on up may be better matched with indium antimonide (InSb) or mercury cadmium telluride (HgCdTe) based FPAs. Obviously multiple FPAs or very large FPAs will in turn drive costs, complexity and instrument geometry. This can be seen in the AVIRIS instrument itself. In order to cover the broad spectral range that it does, AVIRIS uses three different detector materials, silicon for visible light, gallium arsenide for NIR and indium antimonide for short wave infrared (SWIR). The instrument scans along

the path of flight using what is known as a “whisk broom” or side-to-side technique providing a total of 34 degrees field-of-view with a 12 Hz scan rate. (see Fig 1.7).

One of the most challenging aspects of hyperspectral imaging can be the rate of data throughput from the focal plane array. The data rate for AVIRIS is over 20.4 Mbps. Data is stored on a 76GB hard drive. AVIRIS uses air breathing platforms for its data collection flights, so it is easy to download the data taken after each flight. A space-based platform will obviously not have that luxury and data will need to be transmitted to the ground after a collection pass. The other issue that is driven by the data rate is the image processing speed of the focal plane array as well as other important aspects of the mission that rely on the FPA. These will be discussed in detail in subsequent chapters.

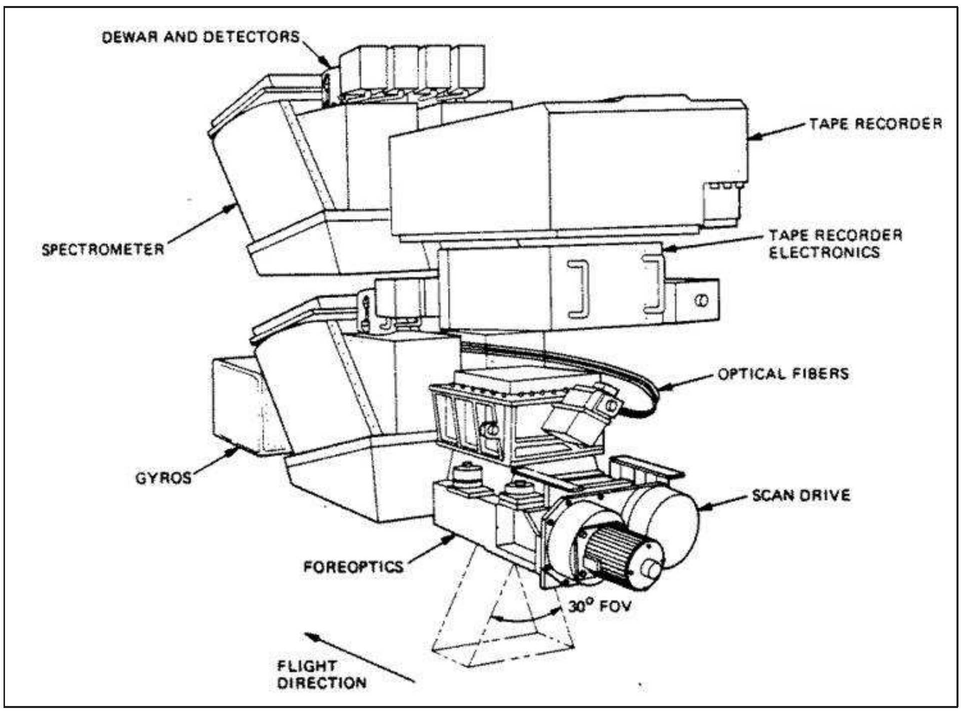

Figure 1.7: The AVIRIS hyperspectral imager [6]

To go further in the discussion of hyperspectral imagery, a representative output from one pixel of the AVIRIS FPA can be examined (Figure 1.8).

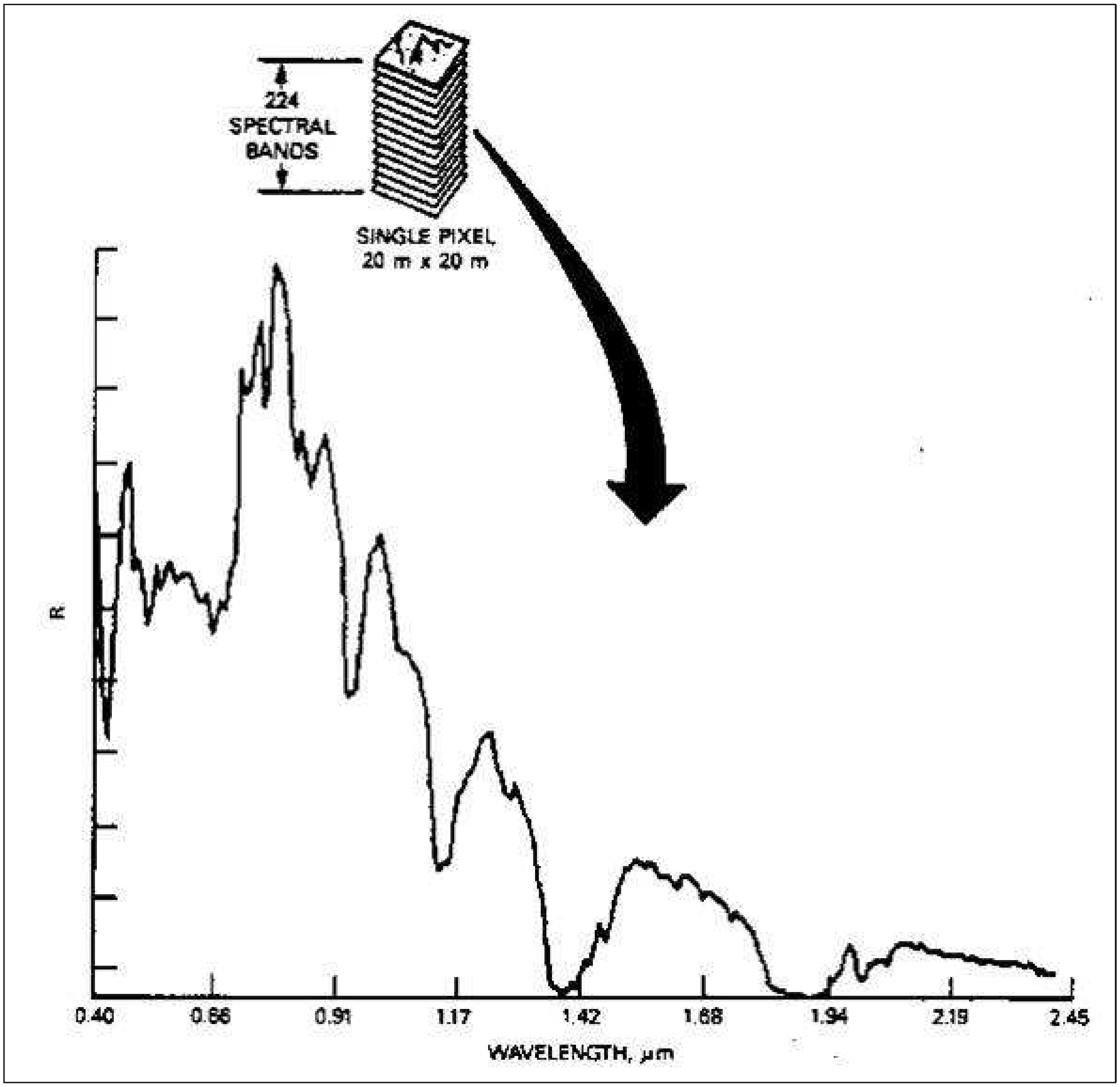

Figure 1.8: One pixel's spatial dimension is repeated over the entire spectral band [8]

The image shows the radiance, the received power, on one pixel of the AVIRIS FPA. The radiance is shown across the entire bandwidth of the instrument from 400 to 2500 nm in each of the 224 spectral bands. Notice that there is both a spatial and spectral extent for each pixel. The spatial extent of the image remains constant but is represented in 224 separate spectral bands. The sum total of all pixels in the 2-D FPA creates a 3-dimensional data cube with x and y spatial components and λ as the spectral extent as shown below. It is important to remain aware of this relationship; that each pixel in the 2-dimensional focal plane array corresponds with a particular portion of the overall image and therefore with a particular piece of geography that is in the optical field of view (FOV) for the instrument as a whole. This does not mean that the FOV corresponds to the size of the FPA. If the light that is incident on the system aperture is not fully focused on the FPA but either extends beyond the edges of the FPA or does not entirely fill the length or width of the FPA, the image produced will not match the instrument field of view. Clearly the greater the number of spectral bands, the better the fidelity of the resulting spectrograph. The end result being a better or poorer ability to identify substances or objects whose reflected or emitted light makes up some portion of the image under consideration.

1.3 Temporal Dimension

Thus far the thesis has described the uses of hyperspectroscopy with a three dimensional hyperspectral cube, two dimensions of physical extent and one of spectral bandwidth. These three dimensions can also be extended to a fourth, time. As already discussed, the spectral content of an image can provide analysts with a great deal of information about the imaged scene. Vegetation, water in liquid or frozen form, geologic minerals, man-made structures and so on can be identified and analyzed through a single hyperspectral image. Certain types of scenes also lend themselves to providing significant additional data through the temporal dimension. Those objects or activities of interest that change rapidly with time produce a changing spectral

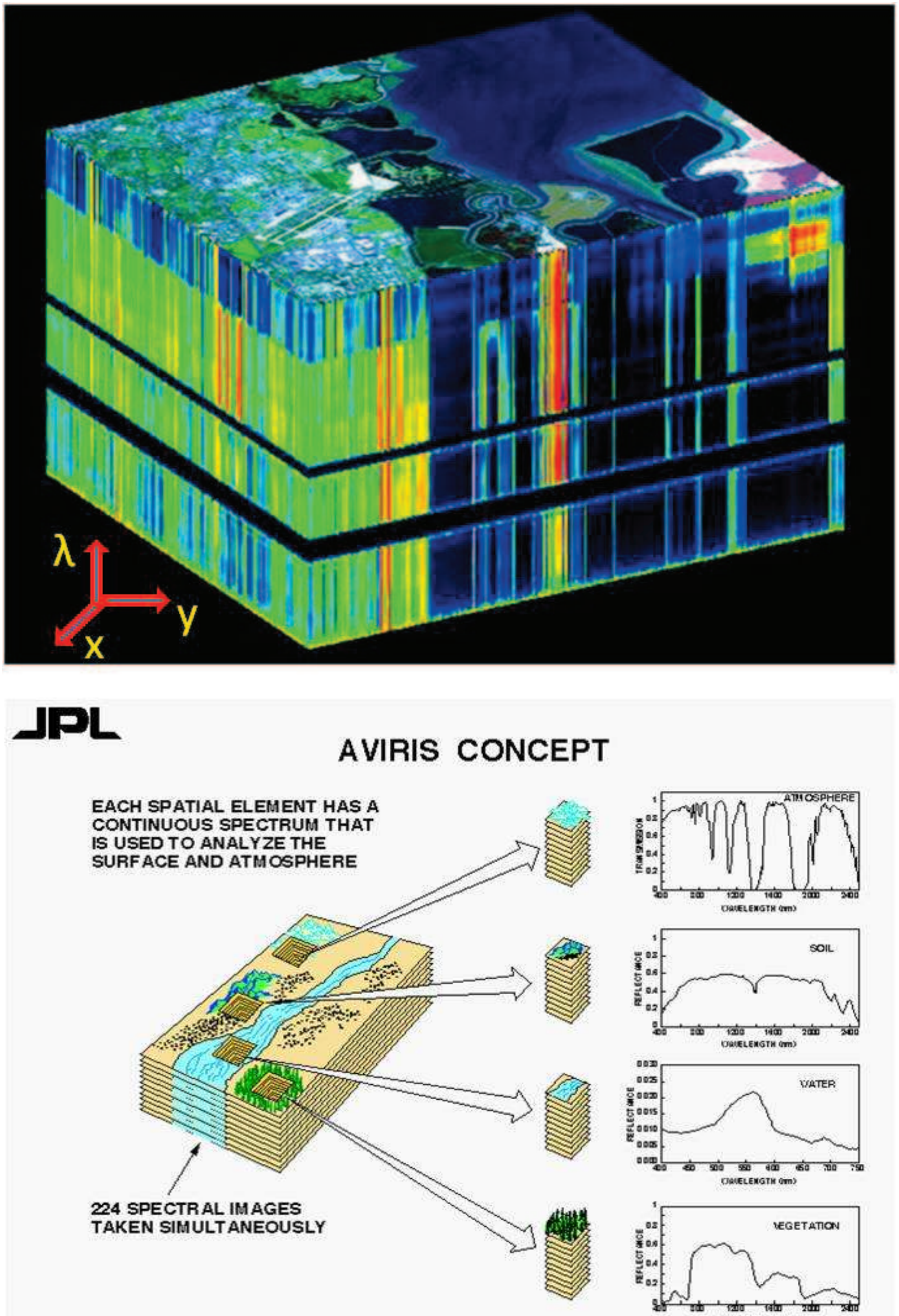

Figure 1.9: A 3-D hyperspectral data cube is created from the convolution of all pixel data [7].

signature in addition to any spatial changes that may occur. Examples of this include jet or rocket engine plumes, explosion fireballs, or any other combustion event.

The detonation of an artillery shell creates a fireball that will rapidly expand and then dissipate. A single hyperspectral image at some point in that progression will capture a snapshot in time of the size and spectral content of the fireball at that instant. However, much more information about the type and quantity of explosive as well as the packaging (shell) of that munition would be discernable if, instead of a single hyperspectral image, a large series of such images over the entire lifetime of the event were available. This would be, in essence, a hyperspectral movie of the event. This application could be used to analyze the evolution of the spectra that the fireball produces over time, in each of however many spectral bands our instrument resolves. This is the essential idea behind the Chromotomographic Hyperspectral Imaging Sensor (CTHIS) as described by Murgia et al. [36]

1.4 Problem Statement and Organization

This thesis uses the CTHIS instrument as a baseline concept for the first-order, engineering trade-space analysis of a proof-of-concept, space based CTHIS instrument. The thesis will be segmented into five chapters. The first, this one, introduces the concepts involved and lays out the problem to be examined. Chapter II provides a background literature and representative instrument review. It goes on to describe the physical layout and concept of operation of the baseline instrument as explained by Murgia et al. as well as a laboratory specimen in use at the Air Force Institute of Technology (AFIT). The third chapter will comprise the majority of the design study. At this point objectives, constraints and restraints for this project will be noted. There will be no assumptions made that any particular launch vehicle will be used to place the instrument into orbit, but that the instrument will be launched to low earth orbit (LEO). The assumption is that the instrument will be placed on the Japanese Experiment Module (JEM) Exposed Facility (EF) on the International Space Station (ISS) and will be constrained by the size, mass and other restrictions

of that facility. This is to be a proof-of-concept experiment and therefore is not expected to be extremely long lived (about one year) and should be designed with budget constraints in mind ($< \$1{,}000{,}000$). Where possible, commercial off-the-shelf (COTS) components should be used to reduce technology risks and lower costs.

Playing "follow the photon" a walk through of the optical and digital path of the instrument from light gathering aperture to data storage/offload will be conducted. This thesis will address the issues, problems and tradeoffs presented at each stage, discuss the merits of each and endeavor to make realistic recommendations for the instrument design.

The fourth chapter will propose a concept-of-operations for the instrument and walk through a hypothetical data collection event. The final chapter will summarize the thesis, pointing out areas that may not be adequately covered and make recommendations for areas of additional study or attention.

II. Hyperspectral Imaging Background Review

In order to ultimately design the instrument under consideration, the basic operation it is intended to perform and how this is accomplished must first be understood. CTEx is to be based on the Chromotomographic Hyperspectral Imaging System (CTHIS) which uses the spectral dispersion characteristics of a prism as a foundation for hyperspectral imaging. CTHIS or similar hyperspectral imaging systems have been studied and written on by several authors since at least 1998 [1]. Indeed, at the time of this writing there is an on-going study of various aspects of the basic system [1]. However, the instrument has never really been examined from an engineering perspective. As this study is aimed at taking a first step towards that end, a sampling of existing space-based multi-and hyperspectral imaging instruments and their operating principles will be discussed. The most recent studies and academic papers focused on CTHIS or similar theoretical or existing hyperspectral instruments will serve as a basis for studying design trade-offs for CTEx. A walk through of the major components of the prism-based CTHIS design will follow to provide more specific explanations of how this instrument is intended to function. This process along with user requirements will provide a baseline of requirements for CTEx. In other words, examining the existing experimental and prototype instruments along with recent academic studies on hyperspectral imagers will help establish a context within which CTEx design trade-space options can be developed.

2.1 Collection Techniques

The first topic to discuss is the general design and operating options for hyperspectral imagers at the present time. There are three general data collection techniques for imaging systems, the whiskbroom method, the pushbroom method and the step stare technique. The whiskbroom method in which the scanner or a mirror assembly scans the scene from side-to-side, perpendicular to the direction of instrument flight, is used by the AVIRIS instrument (Figure 2.1). There are no recent Hyper-

spectral Imager (HSI) designs that use whiskbroom scanning. The preferred method at this time is the pushbroom technique.

The pushbroom scanning technique is by far the most common. Space and airborne systems normally use a two-dimensional focal plane array. In the pushbroom technique light passes through a narrow slit and is focused onto the FPA, matching the field-of-view width. Here the spatial dimension is collected along the direction of the motion of the platform while the spectral dimension is simultaneously collected along the second dimension of the FPA (see Figure 2.1).

A third method of collecting HSI is the step stare technique. In this case the sensor is fixed on a specific ground scene for a period of time before being "stepped" to the next scene. This technique allows for much better signal-to-noise ratio (SNR) since the scene is kept in view for a longer period of time. Some form of this technique is necessary if the objective is to collect on a rapidly changing scene or scene feature as CTEx is designed to do. This method normally requires either a gimballed platform or a moveable mirror to keep a particular FOV under scrutiny while the platform moves along its track [29].

Any HSI system must have some method for separating out the collected light spectrum into the required bands. For this purpose there are three general classes of device: Dispersive spectrometers, Fourier transform interferometers, and narrow band adaptive filters. Dispersive devices use either a diffraction grating or a prism to separate collected light into a continuous spectrum. Fourier transform interferometers split incoming radiation into two beams and then introduce a controlled phase shift before recombining the beams. The combined beam is focused on a detector where the intensity of the light has been modulated by the phase difference between the beams. Since EM waves obey the law of superposition, the result is an additive combination of the two. The amplitude of the recombined beam is sampled at an appropriate rate and a Fourier transform is used to convert the amplitude modulated signal into

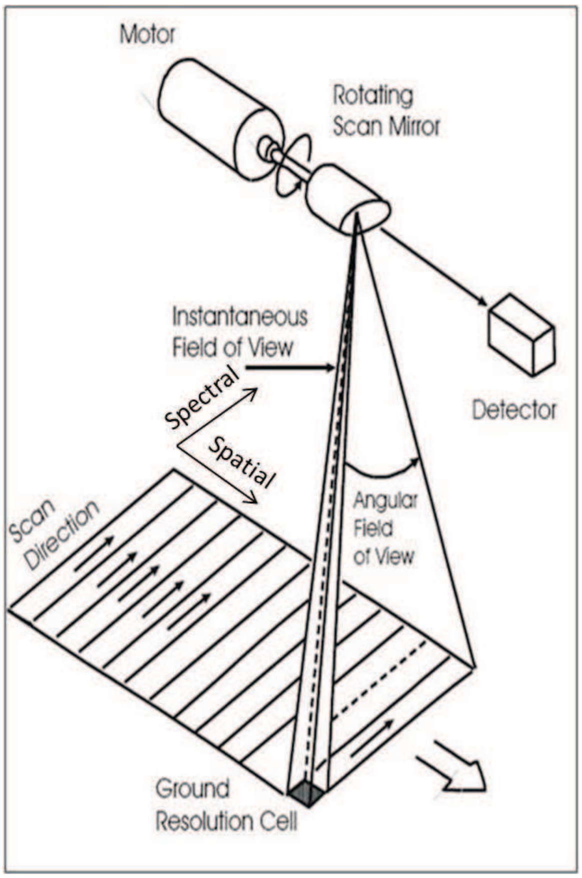

(a) Whiskbroom

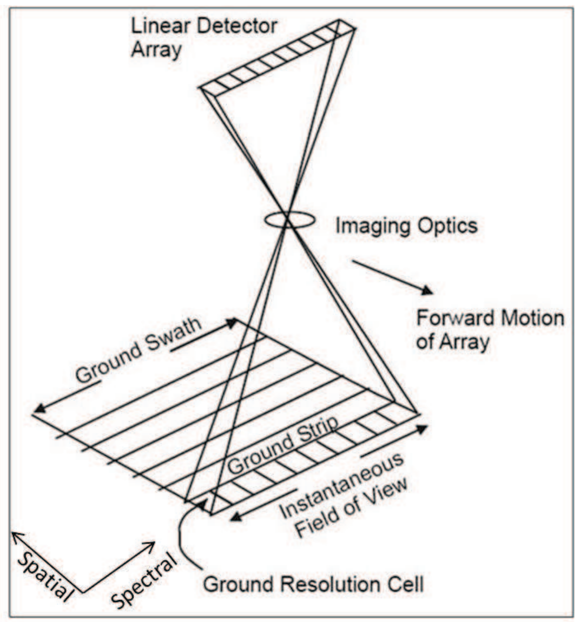

(b) Pushbroom

Figure 2.1: Whiskbroom and Pushbroom collection techniques [39]

a frequency spectrum [45]. This is simply an adaptation of the familiar Michelson interferometer.

There are several different types of spectral filters. The key idea is that EM radiation passes through a filtering material which can be adjusted to allow specific wavelengths through while blocking others. They all operate on some principle of altering a material's diffraction coefficient properties through either stress applied to the material, movement along a wedge, or application of a current or acoustic wave to rapidly change the spectral band of light allowed to pass through that material. Control of these properties allows spectral separation of desired EM bandwidths [40, 45].

Any of these techniques, or combinations of them, can be used for a spectrographic instrument. In practice however, prism or diffraction grating instruments are the most prevalent since these are the simplest, most mature and most reliable techniques. (See table of available devices in Appendix A) Less often seen are filter-based HSIs, although they are not uncommon. It is not unusual to see a combination of spectral filter with a prism or grating. Fourier transform interferometer-based instruments provide good performance, but are rarely used in space-borne applications. This is due to the fact that they have generally been very heavy compared with prism or grating-based HSIs and mass is a serious concern for space flight. One exception to this generalization is the Geostationary Imaging Fourier Transform Spectrometer (GIFTS) on-board NASA's Earth Observer (EO)-3 mission. GIFTS, as the name implies, uses Fourier interferometer techniques for HSI but mass issues have been controlled through the use of cutting edge, lightweight materials such as silicon carbide for the mirrors and other composites in the telescope structure [34].

2.2 Literature Review

An important background study to consider is the paper written by Fisher et al. in 1998, "Comparison of Low-cost Hyperspectral Sensors" [21]. The authors

provide an analysis of the relative merits of an all-reflective spectrograph using a convex grating in an Offner (the Offner spectrometer is discussed in detail below) configuration as well as two off-the-shelf transmission grating spectrographs using volume holograms. The authors conclude that the Offner spectrograph's advantages in lower smile (change of dispersion angle with field position, a type of abberation), larger aperture, fewer components, larger field and broader spectral range outweigh the disadvantages. Disadvantages include the immaturity of the technology for blazing on convex substrates while retaining low polarization and scatter (curved grating production). Fisher proves to be a good judge of developing technology as the Offner configuration is adopted in several proposed and actual instrument designs during the 2000s. As will also be seen, the issue of curved grating production has advanced as well, so the technical maturity disadvantage, as seen by Fisher et al., has diminished over time [21].

The Offner spectrograph, also called the Offner Interferometer, is a compact method of using a diffraction grating to disperse light onto an FPA. Although there are many variations, in general light is introduced through a slit opening and uses a primary mirror to divert the light onto a reflecting, curved grating. The grating is the diffracting element in the optical system. It is configured as a convex reflector to direct the light to the next optical element and to broaden the diffraction pattern. This allows for greater spectral resolution. The diffracted light is then reflected off another, secondary, mirror and sent, usually via some type of collimator, to a focusing lens and hence to the FPA. Besides the curved diffraction grating, an important feature of the Offner design is that the mirrors are spherical mirrors. Spherical mirrors, as opposed to parabolic or hyperbolic mirrors, are much easier to design and manufacture. The wave equations detailing the optical system is far simpler with spherical mirrors. In addition, spherical mirrors generally have shorter focal length and thus the system as a whole is much more compact. Figure 2.2 is a simple schematic of the Offner configuration. The most challenging aspect of this configuration is the manufacture of the convex grating as noted by Fisher in 1998. By 2007 these difficulties were being

overcome, ". . . progress in electron-beam technology has permitted fabrication of the required high performance convex gratings for the relatively difficult design of the Offner spectrometer." [45] The advantages of using a grating in a small volume design make the Offner configuration an attractive option for hyperspectral instrumentation. Beyond this, using an all reflective Offner design (actually any all reflective design) eliminates chromatic aberration [32]. This is an important consideration.

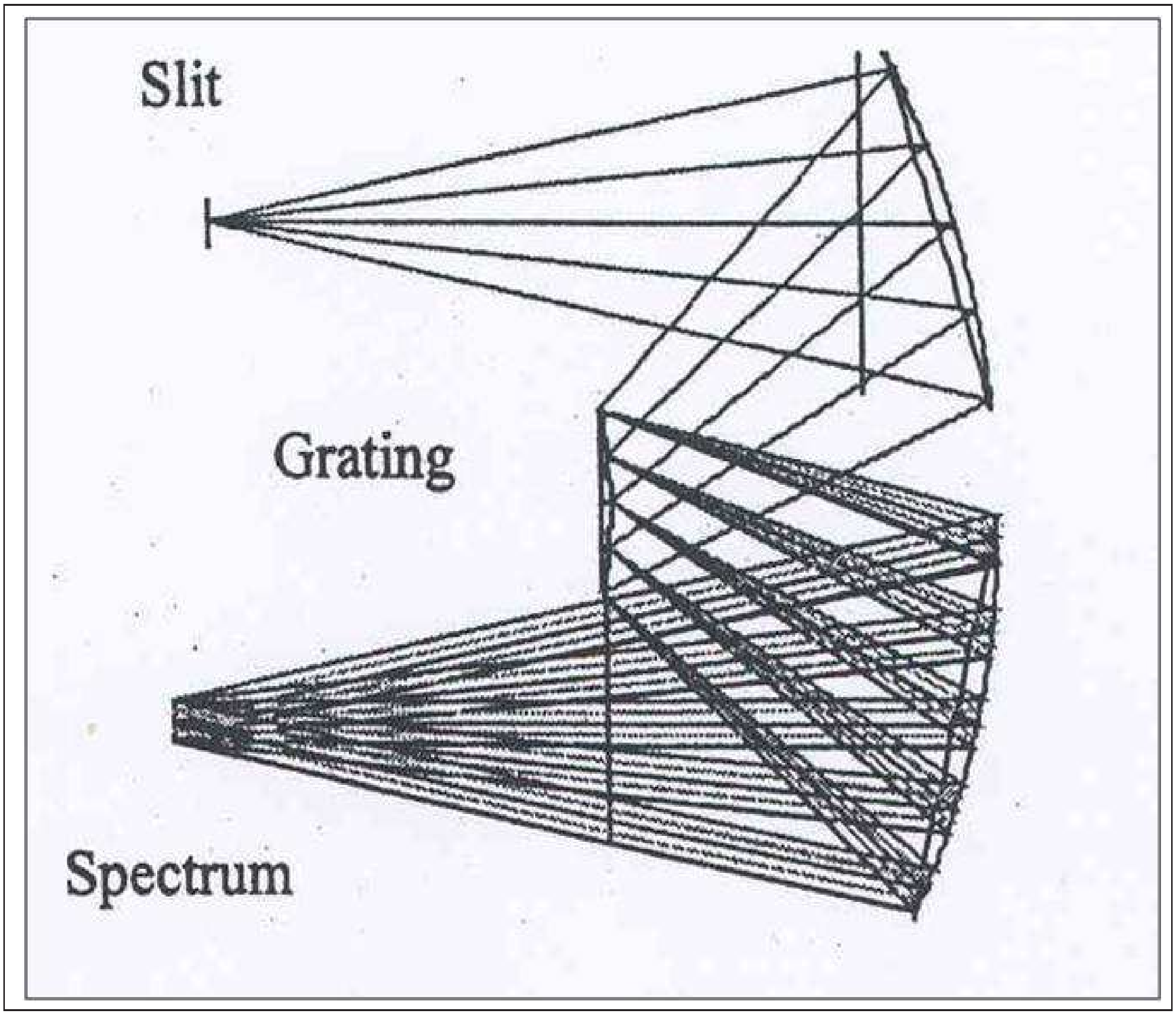

Figure 2.2: Offner interferometer [45]

In surveying the currently proposed or fully designed space-based hyperspectral imaging instruments there are several design characteristics that most of these instruments share. The first is that most incorporate a pushbroom scan technique to gather

spatial and spectral data using a 2-D FPA and gather spatial data in the crosstrack dimension and spectral in the direction of motion [17, 21, 26, 30, 33, 40]. Pushbroom scanning is favored because it is more efficient than whiskbroom and less complicated than low orbit step stare methods. It should be mentioned that there is a subset of the step stare method, simple staring. When an instrument is at geosynchronous orbit and is concerned with continuing surveillance of a fixed piece of terrain it stares at its field-of-view without moving. In this case the instrument would not need to "step" obviously and so would be less complicated since no slewing is involved. Of course at approximately 36,000 km distance from the earth's surface the optics must be considerably more powerful or grossly poorer resolution must be accepted. As mentioned above, one hyperspectral imager that is planned for geosynchronous orbit at this time is the GIFTS instrument on NASA's EO-3 mission. There is no set date for the launch of this satellite.

Advances in optical manufacture have made the Offner type of assembly a very attractive option. Of the proposed constructs since about 2003, use of a convex diffraction grating of some type is by far the most common as documented in studies by Fisher, Murguia, Johnson, and Yiqun et al [21, 30, 32, 36]. These constructs have the advantages of using a reflective optical assembly in a configuration that minimizes the instruments mass and volume, offers good performance and is less complex than a traditional reflecting telescope optic.

This is not to say that the Offner-convex grating is the only type of hyperspectral design being proposed. For example, Chowdhury and Murali's 2006 proposal for a selectable band compact hyperspectral imager uses a very complex combination of lens optics for light gathering and collimation. A two dimensional Linear Variable Filter for spectral separation and selection and an Active Pixel Sensor area array are also employed (Figure 2.3). The authors argue that this design will result in an instrument of less than 4 Kg mass and $\leq$ 10W power requirement with a spectral resolution capability of approximately 6nm in 512 contiguous bands from $.4 - .9\mu$m [17].

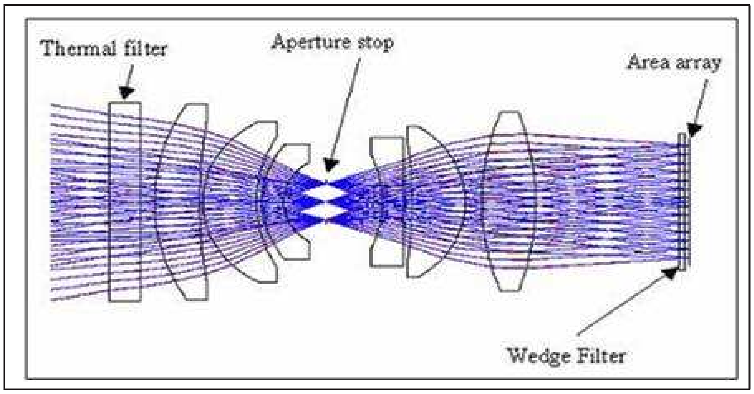

Figure 2.3: The Chowdhury lens-based, compact HSI design [17].

Several other recent papers bring up other intriguing possibilities for space-based hyperspectral remote sensing. Two of these are the 2004 Johnson et al. paper and the very recent (2008) work by Kaiser et al [31, 33]. The Kaiser work discusses the design for the Environmental Mapping and Analysis Program (EnMAP) HSI. EnMAP is a German hyperspectral space mission for environmental monitoring and data collection. It is currently scheduled for launch in 2012.

EnMAP uses an Offner design derivative, but employs a curved prism with a reflective backside rather than a grating as the dispersive element (Figure 2.4). The authors argue that while the Offner design offers very compact dimensions, excellent linearity and low distortion, diffraction gratings are plagued by low optical throughput due to limited diffraction efficiency. Gratings also suffer from high sensitivity to polarization and ghosting due to higher order aberration effects. Prism spectrometers by contrast offer high throughput over a wide spectral range and lower sensitivity to polarization. If used in a double-pass configuration, they also offer high angular dispersion, and therefore greater spectral resolution in a given image space. For this particular instrument the light is split into two bands, VNIR from 400 - 900nm, and SWIR covering 900 - 2450nm. It is designed for a high spectral resolution of about 6.5nm in the VNIR. The use of the Offner design allows the EnMAP spectrometer to be so compact that there is no need for separate collimator and prisms placed in the collimated light beam. Rather, “the prisms are arranged in the diverging and in the

converging beam. This requires the prisms to have curved surfaces as the angles of incidence must be kept constant for single field points and wavelengths." [33]

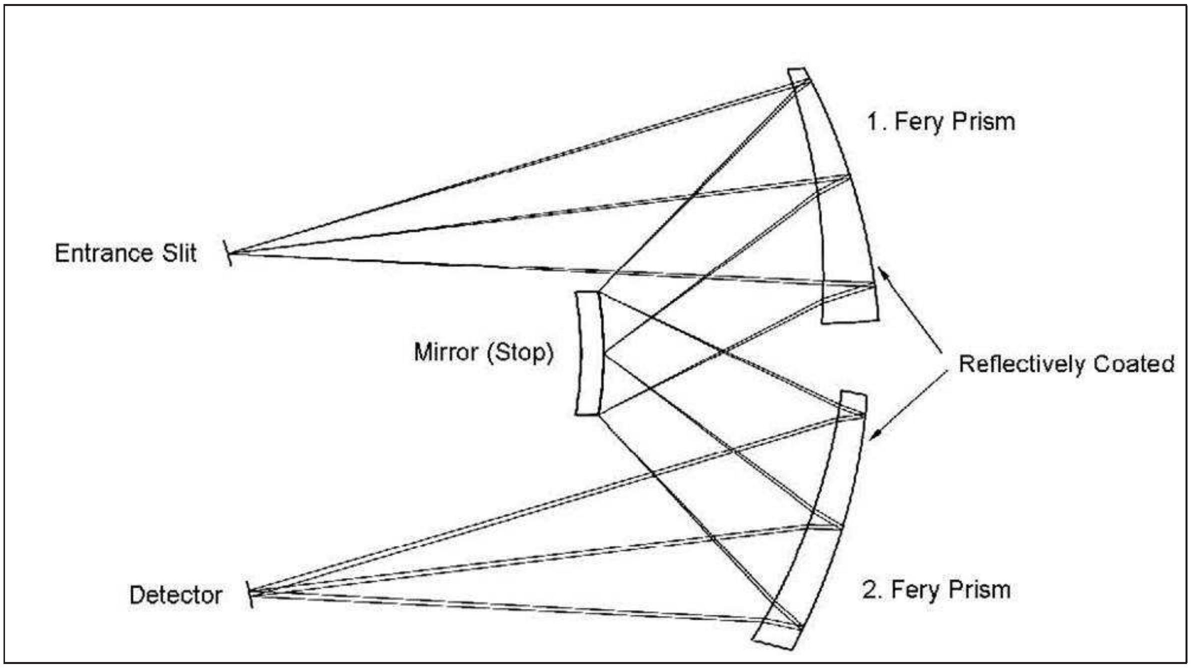

Figure 2.4: Offner spectrograph with curved prisms as the diffractive element [33].

The overall EnMAP system configuration can be seen in Figure 2.5. The front end telescope provides the object radiance to the rest of the instrument. The light is then split, with part going to the VNIR spectrometer and part going to the SWIR spectrometer. Each spectrometer uses two curved prisms and three mirrors as shown.

The Kaiser work is highlighted here to illustrate the rapid and innovative developments that are taking place in the optics field in general, and in hyperspectral imager design specifically. High capability, compact, low power and lightweight instruments are becoming more and more of the norm. These developments must be closely tracked due to their potential to impact design choices for the CTEx and especially any possible follow-on instruments.

The other paper of particular significance is the work of Johnson et al. "An All-Reflective Computed Tomography Imaging Spectrometer," published in 2004. The authors describe the design and laboratory results of an instrument they call the

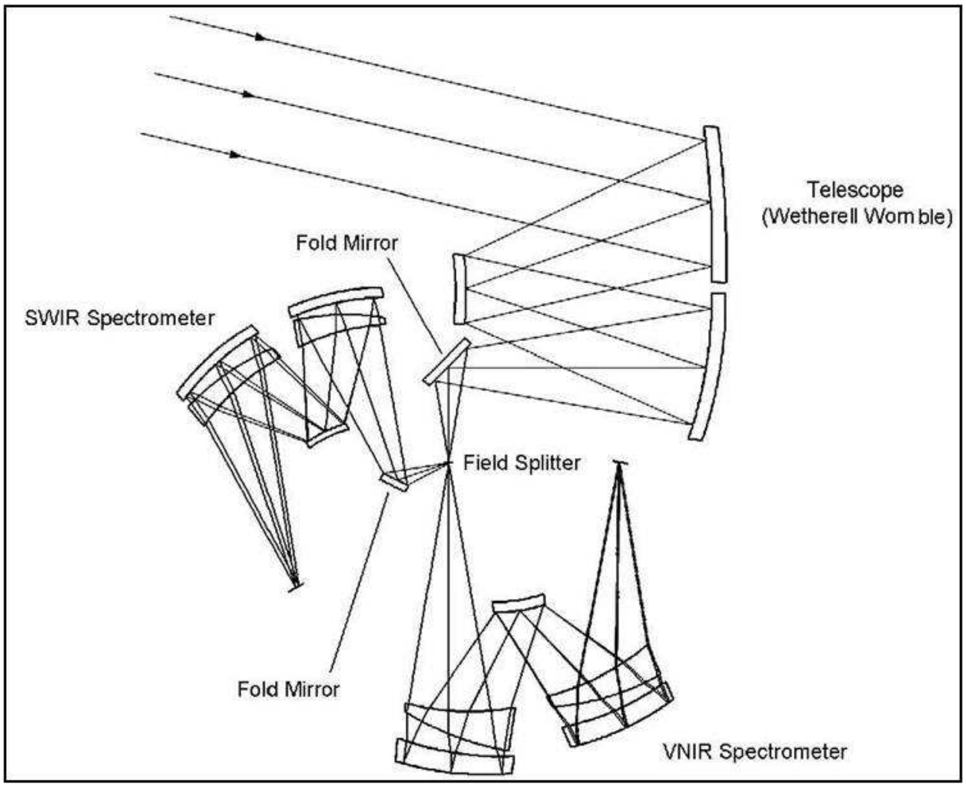

Figure 2.5: EnMAP optical system design [33]

"computed tomographic imaging spectrometer (CTIS)," [32]. They go on to characterize CTIS as an instrument which simultaneously captures spectral and 2-D spatial content. Noting that this implies a temporal capability for the instrument, the authors write, "CTIS accomplishes this by feeding incident scene radiation through a computer generated hologram (CGH) in Fourier space." [32, 88] The paper describes the "standard" CTIS as an objective assembly that images a scene and collimates the light from that scene onto a CGH. A CGH is a type of diffraction grating designed so that light of a particular wavelength band is reflected while another is passed through. Using materials of differing index of refraction, part of the light is split onto paths of varying optical path distance - enabling the use of Fourier techniques as described earlier in this chapter. Figure 2.6 shows an example of the "generalized CTIS" as presented by Johnson et al.

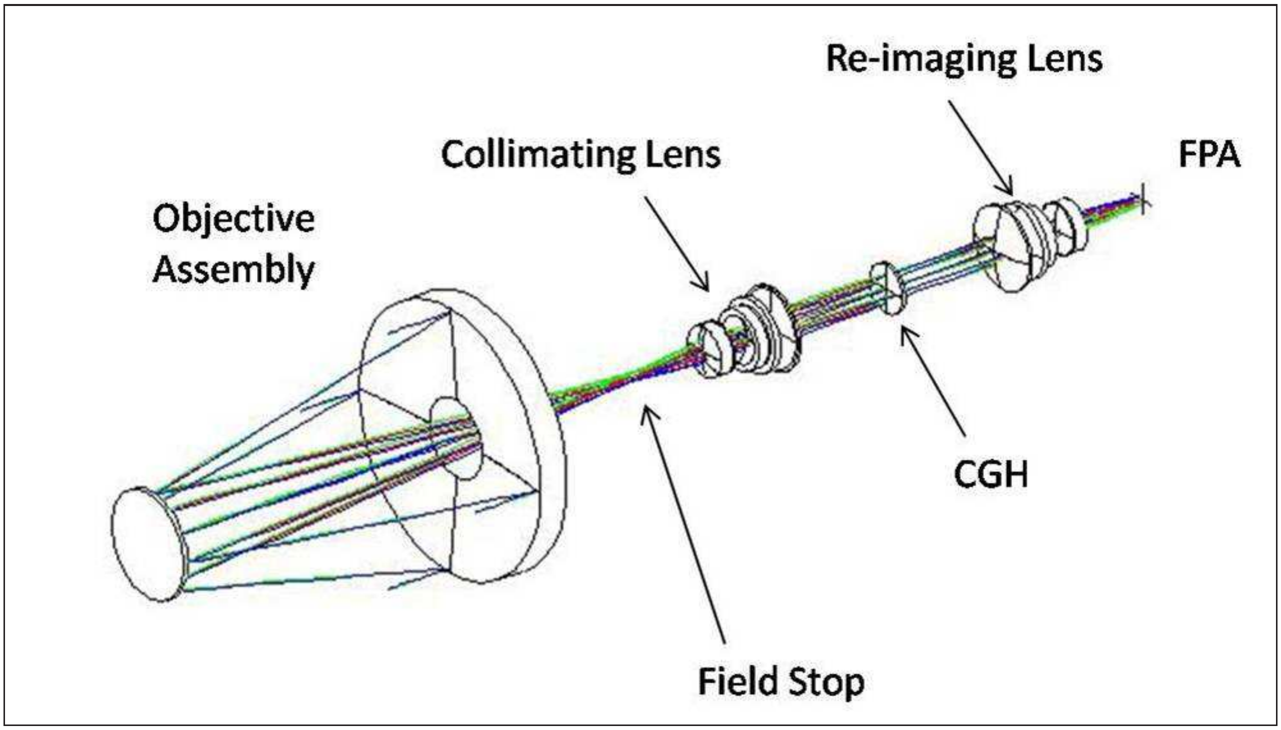

Figure 2.6: Generalized CTIS layout [32, 89]

The Johnson paper goes on to explain how the authors have taken this generalized CTIS layout and adapted it to an Offner spectrometer design (Figure 2.7). This design and its laboratory output appears to provide similar data to CTHIS. However, it is difficult to make direct comparisons between the instruments (see section 2.4 for a full description of the CTHIS laboratory instrument.) The system evaluation provided in the Johnson paper does not provide enough information to form an objective judgment. The evidence suggests there is merit to this form of chromotomographic imaging. Figure 2.8 demonstrates laboratory results of the CTIS laboratory instrument. The image displayed illustrates angular/spectral dispersion of three sources imaged simultaneously: a Mercury Argon source, a red light emitting diode, and a white light source. This result proves the capability of this instrument to perform tomographic projections, the same spectral reconstruction technique used by the CTHIS instrument. Therefore, the Computed Tomography Imaging Spectrometer may be a viable option for gathering rapidly changing spectral data for a dynamic event. However, the fact that the laboratory CTIS instrument uses a Coupled Charge Device

(CCD) for the focal plane array, as noted in the figure, means data throughput is probably limited to relatively slow speed. This would bound its utility for capturing very fast transient events such as explosions. At this time though, there is not enough data to fully evaluate CTIS in comparison with the CTHIS instrument.

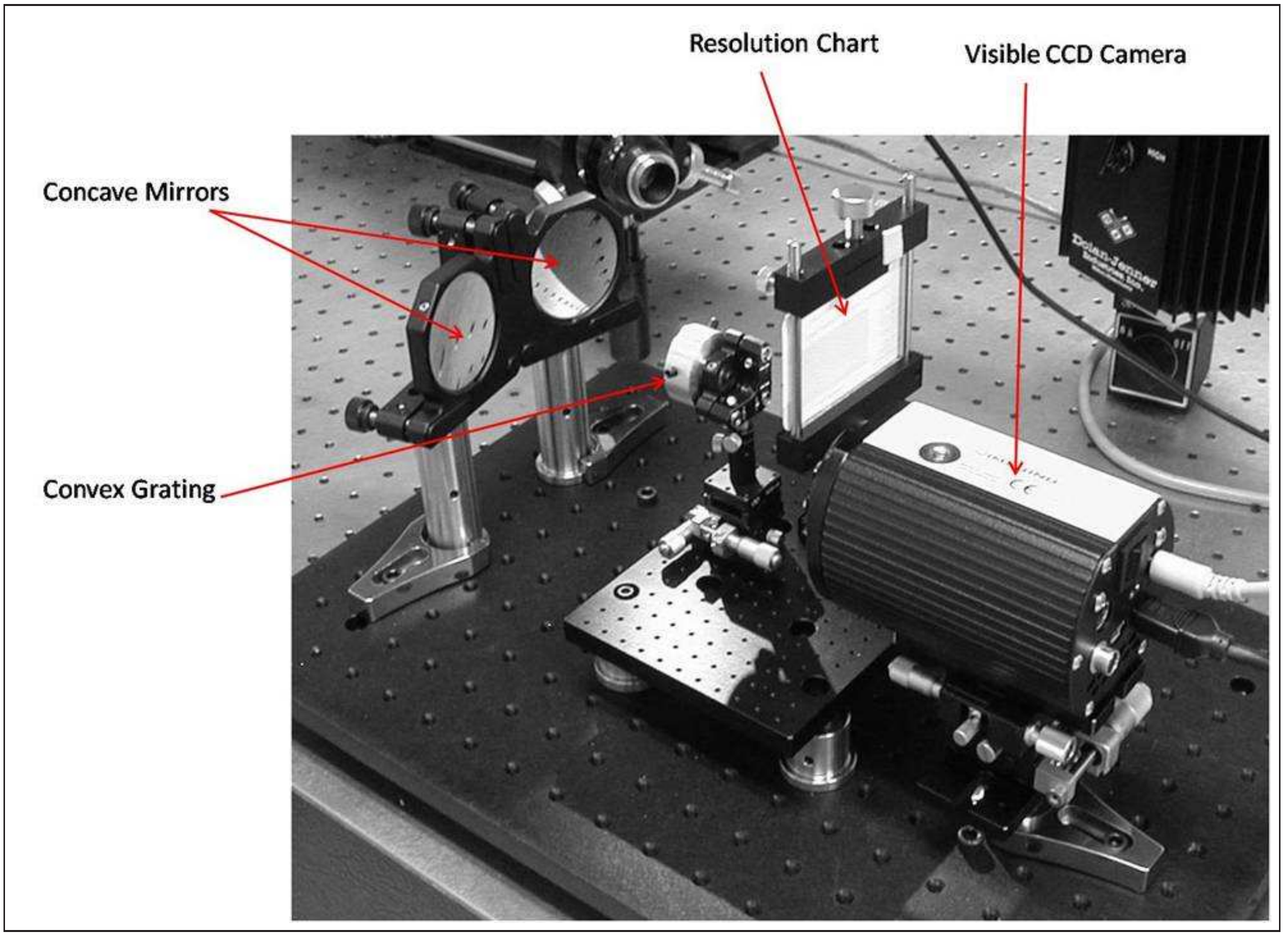

Figure 2.7: Laboratory model of the CTIS spectrometer. Note that the camera is CCD-based [32, 93].

2.3 Operational Instrument Review

The operations of the LandSat Thematic Mapper multispectral and the AVIRIS hyperspectral satellite/instruments were introduced in Chapter I to demonstrate some basic concepts in spectral imaging. Both of these instruments use the "whisk broom" side-to-side sweep for collection and spectral filters with diffraction gratings to sep-

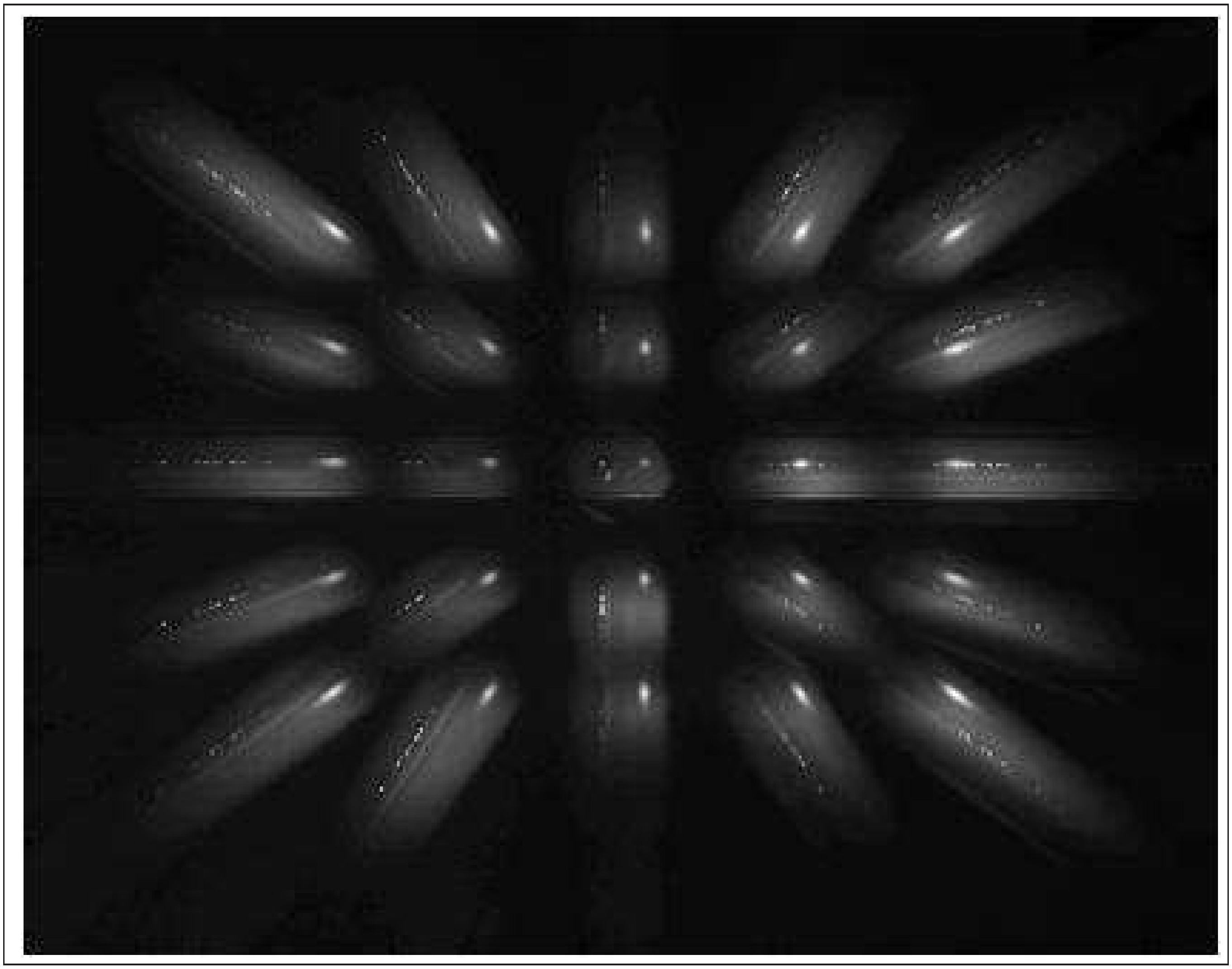

Figure 2.8: Lab result of Offner CTIS showing a Mercury Argon source, red LED, and white light background imaged simultaneously. This image demonstrates high quality tomographic projection [32, 94].

arate spectral bands. While the TM is a multispectral instrument and AVIRIS is hyperspectral, both of these instruments cover a very broad total spectral band, from visible to short or mid wave IR. This being the case, a fairly complicated physical arrangement is necessary since multiple focal plane arrays based on different materials are required. Focal plane array materials are selected depending on the area of the EM spectrum that must be observed. This is due to the fact that photodiode materials have finite areas of the EM spectrum in which they are sensitive.

Silicon-based FPAs, for example, are sensitive from about 300 - 1000 nm, although that range can be extended slightly with the application of particular reflective coatings or through customized physical arrangements. Other common infrared photodiode materials include Indium Antiminide (InSb), Germanium (Ge) and Mercury Cadmium Telluride (HgCdTe). Figure 2.9 shows the spectral ranges of several detectors based on some of these materials. The y-axis of the graph is essentially a scale of signal-to-noise sensitivity. There are multiple HgCdTe detectors shown since the spectral range of this photodiode material can be varied depending on the relative percentages of the three elements making up the material.

There are numerous multi and hyperspectral imagers in use today (Appendix A). To provide a baseline representation for operational instruments and a context for the CTEx instrument, two specific, representative operational hyperspectral imagers will be introduced. One is the Hyperion imager and the other the Mars Observer spectrometer.

The Hyperion hyperspectral instrument was specifically chosen for closer scrutiny in the background section of this thesis because of its clear analogous connections with CTEx. Built by TRW corporation for NASA, Hyperion was designed and operated as an important demonstration and flight-validation instrument for hyperspectral Earth observation. Launched in 2000, it was the first imaging spectrometer to routinely collect science-grade hyperspectral data from orbit [38]. Its mission was to demonstrate and evaluate the capabilities of space-based imaging spectrometry for earth

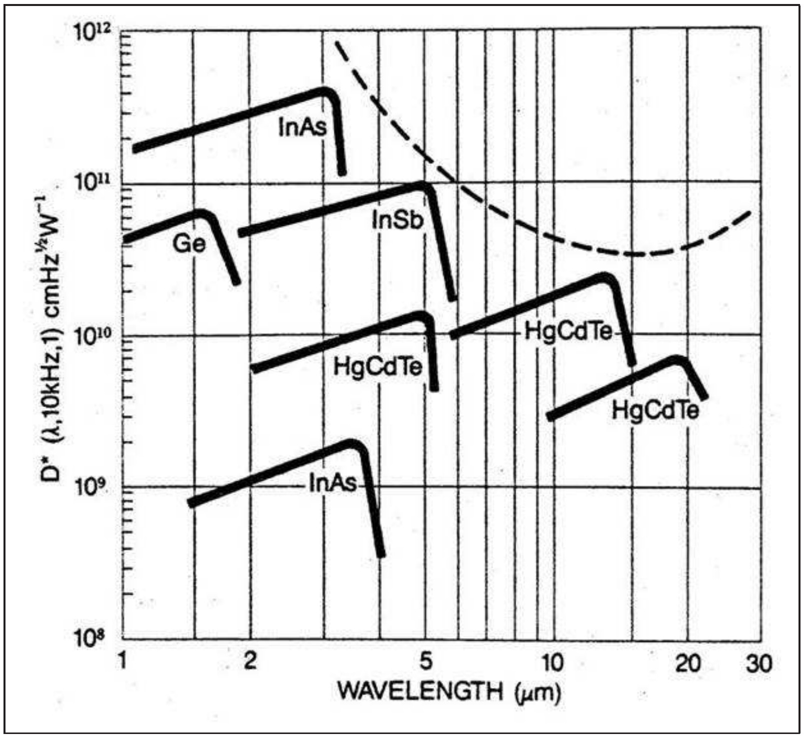

Figure 2.9: Example IR photodiode ranges [39].

observation, to include geological, agricultural, environmental and other earth science fields.

Hyperion is a diffraction-grating based, pushbroom collection type of imager. Its total spectral coverage is from .4 - 2.5 μm broken into VNIR and SWIR bands. The VNIR coverage is from 400 - 1000 nm while the SWIR runs from 900 - 2500 nm. The 100 nm overlap was intentional to allow cross calibration. Each spectral band, VNIR and SWIR, has its own grating spectrometer and focal plane array. There is a common fore-optic telescope that serves both spectrometers. This telescope is a three-mirror anastigmat design. The mirrors, as well as all optical structure, are constructed from the same material, aluminum, to minimize the possibility of induced internal structural stress from variations in material coefficients of thermal expansion. This point will figure prominently in discussions of CTEx issues in Chapter III.

Both of Hyperion's spectrometers use an Offner optical configuration with a convex grating on the secondary element [38]. The SWIR detector is a HgCdTe array

Table 2.1: Hyperion design parameters and on-orbit performance

Parameter	**Hyperion**	**Characteristic**	**On-Orbit**
Volume(L x W x H,cm)	39 x 75 x 66	GSD(m)	30.38
Mass(kg)	49	Swath(km)	7.6
Avg Power(W)	51	VNIR MTF@630nm	0.23-0.27
Aperture(cm)	12	SWIR MTF@1650nm	0.28
IFOV(mrad)	0.043	Spatial Co-Reg:VNIR	.18@Pix # 126
Crosstrack FOV(deg)	0.63	Abs. Radiometry(1 Sigma)	3.40%
Wavelength Range(nm)	400-2500	VNIR SNR (550-700m)	140-190
Spectral Resolution(nm)	10	No. of Spectral Channels	198 Processed
Spectral Bands	220	VNIR (bands 8-57)	427-925nm
Digitization	12	VNIR Bandwidth(nm)	10.19-10.21
Frame Rate(Hz)	223.4	VNIR X-trk Spec. error	2.2nm

cooled to 115 K with a cryocooler during data collection. The significance of this is that detectors in the IR range require cooling for good performance and the addition of cooling increases complexity, power requirements and risk. This will be taken into account in recommended choices for CTEx operating parameters.

The Hyperion's EO-1 host satellite is in a polar, circular, sun-synchronous orbit at 98.7 inclination. The orbit follows that of Landsat-7 by one minute. This orbital configuration was chosen to provide validation and comparison between the two instruments. The close proximity allows Hyperion to image the same scenes as the Landsat TM under essentially the same conditions, providing valid, comparable samples.

Hyperion was designed for a one-year lifetime, although it served for over two before the "Hyperion Validation Report," by Pearlman was written [38]. The design characteristics and on-orbit performance of Hyperion are listed in Table 2.1. One of the most relevant aspects of the Hyperion instrument in relation to the planned design and operation of CTEx is that of calibration. Extensive pre-launch spectral and optical radiometric calibration using National Institute of Standards (NIST) traceable sources/detectors were completed in a thermal vacuum chamber. Additionally, four techniques for on-orbit radiometric calibrations were including in the Hyperion

design/planning. These techniques were solar, lunar, on-board lamps, and vicarious Earth observations. The spacecraft, EO-1, was able to slew to point the Hyperion instrument at the sun or moon which provided known baselines for comparison and biasing of the raw spectral image data being output by the instrument. Internal calibration lamps were included in the system design as well, although many of these failed early in the flight. Vicarious calibration was a technique whereby the instrument would image a characterized test area on the earth's surface. These calibrations were performed using ground instruments to provide on-site surface measurement and atmospheric characterization [38, 6-29]. The author refers to this type of calibration as "vicarious" because the earth imaging calibration was only a substitute and supplement for the other, more precise, methods.

One of the most important lessons to be taken from the Hyperion instrument is that for a technology demonstration, such as with Hyperion or CTEx, it is crucial that some means for precise calibrations are including in the planning. Comparison of the instrument's design capabilities with actual performance against a reliable yardstick is necessary if the experimental results are to be interpreted in a valid, quantifiable way.

One other instrument that is currently in use and is also very relevant to the CTEx design trade-space study is the Compact Reconnaissance Imaging Spectrometer for Mars (CRISM). CRISM is a hyperspectral imager on board the Mars Reconnaissance Orbiter (MRO), launched in August 2005. The MRO entered its science orbit around Mars 13 months after launch. The orbit is a near circular (apogee of 320 km, perigee of 255 km), near polar, sun-synchronous orbit. The expected lifetime of the MRO is about five and a half years on orbit.

CRISM's primary mission is detection and characterization of geological mineral deposits on Mars' surface. It uses a 441-mm focal length Ritchey-Chretien telescope with a 10-cm instrument aperture that brings light to a focus along a slit for its front-end optic. It is designed to use a pushbroom collection technique, where the slit, as

normal, separates the scene into spectral (along flight path) and spatial (crosstrack) elements to create a hyperspectral cube as the instrument operates in orbit. The spectral range is from 383 to 3960nm. Collected light is split by a dichroic into VNIR and SWIR bands (383 - 1071nm and 988 - 3960nm). The instrument uses a modified Offner spectrometer design to spectrally disperse each beam onto its own 2-D FPA. The VNIR FPA is a 640 X 480 pixel silicon photodiode detector array, indium-bump-bonded to a readout integrated circuit (ROIC). The IR FPA is a 640 X 480 pixel HgCdTe detector, also indium-bump-bonded to a ROIC. These CMOS (Complimentary Metal Oxide Semiconductor) FPAs were both designed and produced by the Rockwell Science Center (now part of Teledyne Scientific and Imaging, LLC). Spectral resolution is better than 7 nm per channel with spatial resolution averaging about 17 m (61.5 μrad IFOV) depending on altitude [43]. A schematic of the instrument layout is presented in Figure 2.10.

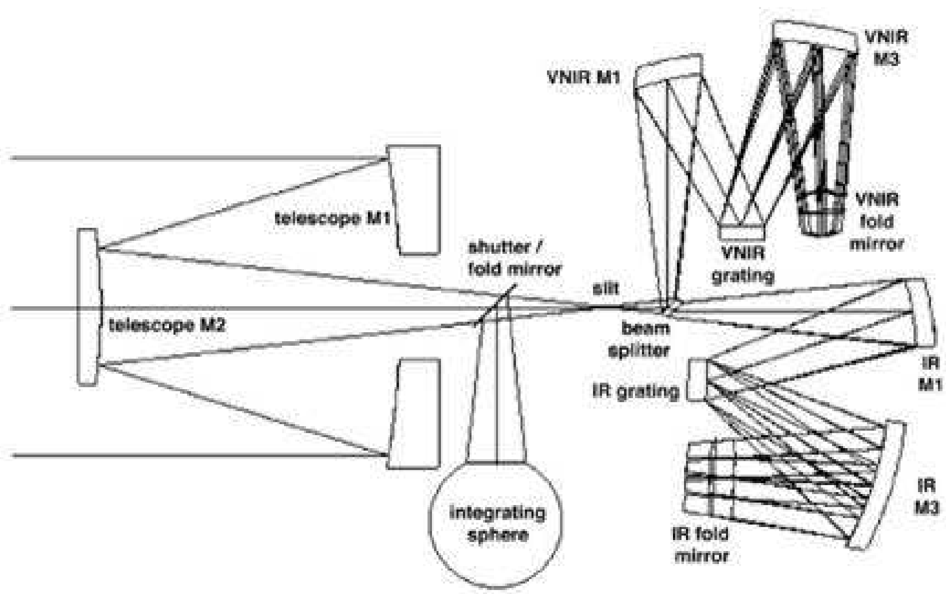

Figure 2.10: CRISM optical design [1]

As for Hyperion, the focus of attention will mainly be directed at the VNIR application. The IR requirement for CRISM makes the instrument much more complicated since it demands active cooling with the inherent supporting structure and

control electronics. One of the aspects of CRISM that is particularly interesting is its optional collection regime. CRISM is designed so that it can perform basic surface mapping with limited resolution through pixel binning (5:1 or 10:1). Pixel binning is an electronic technique whereby groups of pixels in the focal plane array are read as one. This lowers the data throughput requirement (i.e. the reset speed needed for the FPA) at a cost in spatial resolution. In this way CRISM can conduct large scale mapping in a timely manner at a reasonable resolution. When a particular area elicits greater interest, the instrument can be switched to a targeted mode where the full resolution capability, using all pixels separately, is used. In targeted mode, CRISM also has a 60° along track slewing capability. The slewing allows the optics to maintain a particular IFOV and uses a staring collection technique. Staring allows for much better integration and signal-to-noise (SNR) for the area of interest. It also eliminates along-track motion in the field-of-view and so reduces aberration due to smearing. CRISM uses a rotating gimbal to perform slewing maneuvers.

CRISM consists of three main components, the Optical Sensor Unit (OSU), the Gimbal Motor Electronics (GME), and the Data Processing Unit (DPU) Figure 2.12. The optical assembly uses all-aluminum mirrors and structure like Hyperion, to minimize thermal expansion induced-optical misalignment. Even though this material design feature was incorporated into the instrument, thermal vacuum testing was still conducted on the optical subassembly. This testing consisted of six cycles between 30 and -90°C for the telescope and 30 to -115°C for the spectrometers, with dwell time of one hour at each extreme. Results of thermal testing were that focal plane position repeatability was $< 0.1mrad$ in roll and $< 0.18mrad$ in tilt, both of which were better than required. "Decenter repeatability was within 20 microns, and focus repeatability was within 30 microns, both also meeting requirements." [43, 101-102] The authors of the Silverglate et al. study on CRISM characterization results concluded that, "The excellent performance of the OMS (Opto-Mechanical Subsystem) at temperature may be attributed to the use of an all aluminum structure and all aluminum mirrors." [43, 102]

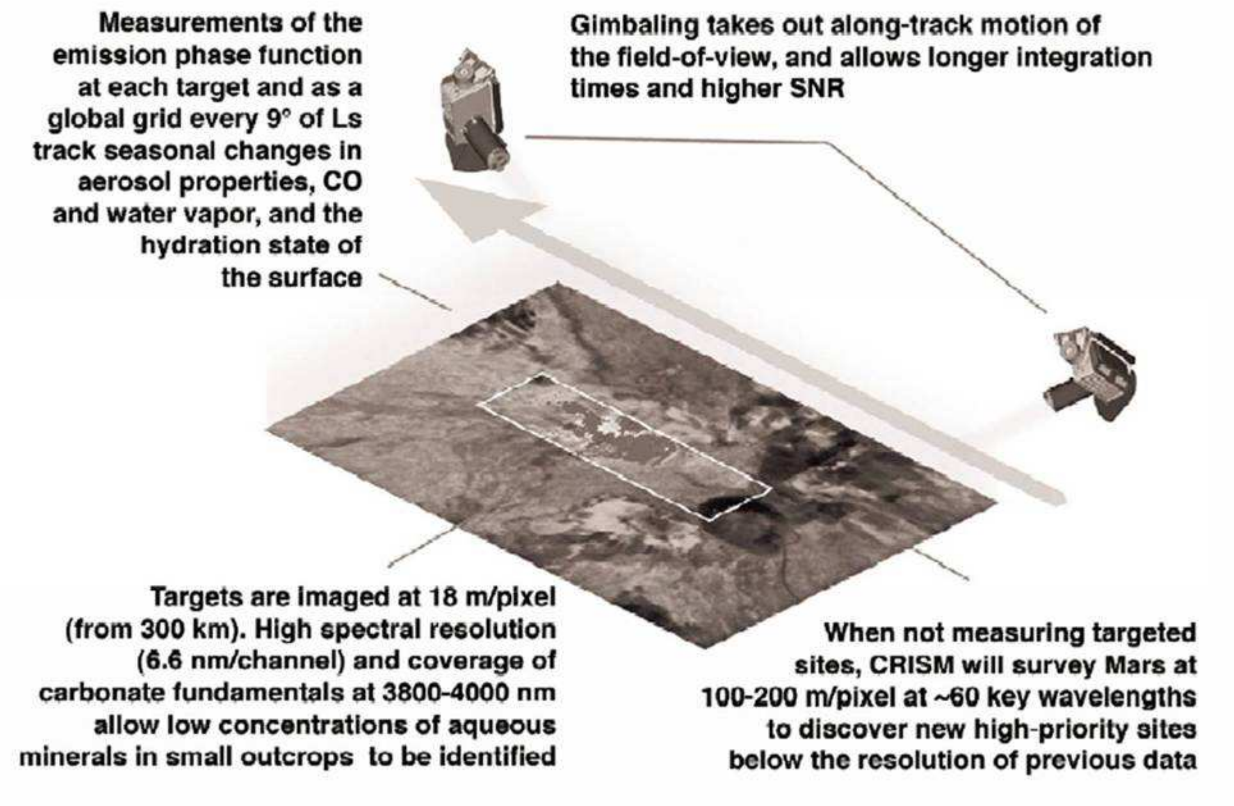

Figure 2.11: CRISM slewing strategy [35]

Other pre-flight testing included vibration testing at 28 g's rms in the lateral axes and 30.5 g's in the thrust axis for one minute [43, 102]. These tests were designed to assess system survivability under the stresses of launch, to include both lift-off associated acceleration and acoustics induced vibration. Ground calibration occurred in a series of stages where the detector arrays were characterized, optical distortion and other biases catalogued, subsystems and the system as a whole were tested at temperature, and system collimation was tested. Several on-orbit calibration capabilities are also incorporated into CRISM. These include shutter-closed "black body" measurements of IR noise, spectral measurements using an internal integrating sphere and internal lamps, as well as the capability to conduct calibration using star measurements.

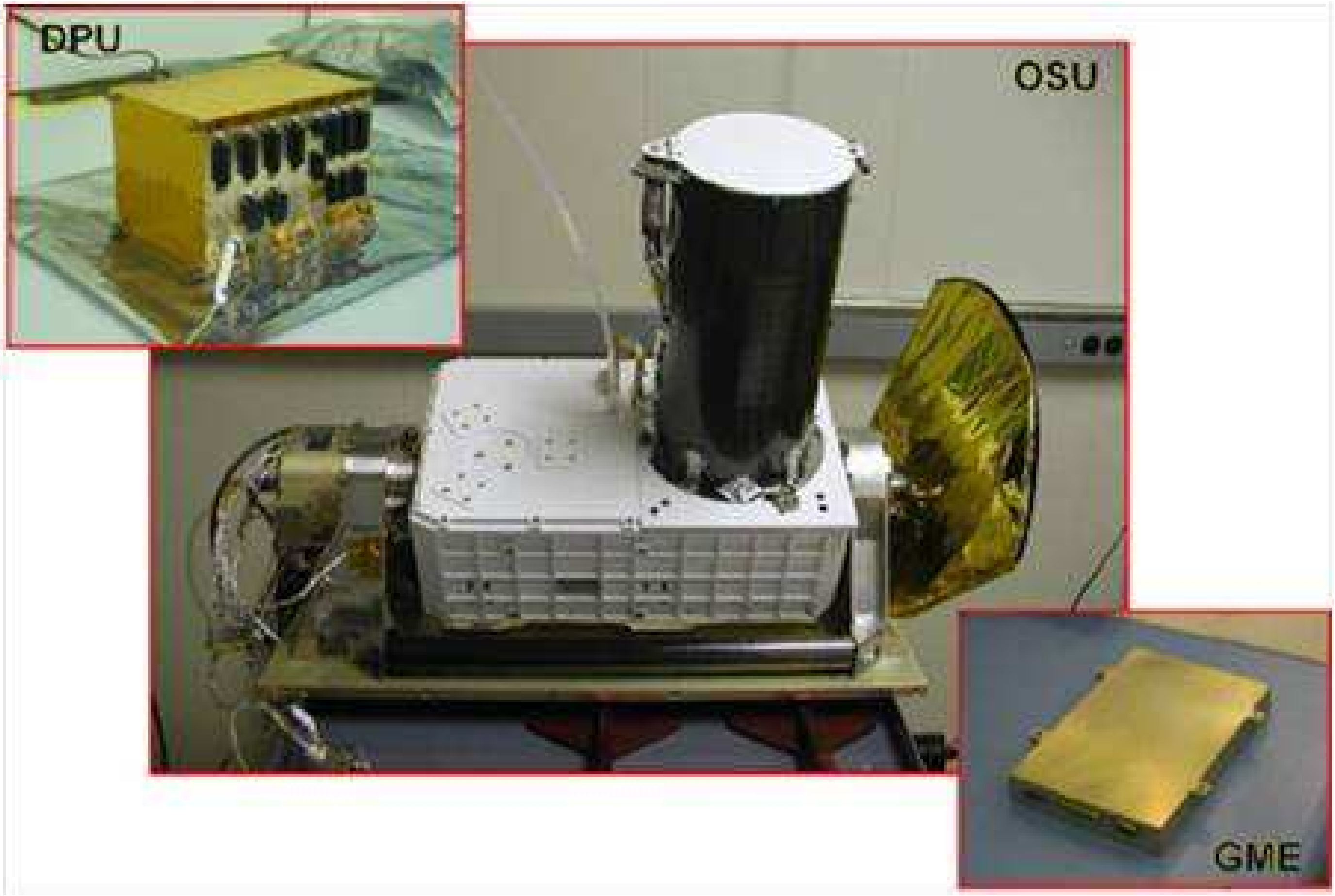

Figure 2.12: CRISM subassemblies [43]

A full schematic of the CRISM design is provided in Figure 2.13. Note how the cooling requirement adds size and complexity to this design.

Even with cooling, the entire instrument has a total mass of only 32.92 kg and power draw during operation of 44.4 - 47.3 W [1]. A view of the optical assembly and a blow up drawing of the entire instrument is provided in Figure 2.14. The light weight and compact size of CRISM are important considerations for design of any space-based hyperspectral imager.

To summarize, Hyperion and CRISM are two examples of space-based hyperspectral imagers which provide excellent baseline trade-space analysis that can be applied to CTEx. The Hyperion an CRISM HSIs both use a polar, near circular, low

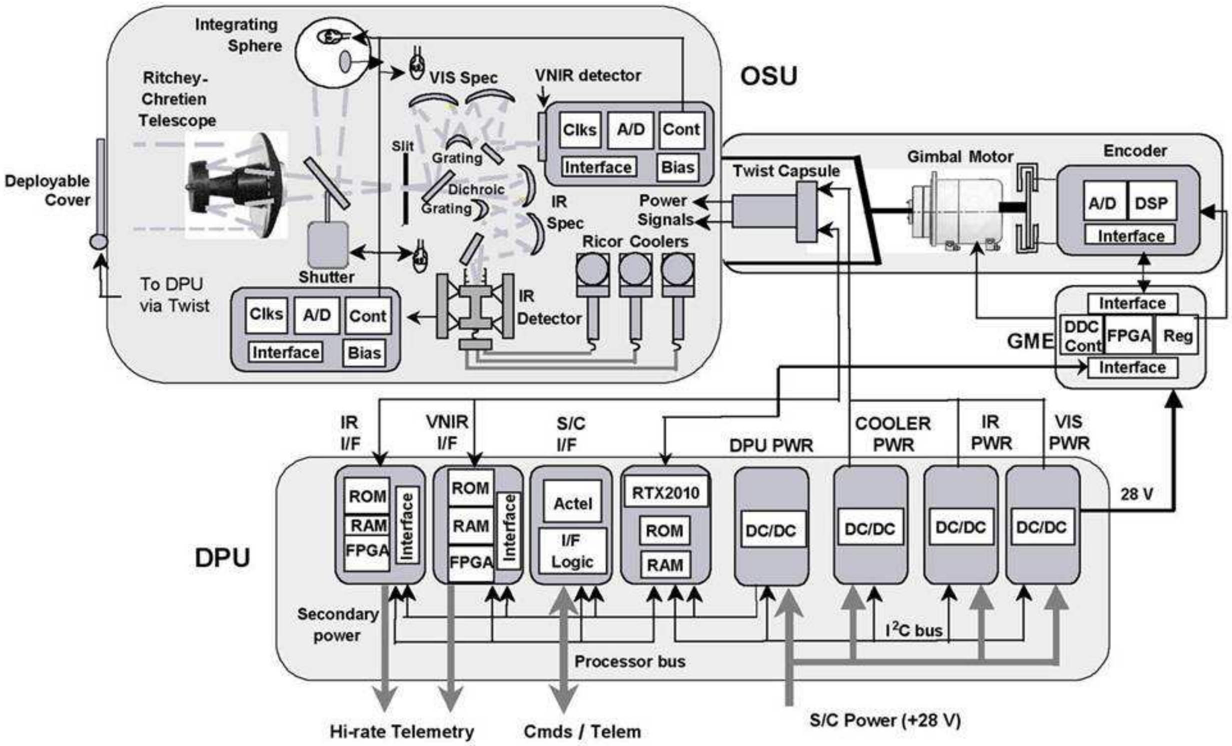

Figure 2.13: Block diagram of CRISM key components [42]

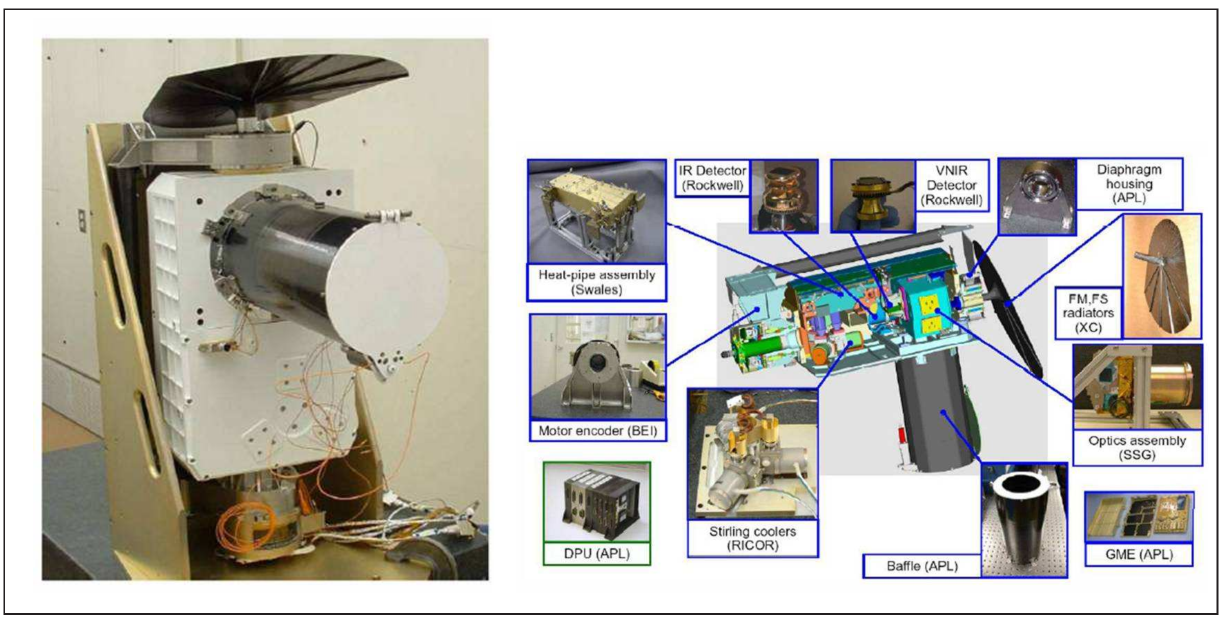

Figure 2.14: CRISM optical assembly and component blow up [43]

orbit, although CRISM is orbiting Mars rather than Earth. The spectral and spatial resolution requirements for these imagers are comparable with CTEx as well. In addition Hyperion and CRISM are designed to produce science-grade hyperspectral data.

The most important aspects of Hyperion and CRISM of which to take note are the compact optical designs, the careful attention paid to structural materials used to mitigate thermal cycling problems, the extensive on-ground testing and calibration performed pre-flight, and the on-orbit calibration capabilities. All of these are directly applicable to design considerations for CTEx and will be discussed in depth in Chapters III and IV of this thesis.

2.4 CTHIS prototype

The CTHIS is in large part a system of optical devices (Figure 2.15). Light is collected and collimated through a front-end optic consisting of two converging lenses with an intervening field stop. That light column then passes through a direct vision prism where it is dispersed according to its wavelength, with one wavelength passing through undeviated. The dispersed light then passes through a converging lens, which focuses the light onto a focal plane array. The FPA is an array of photovoltaic elements which react to the intensity and location of the light, converting the EM energy into electrical signals which are ultimately transferred and stored as digital readout information. The amount of deviation from the central point, the undeviated wavelength, on the array provides information on the wavelength of the light, since the deviation is a function of the wavelength and the prism characteristics.

As the prism rotates, the FPA collects the scene information as described above for each prism rotation angle depending on the reset, or frame rate, of the FPA. One complete revolution of the prism will then constitute a complete hyperspectral cube. Mathematical reconstruction of the multiplexed imaged scene is then possible in any

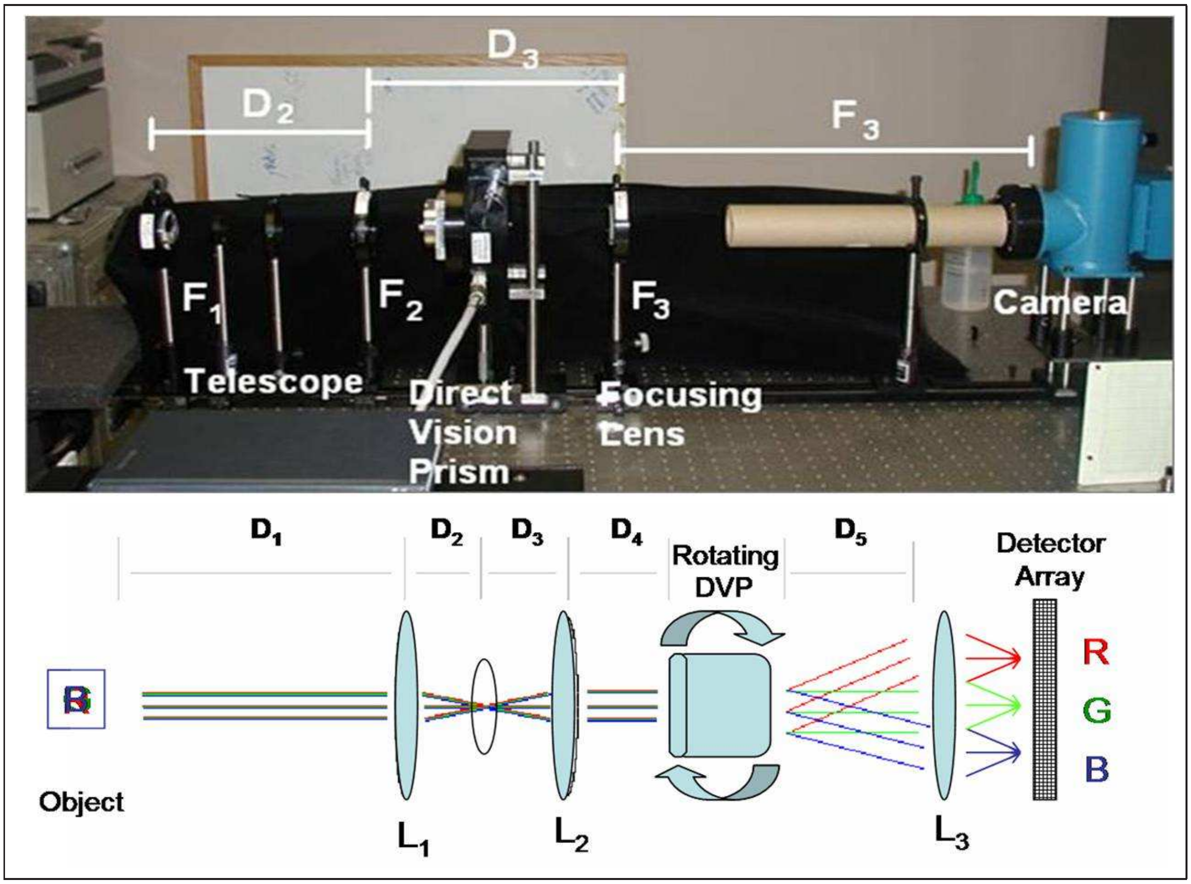

Figure 2.15: CTHIS laboratory design

or all of the spectral bands for which the instrument is designed, that is, according to the spectral resolution. This process is demonstrated in Figure 2.16.

One important aspect that differentiates CTHIS from other hyperspectral imagers is the action of the prism. In this device the prism is rotated at some specified rate over time. This rotation provides a tomographic imaging capability which is important in reconstructing an entire scene. Assuming the device is staring at a particular scene, there are many objects present in that scene and many of them will be reflecting light in the same spectral bands. For example, for simplicities sake assume the scene being imaged consists of a tree, some grass, and a shed. Clearly there will be more than one source of EM energy over the "green" portion of the spectrum. In a single image the light reflected from the scene reaches the prism and is dispersed into its spectrum, which is then focused on the FPA. The spectrum is spread around

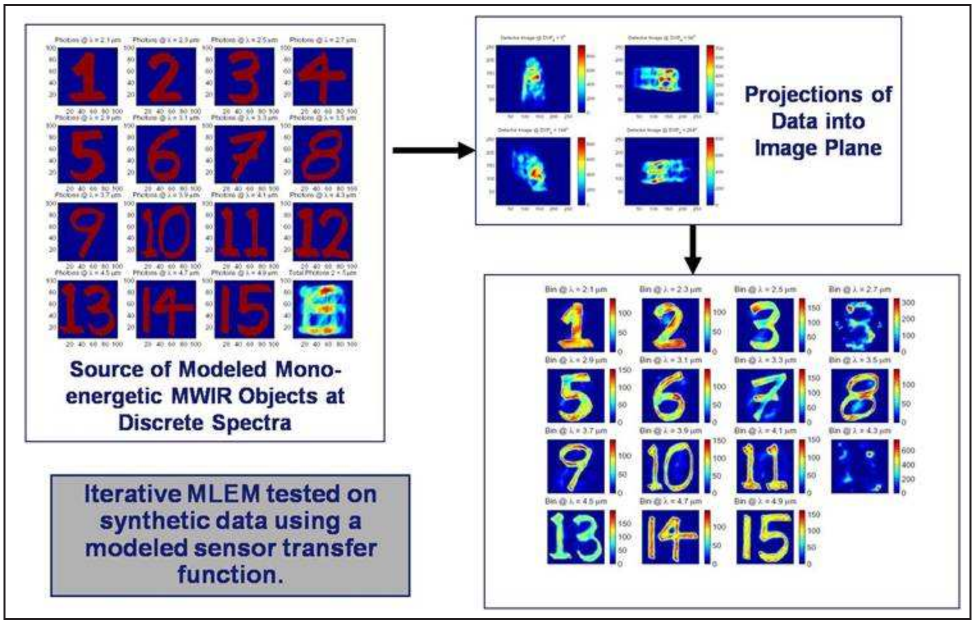

Figure 2.16: Chromotomographic reconstruction of number figures. The original image is all numbers laid on top of one another. Each is in a different spectral band. The demultiplexing of the gathered image data allows reconstruction of each number as a separate image according to its spectra [15].

the undeviated wavelength of the direct vision prism, the angle of diffraction being a function of wavelength and the prism characteristics. Since there are multiple wavelengths at, say 550 nm, how can the image scene be reconstructed? This is where the tomographic aspects of the instrument come into play. As the prism rotates wavelength dependent circles are imaged around the central wavelength point. The process is analogous to medical tomography where, for example, x-rays are passed through the body along varying angles; the images taken along varying planes are multiplexed on top of one another. Through Fourier analysis, the scene in our case, or a particular slice of the body in the medical case, can be reconstructed - pulled out of the multiplexed data. Whereas in the medical case this is accomplished for numerous spatial planes in the body, chromotomography uses the same principles to process data spectrally, reconstructing the scene in any bandwidth of interest.

Depending on the rate of rotation of the prism and the matching camera frame rate, rapidly evolving spatial and spectral events such as explosions or a rocket motor firing can be characterized. As an example, hypothesize that the imager is tracking a plot of ground where there is an explosion. As the fireball expands it changes in both size, the spatial dimension, and in its spectral signature. Both the spatial and spectral changes can now be tracked over time, which provides much more information on which analysis can be done. Aspects of these changing parameters can be analyzed to determine characteristics such as the type, amount, and placement (i.e. above ground, underground etc.) of the explosive. In other words, this instrument adds a temporal dimension to the two spatial and one spectral dimension already present in a "typical" hyperspectral cube. Instead of just a cube, the fourth dimension, time, converts the cube into a segmented, three dimensional rectangle. Rather than a single image, the collected data is more like a movie, where changes in one, several or all spectral bands can be tracked and plotted over time.

Each rotation of the prism provides one complete hyperspectral cube. Therefore the temporal resolution that can be achieved by the instrument is a function of prism rotation rate. If the prism is rotating at 10Hz the temporal segmentation will be .1 second chunks. At 100Hz rotation rate .01 second time steps will be discernable. It is important to understand this time dependent relationship since various events will present different demands for temporal clarity. An explosion may require .01 or smaller time segments to allow for data analysis of such a rapid event. A test rocket motor firing may only require .1 second steps since the rocket plume maintains a more steady state over time than the explosion fireball.

As can be seen in Figure 2.15 after dispersal into its spectrum the light is focused onto the 2-D focal plane array of a fast framing camera. This is the point at which the image data is taken into digital form and recorded for processing. One of the limiting factors for the instrument will be the refresh rate of the FPA. The speed at which optical information can be transformed from photonic to an electric potential and then to analog or digital information is the throughput rate of the FPA. The angular

image capture rate then is equal to the camera frame rate. This defines the amount of image data taken for each hyperspectral cube. To illustrate, if the rotation rate of the prism is 1Hz and the camera frame rate is 4Hz, then each hyperspectral cube will be constructed from image data taken at 90, 180, 270 and 360 degrees of rotation, or four images. The greater the frame rate for a given prism rotation rate, the more images available for convolution and tomographic processing. Thus, the faster the FPA throughput capability, the better the fidelity of the resulting data cube.

Besides data throughput, the size, pixel center-to-center distance, material and type of processing of the FPA are crucially important for defining maximum spectral and spatial resolution, bandwidth sensitivity, and cost for the instrument as a whole. The raw data from CTHIS is stored on a normal hard disk. At the time of this writing there is no commercially available software for conducting the image reconstruction and spectral analysis. However, several researchers have written or outlined algorithms for doing so [19, 23]. Hyperspectral imagery tends to generate large amounts of data very rapidly so another important aspect to performing these operations is having a data bus capable of transferring data off the imaging system to storage, and of course adequate storage capability for reasonable amounts of imaging time before processing or data compression.

2.4.1 Geometric Optics. The system being used as the basis for the instrument design, as seen in Figure 2.17, begins with a converging lens, followed by a stop then another converging lens.

The essential principles for the use and placement of this lens configuration become clearer upon briefly examining some basic geometric optics. The essential relationship for thin lenses is noted in Equation 2.1

$$\frac{1}{s_o} + \frac{1}{s_i} = \frac{1}{f} \tag{2.1}$$

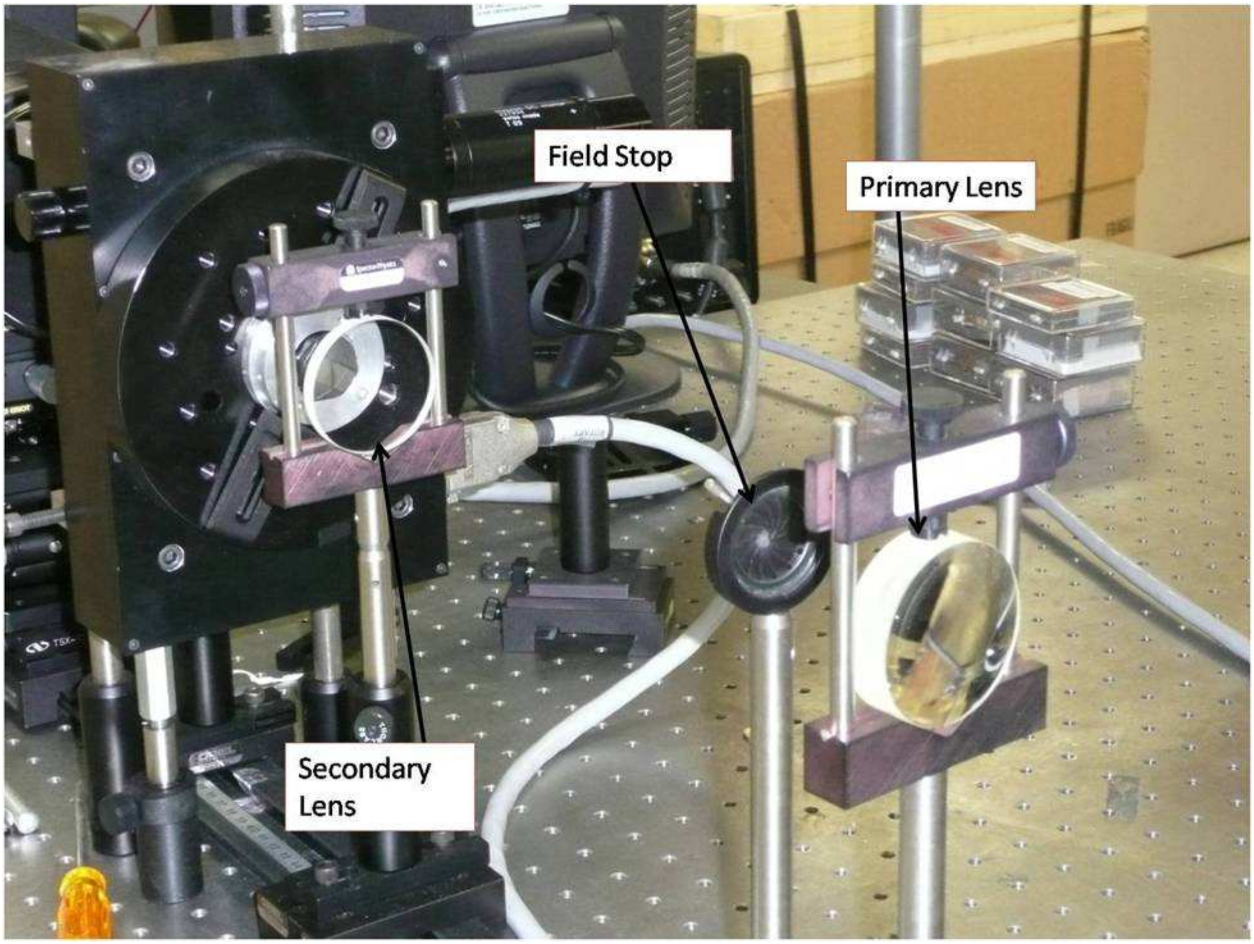

Figure 2.17: CTHIS lab instrument front-end optics

where s_o is the object distance from the lens, s_i is the image distance and f is the focal length. If an object is placed a great distance away from a converging lens in comparison with the lens' focal length, the image distance will converge to that focal length. Similarly if an object is placed at the focal length, its image distance approaches infinity - meaning that the light from the object will be collimated after passing through the lens. So using two thin converging lenses, if the image from the first lens serves as the object for the second (that is their focal points are coincident) the light passing through the optical system will be collimated. The stop between the two lenses serves to isolate the desired object/image from stray light. These principles are demonstrated in Figure 2.18

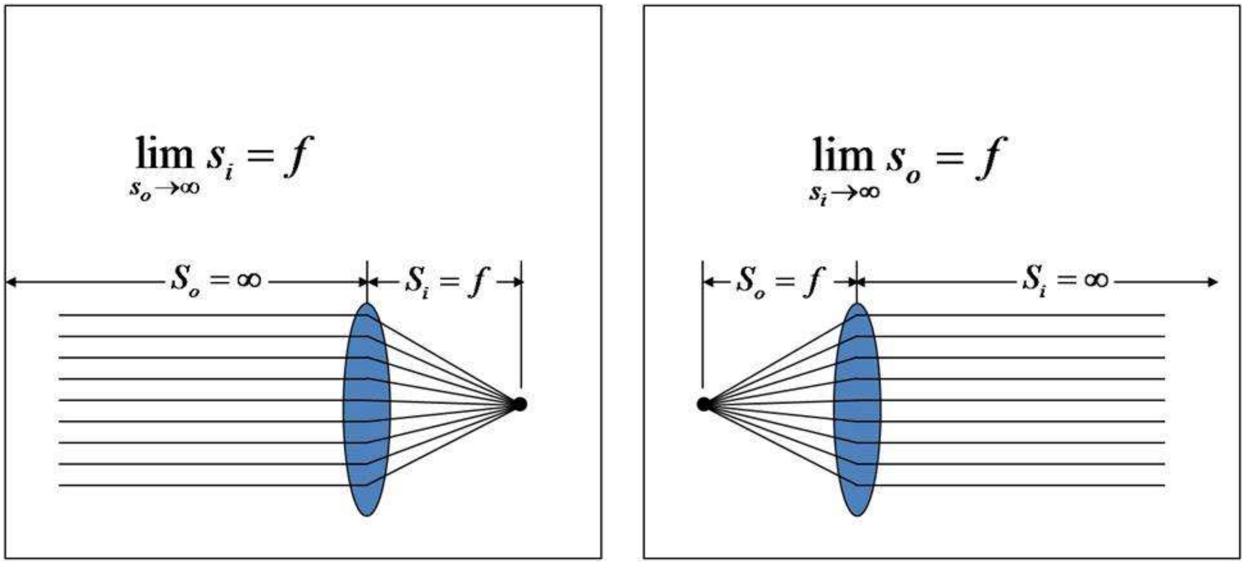

Figure 2.18: Thin lens optics for light collimation

As can be seen in Figure 2.17, the actual optics in the CTHIS are rather more complicated.

The primary and secondary lenses are not, in fact, thin lenses. Instead they are achromatic doublets. Because the index of refraction of any given material is based on the wavelength of light passing through it, light of different wavelengths will be refracted by different amounts in the same material. Thus the focal length of a lens changes slightly with the wavelength of the light passing through it. As shown by the Lens Maker's Equation below (2.2) the focal length of a lens depends on the difference in index of refraction between two media where light is passing from one to the other. As index of refraction is dependent on wavelength, light of differing wavelengths will be refracted by different amounts passing through the same lens; therefore the focal plane will also be different for different wavelengths.

$$\frac{1}{s_{o1}} + \frac{1}{s_{i2}} = (\frac{1}{R_1} - \frac{1}{R_2})(\frac{n_2}{n_1} - 1) = \frac{1}{f} \tag{2.2}$$

Figure 2.19 demonstrates this phenomena graphically. As shown, when white light passes through the lens, the focal length for the blue wavelength (F_B) is shorter than that for the red (F_R).

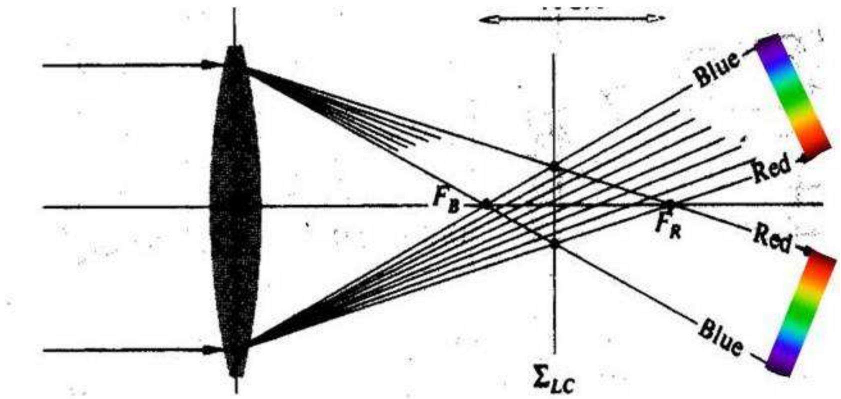

Figure 2.19: Chromatic Aberration [28]

As a result, optical systems using lenses often use an achromatic doublet lens design. Here material of two different indices of refraction are mated together in order to produce a coincident focal point for both red and blue wavelengths. Obviously this is still not a perfect solution since wavelengths of light between red and blue will still not have the same focal point. The yellow focal point in Figure 2.20 below illustrates this problem. The lens in the figure is a compound mating of two materials, labeled H_1 and H_2. In fact more than two materials can be used to further reduce chromatic aberration, however it can never be completely eliminated and the bonding surfaces between materials introduce their own aberrations as well.

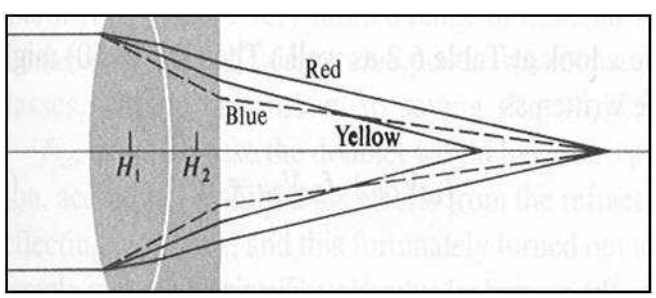

Figure 2.20: Achromatic Doublet [28]

From the second lens, the collimated light passes into and through the direct vision prism as in the schematic in Figure 2.15. A direct vision prism, like an achromatic doublet, is made from two different materials with different indices of refraction. In this case though, the desired effect is to have one wavelength pass directly through the prism with no deviation from the optical axis. All other wavelengths will be refracted according to their wavelength by the angle of refraction of the prism. Prism characteristics can be customized to provide a greater or lesser angular deviation. The angular deviation - δ, as shown is Figure 2.21, is wavelength dependent. The unique property of the direct vision prism is that for one specific wavelength the angular deviation is zero. This is the key operating principle that enables chromotomographic reconstruction.

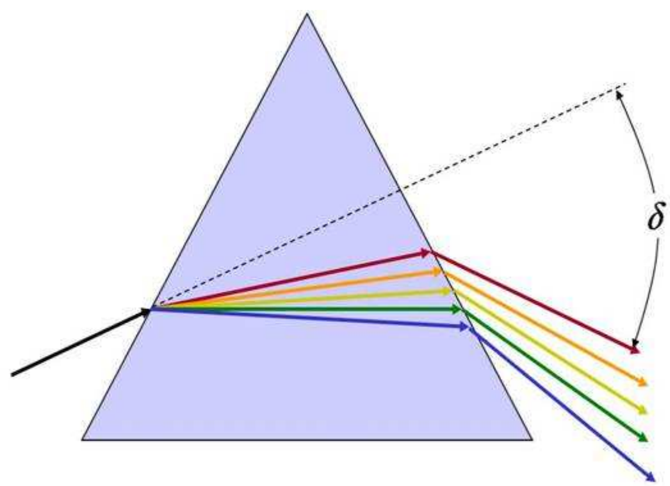

Figure 2.21: Dispersing prism

In the laboratory CTHIS instrument the direct vision prism is a custom-made piece from Schott Optisches Glas of Germany. Prism characteristics are available in Appendix B.

From the direct vision prism the dispersed light is passed through a focusing lens which directs the image onto the focal plane array of the instrument. In the laboratory instrument the focusing lens and FPA are contained in a single fast-framing video camera, seen in Figure 2.22 to the left of the prism instrument. The image is

transferred as digital data from the camera to a desk top computer where it can be demultiplexed and manipulated according with Fourier transform algorithms as discussed by Dearinger, Gould and Bostick [16, 19, 23]

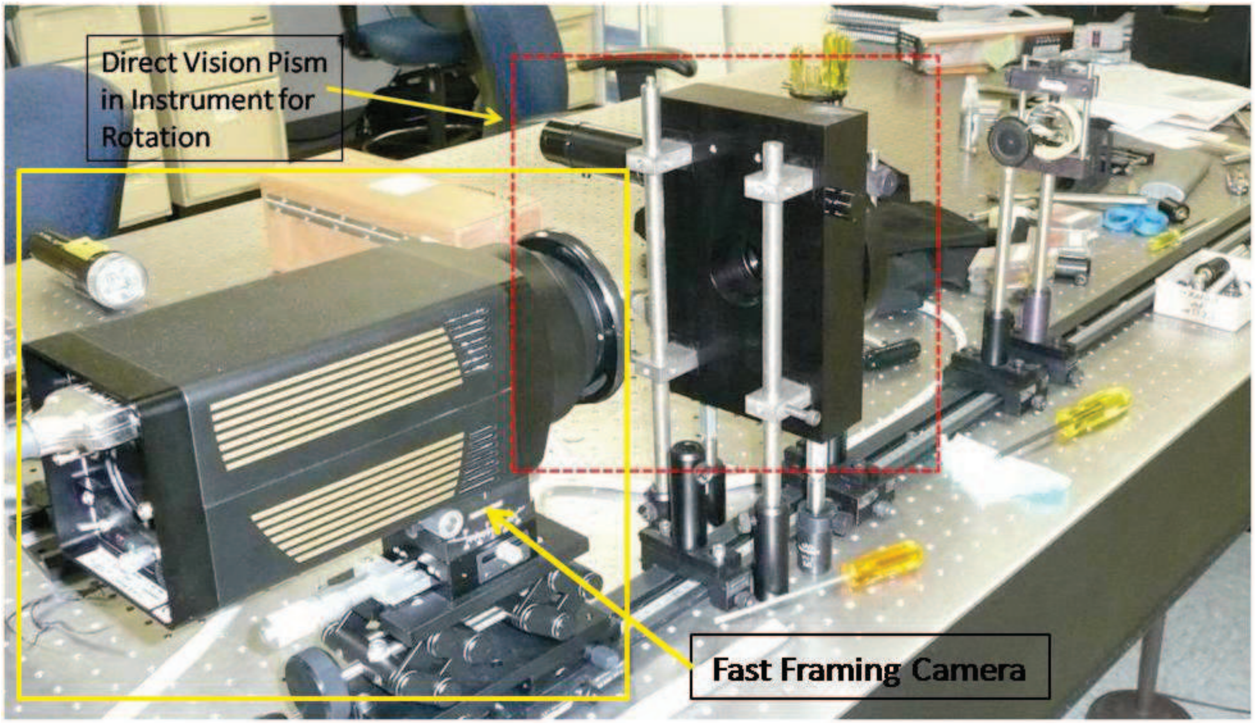

Figure 2.22: Direct vision prism in rotator

This prototype laboratory device then forms the basis upon which the CTEx instrument will be designed. The first order engineering analysis is presented in Chapter III.

III. CTEx Design and Trade Space

The objective of this chapter is to take the principles for chromotomographic imaging as described for the CTHIS laboratory model in the last chapter and translate them into a proposed design for the space-based experiment, the CTEx. The requirements for the CTEx instrument are rather straightforward and would seem to allow for a great deal of design choice. Fundamentally, there a several requirements that will tend to override most other considerations. These are discussed in the next section.

3.1 Requirements and Assumptions

The CTEx is required to demonstrate multispectral chromotomographic imaging from orbit using a rotating prism as the dispersive element. It will operate in orbit, taking imagery of selected ground-based targets to determine if the instrument can gather useful hyperspectral data. It should also demonstrate unique capabilities, or the potential for those capabilities, which will distinguish it from other hyperspectral imagers already in operation. There are three goals defining success for CTEx:

1. Obtain hyperspectral imagery of a static scene.
2. Obtain hyperspectral imagery of a large-scale event that changes spectrally and spatially in time, but at a relatively moderate rate.
3. Collect hyperspectral data on a very rapidly changing target.

Examples of each of these are:

a) A single hyperspectral image of a basically static scene such as a farm field.

b) Hyperspectral data that changes moderately over time on the scale of seconds, such as with a forest fire.

c) Hyperspectral data that changes rapidly over time using a small scale event such as an explosion.

Of these three goals the one that chiefly distinguishes CTEx from all predecessors is the third, the ability to obtain hyperspectral data with a temporal dimension of very

rapid, transient events. This will be the main area of focus for all following discussion of CTEx design requirements and trade-space analysis.

While accomplishing these goals one of the major driving design parameters is that CTEx must be a very simple design. In practical terms this means that the instrument needs to be able to be assembled to a large degree in a university lab by students, professors and lab technicians. Also, related to these requirements is that of cost. Although it will not be possible to cite precise cost figure at this initial stage of design, most components for the instrument should be either commercial off-the-shelf (COTS) pieces, or already available through other U.S. governmental entities such as the Air Force Research Laboratories. A nominal figure for design and construction of the instrument (though not of launch) is less than $1,000,000.

Further, because this is already an experimental instrument, it is highly desirable that those instrument functions that are outside of the direct experimental aspect (i.e. front-end optics or slewing mechanism) be proven, low technical risk items. This strategy should help keep costs down and overall reliability high. It will also help ensure that the basic experiment is the focus of experimental operations rather than other aspects of instrument operation.

Defining requirements for spatial and spectral resolution are somewhat subjective. However, 10nm spectral resolution should provide enough fidelity to allow for definitive experimental results demonstrating the utility of this form of hyperspectral imaging. The choice of a spatial resolution goal of 10m, meaning two objects which are 10 meters apart will be discernable as two separate objects, may be somewhat overambitious. Given an instrument aperture of 10cm and an operating altitude of 400km, the diffraction limited ground resolution should be well under 10 meters, as shown in Equation 3.1:

$$\theta = 1.22(\frac{\lambda}{D}) \tag{3.1}$$

where λ is the specific wavelength and D is the aperture diameter. Using 550 nm as a representative wavelength,

$$1.22(\frac{550nm}{10cm}) = 6.71\mu rad \tag{3.2}$$

Multiplying by the altitude provides the diffraction limited ground resolution:

$$400km * 6.71\mu rad \approx 2.7m \tag{3.3}$$

which would appear to be well within the spatial resolution goal of 10m. However, as the actual spatial resolution figures for CRISM in Figure 3.1 shows, spatial resolution is not necessarily a simple function of diffraction, but of the projection of the Instantaneous Field of View (IFOV) onto the focal plane array. There, the pixel size and density as well as the overall focal plane array dimensions define the ground resolution. The smallest piece of the projected ground area that can be resolved is that corresponding to an individual pixel. This is what limits the ground resolution of the CRISM instrument to approximately an order of magnitude greater than would be the case purely with diffraction limits.

Using the CRISM requirements as a general model, preliminary CTEx requirements have been formulated. Overall top-level requirements for CTEx are listed in Table 3.1. Among the assumptions being taken into account for this project are that CTEx will be deployed on the International Space Station (ISS). There are several options for placement available on the ISS. The Japanese Experimental Module-Exposed Facility (JEM-EF) on the ISS is used throughout the remainder of this thesis as the representative deployed site for CTEx. There is no significant impact on CTEx between choice of one ISS experiment berth and another. Deploying CTEx on the ISS itself, of course, imposes bounds on available power, communications links with ground stations, heating or cooling, platform stability, vibration and orbit parameters. It also has the overwhelming advantage of greatly simplifying questions of "care and feeding" of the instrument since external support is provided. Since a specific

Requirement	Required Value	Achieved	Comment/Justification
Primary requirements, driven by the MRO Project			
Spectral Range	400-3600 nm to 4050 goal	383 – 3960 nm	Misalignment of IR order-sorting filter; allows carbonate band to be measured
Spectral Sampling	Better than 10 nm	VNIR = 6.55 nm IR = 6.63 nm	Measured dispersion
Swath Width	> 7.5 km at 300 km	9.4 to 11.9 km	Slit 2.12° wide, MRO Orbit
Spatial Sampling	Resolve 50-m spot	15.7 to 19.7 m/pixel	IFOV = 61.5 μrad, MRO orbit (nominal) 255 km x 320 km
Lifetime	1.8 years; goal 5.4	4 years	Estimate based on heat load, MTTF of 12000 hrs per cryocooler
Selected secondary requirements, internal to CRISM			
IR detector temperature	<120K	~100K attainable	Operational temperature commandable
Spectrometer housing temperature	<198K	<194K	184K to 194K depending on orbit
SNR	> 400 at 2300 nm	450 at 2300 nm	Best estimate from calibration data
System MTF	0.2 at 9.25 cycles/mm	0.73 VNIR; 0.4 IR	Analysis uses as built measurements of PSF, pointing jitter, estimate of orbital smear
Pointing	±60° Along Track	±60° Along Track	Flight subsystem test, dummy mass
Scan Jitter	48 μrad (3σ)	25 μrad (3σ)	
Spectral Full Width Half-Max	Better than 20 nm; goal <9 nm	8.5 –11.8 nm VNIR 9.3 –15.2 nm IR	Diffraction, FOV effects; acceptable
Spectral Smile (VNIR)	<1.2 pixels	1.3 pixels	Stepped monochromator point source
Keystone (VNIR)	< ± 0.4 pixels	<± 0.42 pxls	Measured point source dispersion
Smile (IR)	<1.2 pixels	1.3 pixels	Stepped monochromator point source
Keystone (IR)	< ± 0.4 pixels	< ± 0.42 pxls	Measured point source dispersion
Spectral Profile, VNIR	<2%, 3 pixels from peak	1.1%	Measured response to monochromator
Spectral Profile, IR		2%	
Out of Field Stray Light	< 2%	< 1%	Quartz halogen lamp out of field

Figure 3.1: Requirements for the CRISM Hyperspectral Instrument [35]

launch vehicle for the instrument cannot be projected at this time, generic standards of survivability for launch will be applied. Service life for CTEx is set at one year from placement on the ISS. The operating demands are not well defined at this point beyond successfully taking data in the three regimes discussed at the beginning of this section.

3.2 Front-end Optics

The front-end optics for this instrument amounts to some sort of telescope and collimator which will provide the required collimated light sample to the prism mechanism. There are essentially two choices here. Either use the design of the CTHIS laboratory instrument with two converging lenses at the front end, or some form of mirrored, reflecting telescope.

Table 3.1: CTEx Driving Requirements

Requirement	Requirement Value	Comment/Justification
Spectral Range	400 - 900 nm	VNIR coverage allows single FPA
Spectral Sampling	Better than 5 nm/channel	Provides for useful discrimination between chemical salts
Ground Sample Distance	<10 m	Diffraction limited resolution = 1.9 m @ 400 km, 10 cm aperature
# Spectral Bands	100	Derived from spectral resolution
Data Cube production	10 Hz	10Hz prism rotation and 1000 frames per second
Scan Jitter	5μrad (3σ)	Testing needed
Lifetime	$\geq$ 1yr	On-orbit
Data Volume	1Tb	Nominal on-instrument data storage
Collection time/event	$\geq$ 10sec	One ground target
Max Mass	$\leq$550 kg	JEM-EF Standard site
Max Volume	1.5 m^3	JEM-EF Standard site
Power	$\leq$ 3kW	JEM-EF Standard site

3.2.1 Reflection vs Refraction. There are many advantages to using a reflecting versus a refracting telescope. As discussed in Chapter II, refracting lenses, even achromatics, will introduce chromatic aberration into the resulting image. Although this may be small enough (and the degree of chromatic dispersion is a function of lens index of refraction and focal length), experience shows that in this application chromatic aberration is a real concern. Bostick, in his research on the function of the CTHIS instrument, has noted that chromatic aberration is a problem in obtaining high fidelity results [16]. Mirrored surfaces do not introduce any chromatic aberrations since the angle of reflection is not dependent on wavelength and is therefore the same for all λ (Equation 3.4) as shown in Figure 3.2.

Law of Reflection

$$\theta_i = \theta_r \tag{3.4}$$

Angle of incidence = Angle of Reflection

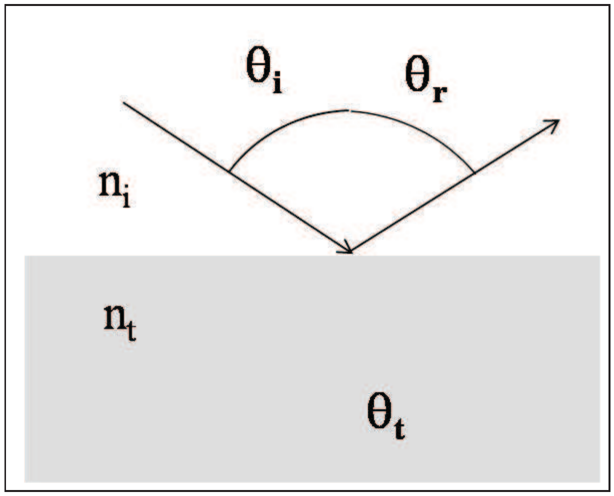

Figure 3.2: Incident angle equals reflected angle for all wavelengths [28]

Another advantage of using reflection is that the mirrored surface provides a more stable structure than lenses. Since the light does not pass through a mirror, a fully supporting structure on the mirror's backside can be designed that provides much greater stability. A lens must allow light to pass through with as little structural impediment as possible. So a lens is normally only supported and attached to the telescope structure along the lens' outer edge. An important aspect of the space-based instrument, and for any space-based optic, is that alignment along the optical axis must be maintained as closely as possible since it is either impossible, or very difficult and expensive, to align the optical elements (collimate them) once the instrument is in orbit. The greatest stresses that will be applied to the instrument are at launch. The better supported the optical elements are, the better chances of surviving launch within collimation tolerances.

A third possible reason for selecting a reflecting telescope over refracting lenses for our application is that the mirror(s) and the structural elements can be constructed

of the same or very similar materials. In this case the use of polished aluminum for the mirrors and the tube structure allows maintenance of a low or zero differential for coefficients of thermal expansion for the various telescope parts. In the space regime where the instrument may experience a range of temperature from -40 to +80 C or even greater, any significant differences in materials' thermal expansion properties may result in asymmetric expansion or contraction resulting in internal stresses that can distort the optical system. This has clearly been identified as a significant issue in currently employed space-based instruments as exemplified in the CRISM hyperspectral instrument orbiting Mars. Though noted in Chapter II, it bears repeating that in CRISM the opto-mechanical subsystem was tested for consistency over six thermal cycles between 30C and -90C with a dwell time of one hour at each extreme per cycle. There was no measurable change in instrument interferograms taken before and after the cycling. This was attributed to the use of an all aluminum structure and all aluminum mirrors [42,43]. In a design using lenses, the lenses must be made with an optical material like crown glass while the structure is constructed with something else. Differences in thermal expansion properties between these elements are unavoidable.

Finally, mirrored elements do not increase in weight with size at nearly the rate of refracting lenses. With mirrors, the reflecting surface only needs to be a thin film applied over a base substrate. Even if the material required for the reflection is relatively dense, it can be kept quite thin and still provide the needed optical properties. Lenses must allow light to pass through and quickly begin to distort under their own weight as size grows. Physical sagging then results in optical distortion. This would not likely be a problem for the proposed CTEx instrument, given its expected modest size. However it is still a factor to take into consideration since CTEx is a proof-of-concept that may lead to a similar, larger operational instrument sometime in the future.

Mirrors have been used extensively in space for many years. Reflective optics for space is a mature technology and its use in CTEx provides good advantages at no

increased risk. Although design of the CTEx instrument, as in the current lab models with refracting lenses, could certainly be accomplished, the advantages of changing over to reflection for the telescope front-end outweigh the very minor disadvantage of making this change. In fact, there may be no disadvantage at all since the instrument would have to be resized in any case to take into account the instrument's operating altitude over the ground.

The one advantage refractive lenses might hold over using a reflecting design is that the current laboratory instrument uses refracting lenses and is a straightforward design where all elements are centered along a single optical axis. A specific disadvantage of this design involves problems with achromatic lenses in a space environment. Achromats, as discussed in the previous chapter, partially compensate for chromatic abberation by bonding two or more materials with differing indices of refraction. The inherent problem with this is that the same properties which are used to reduce chromatic aberration in achromatic lenses, that is different materials with different indices of refraction, also means the materials have different coefficients of thermal expansion. Thermal cycling, which is a condition expected to occur with the CTEx instrument as it orbits the Earth on the ISS, will then produce expansion and contraction stress along the bonding plane between the two materials. This results in an unacceptable risk of lens separation, which would mean mission failure. This issue will surface again in the next section on the prism. The overwhelming advantages of reflecting over refracting telescopes for space operations clearly leads to the conclusion that a reflecting telescope in the CTEx design is the better design choice.

3.2.2 Telescope Design. There are many options available for reflecting telescopes. So many in fact that it is beyond the scope of this thesis to provide a detailed analysis of the universe of possibilities. Some general characteristics of any telescope used for CTEx will include a compact design, yet as simple as possible. The light must be brought to a focus at a point where a field stop can be incorporated. Light will also need to be collimated prior to passing through the direct vision prism.

Some preliminary optical design study has been accomplished and a viable and practical choice which incorporates the characteristics above has been made. An off-axis Mersenne telescope design provides the desirable characteristics of using an all-reflective optic to bring light to the rotating prism, to include collimation of that light. It is relatively compact, yet provides a space for the field stop, which is absolutely necessary to limit the bounds of the image. A graphic of the proposed design is provided here in Figure 3.3 for illustration [25].

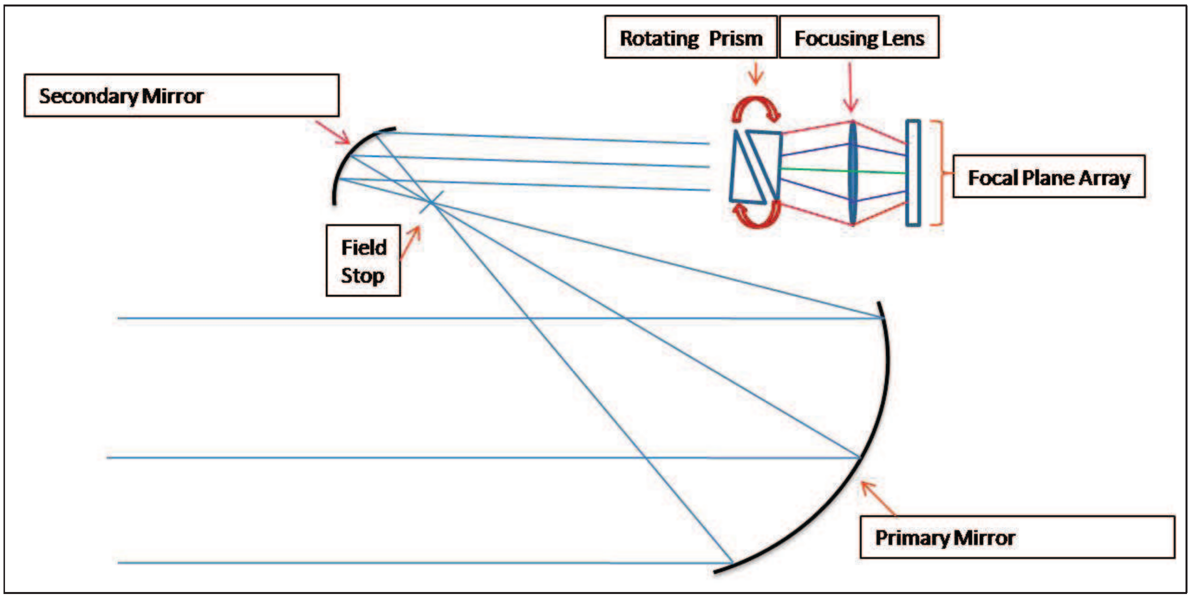

Figure 3.3: Proposed Mersenne Telescope Design.

3.3 Prism

The rotating prism is a key element of the CTEx instrument. It goes to the heart of the operating principles for hyperspectral chromotomography. For the application in CTEx, a nominal rotation rate of 10 Hz for the prism is specified. The prism rotation rate defines the number of hyperspectral cubes produced in a given time frame - 1 cube per full rotation. At 10 Hz the instrument is producing 10 data cubes a second. This means transient changes can be tracked over .1 second increments. The trade-space issues this brings up are considerations of rotating speed versus transient event capture. In other words, while .1 sec time capture increments may be perfectly

satisfactory for some events, such as a rocket engine test, it may not be nearly fast enough for others, like an explosion due to the much quicker rate of change in both the spatial and spectral dimensions for an expanding fireball over an engine plume.

A controllable variable rotation rate would be very useful then. However this would also increase the complexity of the instrument versus a single set speed. A good compromise would be to have a small number of set rotation rates that could be selected depending on the users requirements for a particular collection event. A reasonable base line would be an exponential scale of 0 - 2 corresponding to rotation rates of 1, 10 and 100 Hz. This will provide flexibility to adapt the instrument operation to varying test events while maintaining enough simplicity to keep costs down and reliability high.

The prism itself, as used in the laboratory CT instrument, is quite small - only 38 mm in diameter. The small mass of the prism means that rapid spin up and slow down is possible and should allow for precise rotation rate control. This is very important since the rate of prism rotation along with the camera frame rate will be needed for solving the tomographic Fourier transform used to ultimately extract the desired spectral data. Knowledge of the exact prism position at any time is also important in matching the prism angle with each frame during operation. It will be highly desirable to have some form of feedback either to provide on-orbit calibration capability or simply to have the true rotation rate and position for input into the algorithm as mentioned.

There is another inherent problem however, with the laboratory CT prism. As described in Chapter II, this is a direct vision prism. So, just as with the achromatic lenses, it consists of two different materials bonded together, as shown in Appendix B which provides the optical properties of both parts of the prism. The direct vision prism uses two bonded materials of differing indices of refraction to allow one wavelength of light to pass through the prism undeviated. The undeviated wavelength then passes through the focusing lens onto the focal plane array. The result is illus-

trated in Figure 3.4, where the undeviated green wavelength is in the image center. Other wavelengths of light form a circle around the undeviated wavelength and the angle of dispersion (θ) and distance from center (x,y) provide spectral and spatial information.

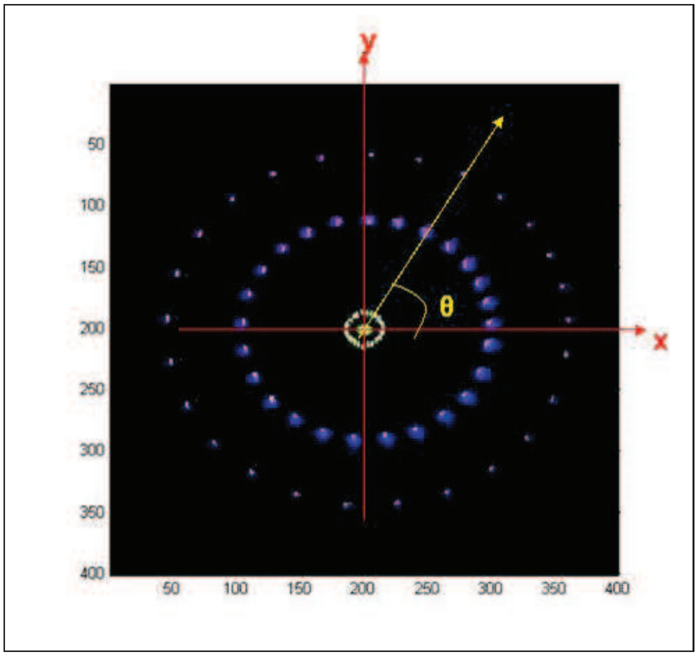

Figure 3.4: Spectral dispersion around undeviated green wavelength [15]

It is apparent then that having an undeviated light wavelength to provide a reference frame is essential to the operation of the instrument. Therefore the direct vision prism is an absolutely essential optical component in the instrument. There is a problem of differing coefficients of thermal expansion between the materials making up the prism, as with achromatic lenses, which may be fatal to CTEx operation if not addressed. The specific problem is that the materials used in the prism expand or contract with changes in their temperature at different rates. The orbit of the ISS around the Earth will take CTEx in and out of sunlight repeatedly every day. Not knowing precisely where the instrument will be positioned on the space station it isn't possible to determine the exact time periods of sunlight/shadow. There is bound to be some measure of thermal cycling in any case. As temperature changes, the prism materials (SFL6 and LaSF 30; properties listed in Appendix B) differences in size

will create stresses on the materials but particularly along the bonding plane between the two. This stress will cycle periodically with the thermal fluctuations related to the orbit. Even if a single application of this stress presents no significant danger of prism failure, the repeated cycling of that stress may result in a high probability of failure. If the prism were to separate along the bonding plane, the functionality of CTEx would be severely degraded.

Equations leading to the total force along the bonding plane in the prism are presented below. Coefficients of thermal expansion and Young's Modulus are taken from the cited references. The dimensions of the CTHIS instrument prism are used for these calculations. Assumptions were made on the temperature differences as follows: It was assumed that baseline temperature of the prism, the temperature at which bonding was applied and stress between materials was zero, was about $25°C$. Extensive NASA reporting on the Hubble Space Telescope indicates that Teflon thermal shielding on direct sunlight exposed surfaces reach temperatures of $130°C$ on-orbit [24, 1]. Using this as a "worst case" figure that temperature was modified and a maximum temperature of $85°C$ was used in the stress calculations. This was done because the prism itself will probably not be exposed to direct sunlight. Cooling below $25°C$ was also not taken into account. A temperature cycle of $60°C$ is used as a compromise figure in these calculations.

Given the coefficients of thermal expansion for the materials making up the direct vision prism, the level of stress that may be applied to the bonded interface can be determined. This is demonstrated mathematically here and graphically in Figure 3.5.

$\alpha_{SF6} = 9E^{-}6$ - Coefficient of Thermal Expansion for SF6 $(°C)^{-1}$ [3]

$\alpha_{LaSF30} = 6.2E^{-}6$ - Coefficient of Thermal Expansion for LaSF30 $(°C)^{-1}$ [46]

$Y_{SF6} = 531$ - Young's Modulus for SF6 $(10^8 N/m^2)$ [3]

$L_i = 38mm$ - Initial prism diameter (length)

$\Delta T = 25°C - 85°C =^{-} 60°C$ - Temperature change assuming initial temp on Earth of $25°C$

$\Delta L = \alpha L_i \Delta T$ - Formula for determining material change in length with temperature

$\Delta L_{SF6} = (9E^{-}6)(38mm)(60) = .02052mm$ - Length change for SF6 material

$\Delta L_{LaSF30} = (6.2E^{-}6)(38mm)(60) = .0014136mm$ - Length change for LaSF30 material

$\Delta L_T = \Delta L_{SF6} - \Delta L_{LaSF30} = .006348mm$ - Difference in length change between SF6 and LaSF30

Tensile Stress

$$Y(\frac{\Delta L_T}{L_i}) = 531E8(N/m^2)(\frac{6.35E^{-}6m}{38E^{-}3m}) = 8.873E6(N/m^2) \tag{3.5}$$

Cross Sectional Area of Prism

$$\approx \pi r^2 = \pi(19E^{-}3m)^2 \approx 1.134E^{-}3m^2$$

Shear Force Along the Bonding Plane

$$1.134E^{-}3m^2 \cdot 8.873E6(N/m^2) = \mathbf{10{,}061N} \tag{3.6}$$

Although there is no empirical data specifying the strength of the bonded layer between the two prism materials it seems clear that at this level of stress it would be prudent to assume there is a significant danger of shear failure at some point during the instrument lifetime. The ISS orbit altitude is between 350 - 400 km. Using the higher altitude to calculate a conservative orbital period:

$P = 2\pi/\sqrt{\frac{\mu}{a^3}}$
where $a \approx r \approx 6350 + 400km$

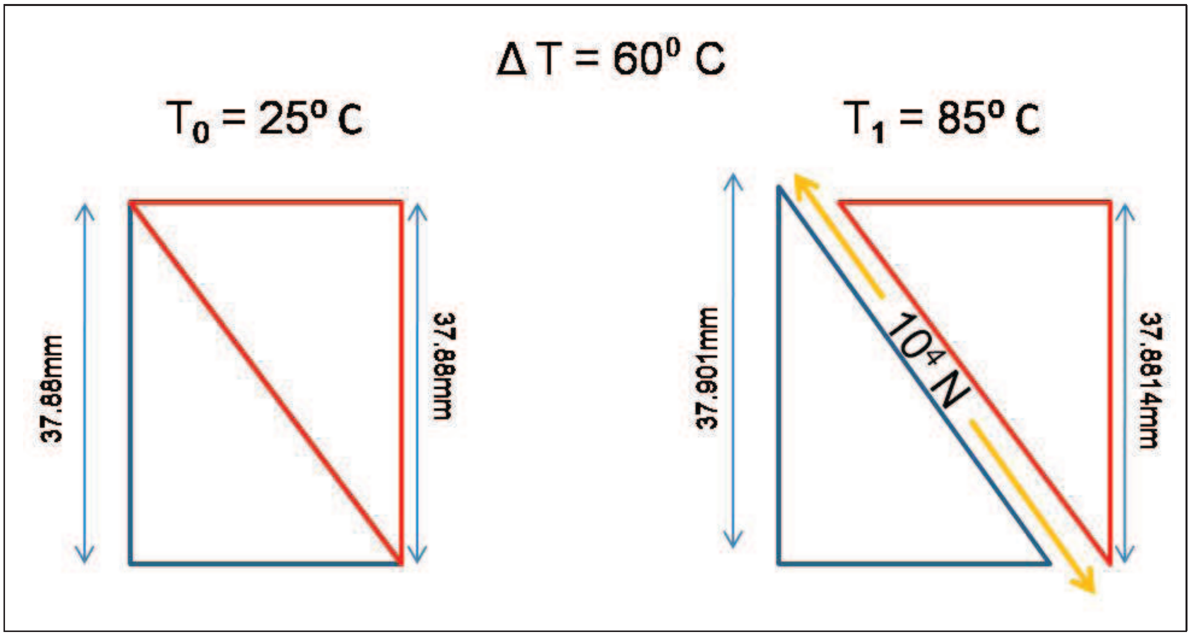

Figure 3.5: Differing coefficients of thermal expansion cause the two materials making up the prism to expand at different rates. This results in large stresses across the bonding plane even for small differences in expansion.

then $P \approx 92mins$ meaning the instrument would orbit the earth approximately 15 times/day. If it's assumed this is the rate of thermal cycling for the instrument there appears to be a need to take measures to ensure that the prism has a high probability of surviving these conditions.

In addition to the stresses of thermal cycling, any imperfections in the bonding surface between the materials may also introduce further stresses due to trapped air pressure in the near vacuum environment of low-earth orbit. Microbubbles within the bonded material interface will add to the thermal stress. The first action that should be taken is to conduct thorough vacuum and thermal cycling of the prism to obtain empirical data on the likelihood of failure. Testing will be specifically addressed in a later section of this chapter.

Making the assumption that the prism, as constructed in the laboratory instrument, would present a significant risk of failure through the mechanism discussed above, options for mitigating that risk must be explored. One option is to control

for instrument temperature through heating/cooling devices. A passive approach using insulation around the entire instrument may significantly limit the range of temperatures across which the prism would cycle, although Groh's study on insulation degradation on Hubble indicates a substantial reduction in effectiveness over time [24]. More active devices such as on-board cryo-coolers or radiative heaters is a further possibility. This option would greatly increase the cost and complexity of the instrument which in itself increases the risk of overall failure.

Addressing the problem with the prism directly, the prism can be designed as a two-piece element with space gap between the elements. This gap would eliminate the possibility of bonding failure completely. The prism design would increase in complexity and therefore probably in cost too, but the final product would not be more complex and reliability would be enhanced. Another essential feature of the prism portion of the CTEx instrument is the rotation of that prism. Since the prism is held in a rotating assembly in any case, using a two-piece element the assembly will serve to rigidly hold each piece, ensuring that alignment is maintained. The difficulty of the gapped materials prism is that the prism halves will need to be installed in the rotation ring extremely precisely. Not only will each piece have to be positioned accurately such that the vertical plane of the prisms are aligned to that of the rotation stage, the prisms must be accurately aligned with one another.

The spin rate requirement for the rotation mechanism was addressed above. One other aspect of this rotation is the precision requirement. Examples of high-accuracy rotation stages with direct reading encoder and better than 0.00001° resolution are available from Newport Corporation. Unfortunately, while these rotation stages offer outstanding precision, they are not designed for continuous rotation nor for the angular velocities required for the CTEx instrument. Maximum rotation rates are 720°/sec, 2 Hz, which is nowhere near the rates of 10 - 100 Hz required. Specifications for a high precision Rotation Table manufactured by Newport are available in Appendix F. Computer Optical Products does produce a rotation stage and optical encoder (position readout) that appears to meet requirements. Their CM-5000 series

is a high performance brushless DC motor with integral optical encoder. It offers a maximum rotation speed of 1500 rpm, well above our maximum requirement of 1000 rpm. Specification for this product are available in Appendix G. However, as with many of the COTS components the CM-5000 is not space-rated. This issue will be discussed further in the concluding chapter of the thesis.

3.4 Focal Plane Array and Camera

The focal plane array (FPA) lies at the heart of any electro-optical imaging instrument. All imagers require some form of optic to bring the light that has passed through the front-end instrumentation into focus on a two-dimensional array of photosensitive elements (pixels). There are two major classes of FPAs in use today. These are charge-coupled devices (CCDs) and complementary metal oxide semiconductors (CMOS).

CCDs fundamentally work like a bucket brigade. Rain falls on an array of buckets in a given time frame. By passing the bucket contents horizontally until it reaches the end of each line, and then vertically down the array, the overall content is then measured. Figure 3.6. In a similar fashion, photosensitive pixels making up a CCD array are bombarded with photons, which they convert to a charge as depicted in Figure 3.7.

CCD focal plane arrays offer many good characteristics for imaging. Among these are: good spatial resolution; very high quantum efficiency (often 90% or better); a large spectral window; low noise; high dynamic range (ability to handle large variations in signal strength); high photometric precision; and very good linearity [13, 14, 20]. CCDs were developed in the 1960s and have been used extensively for over three decades. This maturity is also an attractive factor for limiting technical risk.

CMOS imaging arrays are a more recent development. However, technological improvements in this array type have been proceeding at a very rapid pace over the last

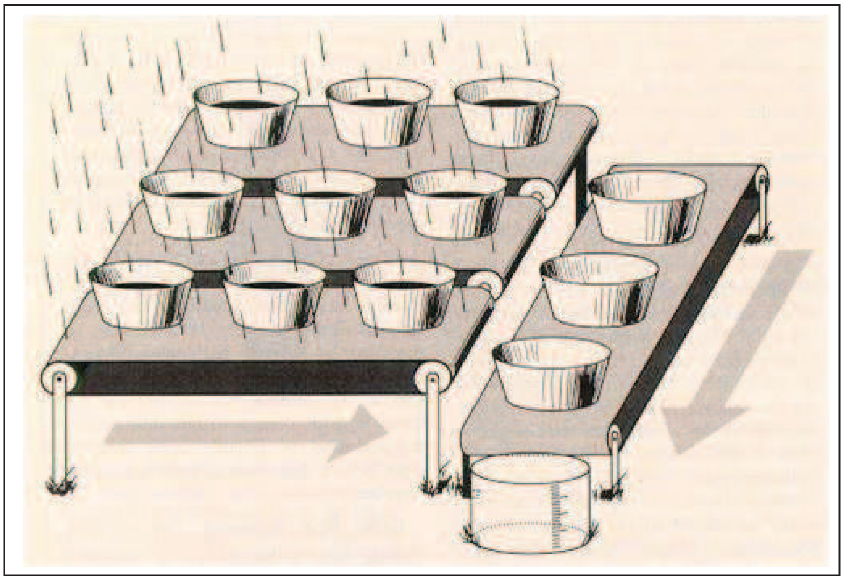

Figure 3.6: As rain fills the buckets the water is passed horizontally, then vertically at the end of each line. [20]

five or six years. Issues that were once serious disadvantages, such as low quantum efficiency, have largely been addressed and the capability contrast between CMOS and CCD arrays has been substantially reduced. An example is the comparison in quantum efficiency between commercially available CCDs and CMOS arrays. The CMOS silicon array with visible antireflectance coating is quite competitive with the backside illuminated CCD (Figure 3.8).

The major difference in operation between a CMOS array and a CCD is that in a CMOS array the photoelectric elements are connected directly with a Read Out Integrated Circuit (ROIC). What this means is that each pixel in the array is read independently of the others, directly into output. There are two major types of CMOS arrays, monolithic and hybrid. Monolithic arrays have the integrated circuit on the same chip as the pixel array. The hybrid design uses a 3-D scheme where the pixels are bonded to the integrated circuit in a sandwich arrangement (Figure 3.9).

As can be seen in Figure 3.10 the differences between CCD and CMOS arrays are founded at the most fundamental level. The pixel readout technique defines the

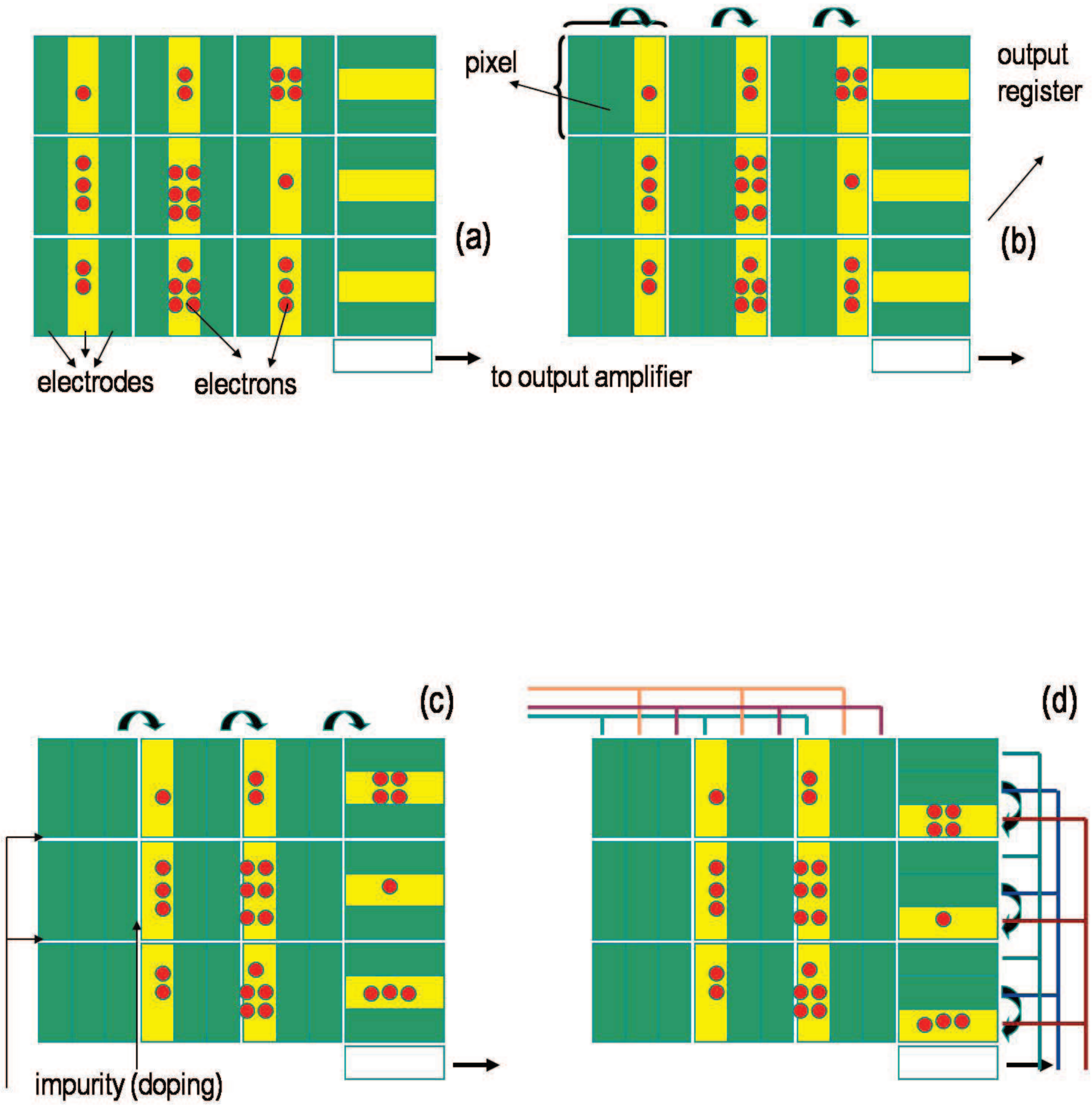

Figure 3.7: (a) For the charge collection process during an exposure the central electrode of each pixel is maintained at a higher potential (yellow) than the others (green). (b) At the end of the exposure, the electrodes potentials are changed and the charges transferred from one electrode to the other. (c) By changing the potential of the electrodes in a synchronized way, electrons are transferred from pixel to pixel. Charges on the right are guided to the output register. (d) The horizontal transfer of charges is then stopped and each charge package at the output register is transferred vertically to an output amplifier and then read one by one. The cycle starts again until all the charges have been read. The reading time amounts to about one minute for a large CCD. [20, 5-6]

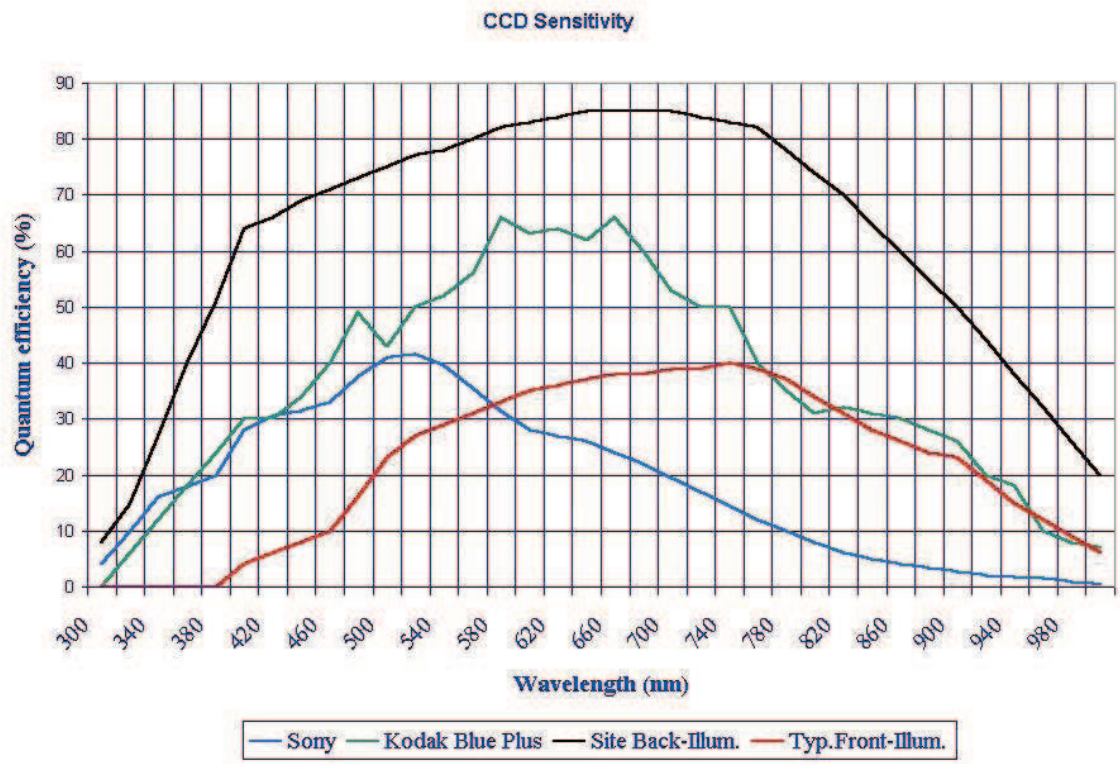

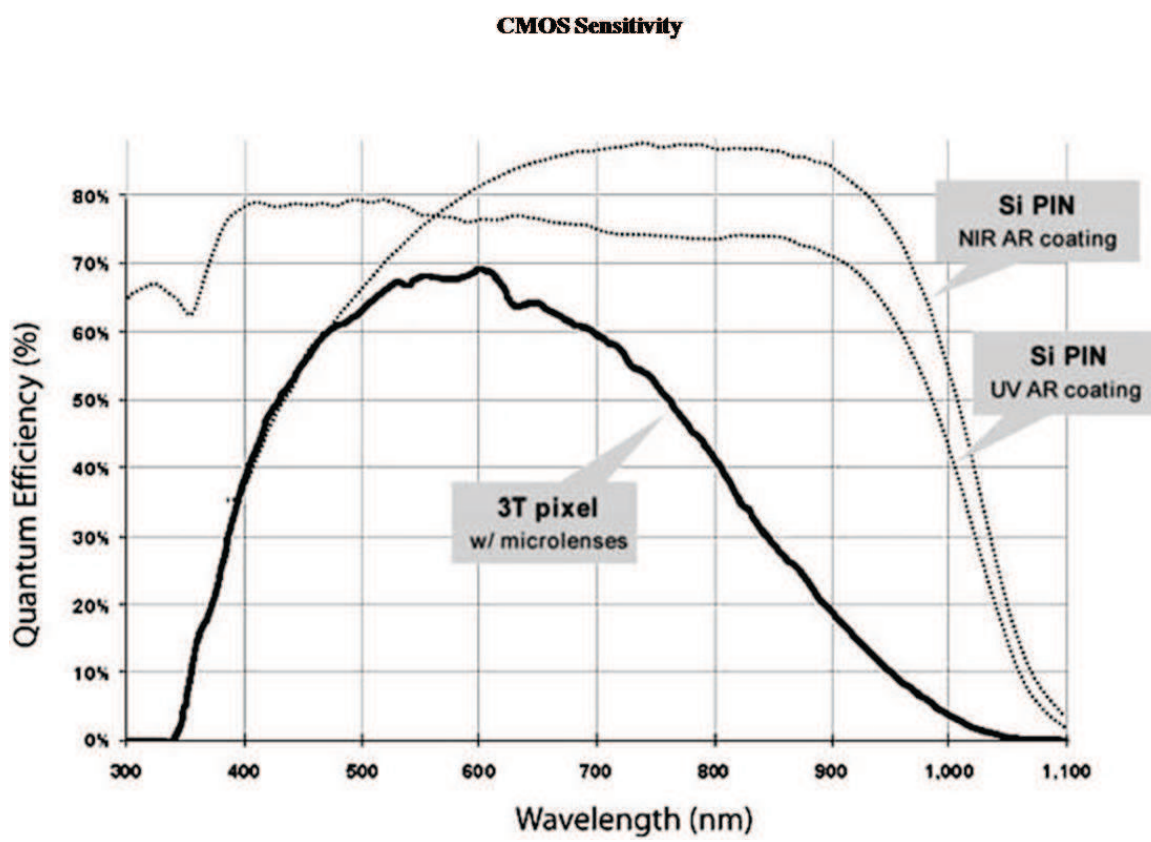

Figure 3.8: CCD vs CMOS quantum efficiency [9, 27].

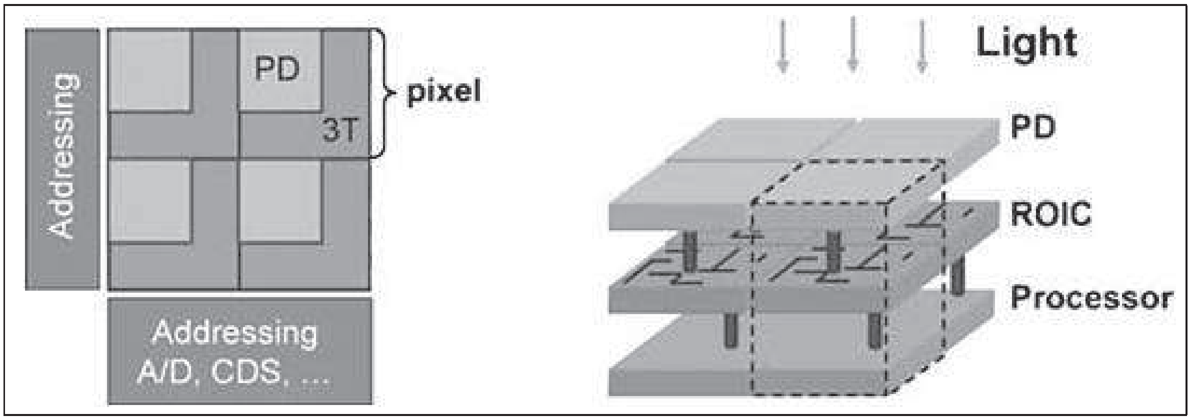

Figure 3.9: Monolithic CMOS chip (left) and hybrid (right). [27, 130]

operating principles of these two array types and characterizes the advantages and disadvantages of each relative to a given application.

For designing the CTEx FPA, there are some significant advantages of the CMOS array over the CCD. Because the photodiode and integrated circuit are on the same chip, various processes such as amplification, timing and analog-to-digital conversion (ADC) can be accomplished right on the chip (Figure 3.11). On-chip integration results in low power requirements, smaller system dimensions and higher speeds. In addition, because of the individual pixel readout capabilities of the CMOS architecture, it is easy to implement various scanning strategies to isolate or enhance particular aspects of the scene under consideration. Examples of these include windowing, subsampling, random access and pixel binning (Figure 3.12). Windowing in particular will provide options for data collection that will be discussed further later in this chapter.

One of the major difficulties in developing an operational CT instrument is the demand for high data throughput. The nominal requirement is for 1000 frames per second (fps). This speed far exceeds that of any hyperspectral imager ever launched. This alone virtually requires the use of a CMOS-based FPA due to the reset speeds involved. In addition, the low power requirement, resistance to radiation, including Single Event Upset (SEUs), and compact size strongly recommend a CMOS versus

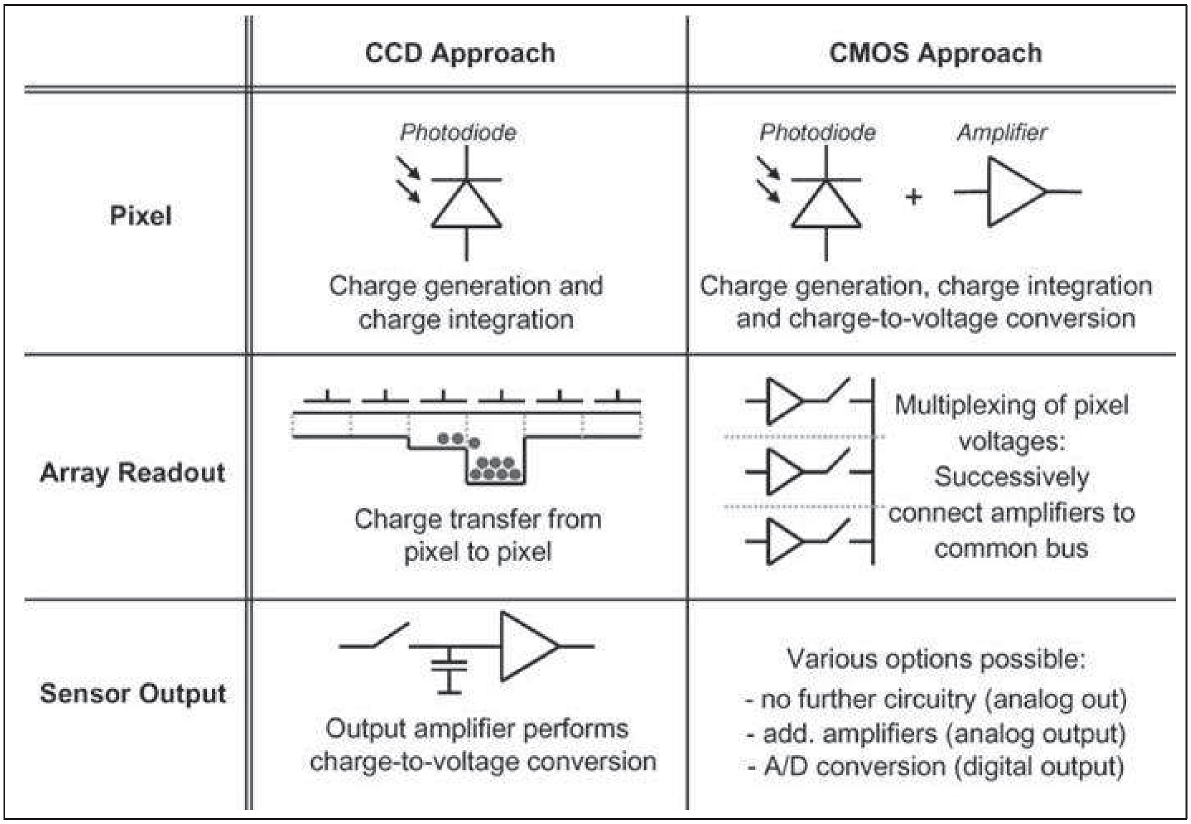

Figure 3.10: Comparison between CCD and CMOS at the pixel level. [27, 112]

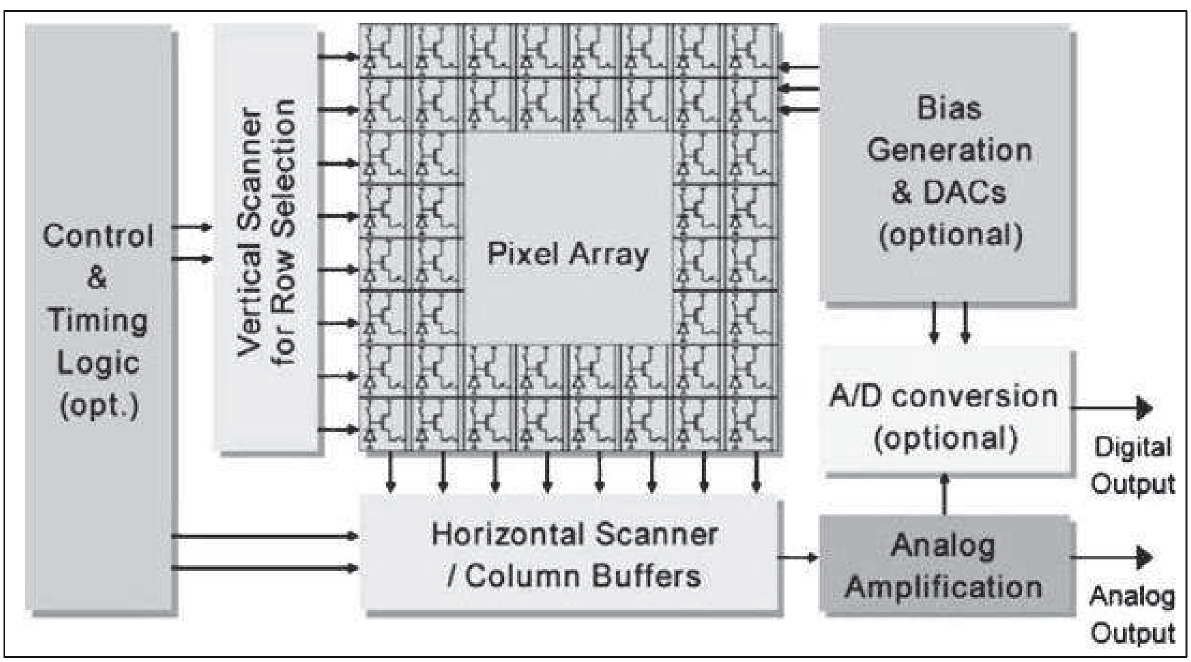

Figure 3.11: Generic Monolithic CMOS chip. [27, 113]

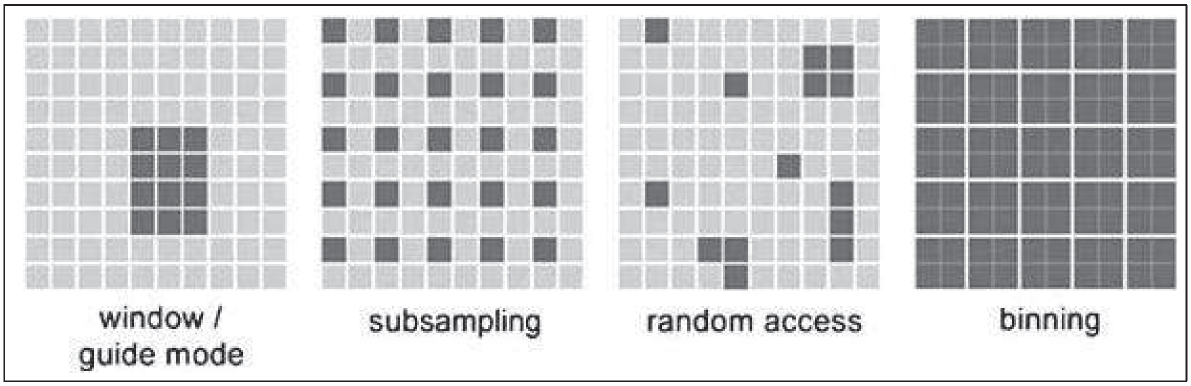

Figure 3.12: In window mode a particular scene feature can be isolated and tracked as it passes under an overhead imager. Subsampling allows a scene to be roughly imaged using only a percentage of the total array. Random access allows multiple, particular features to be imaged while background is ignored. Pixel binning convolves groups of pixels which may be used to improve signal-to-noise for poorly illuminated scenes. [27, 114-115]

CCD FPA for CTEx. One final determining factor is the commercial availability of appropriate, high-speed cameras. While there are two major companies that produce very high-speed, CMOS-based cameras no CCD-based equipment can produce anywhere near the required FPA reset rate.

For the best spectral and spatial resolution it is desirable to have as large a physical array as possible with the smallest pixel size. However, it is also the case that larger pixels are more sensitive to light since they provide a larger surface area for photon detection (larger total photon flux). For CTEx the image on the focal plane should be oversampled, that is the image size is smaller than the array dimensions. Although at first glance this appears to be wastefully inefficient, it is necessary for several reasons. The first is that perfect sampling, where the image size exactly matches the FPA, at the zero prism angle will mean lost data (undersampling) on the edges as the prism and thus the image rotates. Secondly, if electronic windowing is used to collect event data as illustrated in Figure 3.12, large numbers of pixels within the array is essential. A hypothetic may better illustrate this idea.

Assume the total IFOV is 50 km^2. CTEx is taking data on a rocket engine test in a known location at a know time. In order to capture the imagery data from

the engine plume, the actual target of interest is the 10 m^2 area encompassing the engine test. As the instrument passes directly over the target area, the 10 m^2 area of interest enters the far left side of the IFOV. The IFOV will be translating to the left at the ground speed of the instrument. As the instrument passes over, the target area of interest will enter the IFOV, essentially "move" through it, and then exit at the far right. Through windowing and precise knowledge of the instrument and target locations and the instrument orbit the target engine test can be tracked across the FPA (Figure 3.13).

Using representative numbers it is possible to analyze the practicality of using the windowing method for data collection. Starting with the ground sample distance (GSD) of 10 m, which is driven by the instrument ground resolution requirement, the total IFOV can be determined. By definition of the GSD, each pixel will correspond to 10 m on the ground. The minimum number of pixels required for determining a two-color source spectral separation is two pixels. So for purposes of hypothetical demonstration, assume a 2X2 pixel block for the window of interest. The total block size doesn't matter for the following calculation though, as long there are enough "windows" across the array to amount to a useable data collection event.

$$\frac{10m}{pixel} \times \frac{2048pixels}{array} = 20.5km$$

The velocity of the ISS at an altitude of 357 km is determined by:

$$v = \sqrt{\frac{\mu}{r}}$$

where

$\mu = Earth\ gravitional\ constant \times Earthmass$

$r = circular\ orbit\ radius$ (although the ISS orbit is not perfectly circular, it is a reasonable approximation since its eccentricity is only .0008)

$$v = \sqrt{\frac{398600km^3/s^2}{6735km}} = 7.69km/sec$$

At that velocity the instrument will move from one end of any particular IFOV to the other in about 2.5 seconds.

$$20.5km \div 7.69km/s = 2.666sec$$

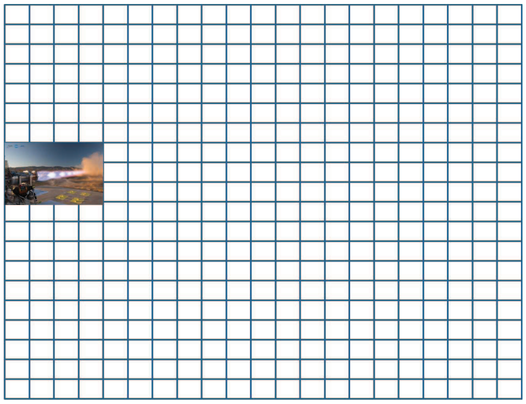

(a) Position1

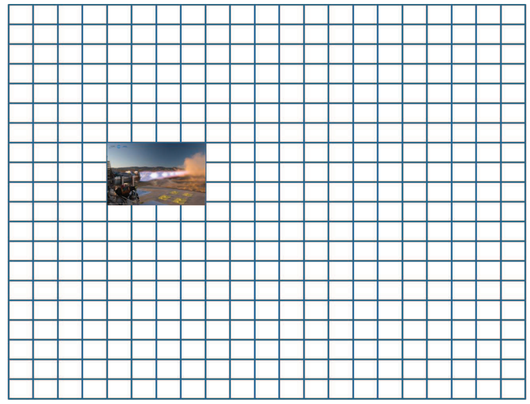

(b) Position2

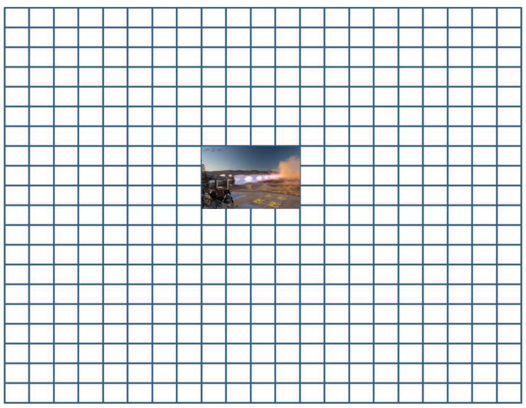

(c) Position3

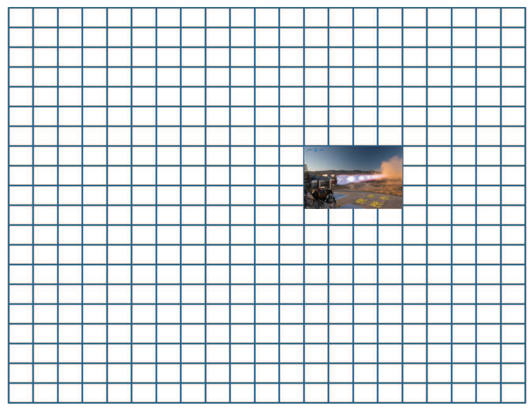

(d) Position4

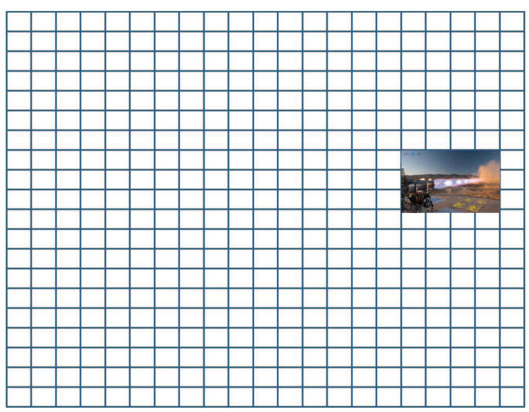

(e) Position5

Figure 3.13: Hypothetical Windowing concept. The image of the rocket test moves across the focal plane as the instrument passes overhead.

The problem with windowing, as illustrated, is the desired data event time of 10 seconds cannot be met. The most direct option is to reduce the data take time to 2.5 seconds. The next option is a trade-off between data take time and spatial resolution. As GSD increases to, for example 20 m, the IFOV grows and there is a doubling of the time the test event will be in view. This trade-off though, is not dynamic. Because the GSD is a function of the focal length of the instrument's focusing lens, once designed into the instrument and launched it cannot be changed.

The discussion above begs the question of other methods for taking event data. The obvious solution is designing a slewing ability into the instrument so staring at a field-of-view as the ISS passes over is possible. For this option either the instrument itself or just the FOV must be able to slew at the angular rate of the ISS passing over a spot on the Earth. Assuming an altitude of 350 km and ignoring the curvature and rotation of the Earth since these will be very small for a five second data pass, the angular slewing speed will be:

$\omega = \frac{\nu}{r}$

where

ν = velocity in direction of motion = 7.69km/sec

r = distance to earth surface = 350km

then

$\omega = \frac{7.69km/sec}{350km} = .0022rad/sec$ or about 1.22 degrees/sec

To slew the entire instrument will require CTEx to be mounted on a slewing table with precision control for rate and position and total along-axis motion of $\pm 6°$ for the capability to collect for roughly 10 seconds at a time. The Navy Research Laboratory's Hyperspectral Imager for the Coastal Ocean (HICO) uses this type of slewing table, but for cross-track collection opportunities, not along track staring [18]. The HICO design with slew table emphasized is shown here in Figure 3.14. It is scheduled to be launched in June, 2009.

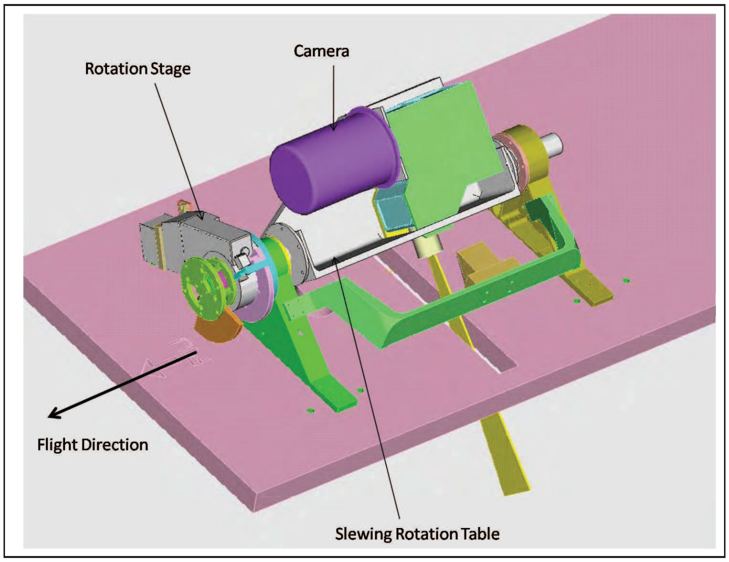

Figure 3.14: HICO instrument design [18]

The more elegant mechanical slewing option is to use a rotating mirror assembly at the optic aperture to accomplish the same along-track scene staring function. This is the design option exercised on the Landsat Thematic Mapper. As shown here in Figure 3.15 in two views, this application is used for cross-track collection. There are serious issues involved with use of a scanning mirror that also must be taken into account. Referring back to the CRISM Mars Orbiter instrument, a single scanning flat mirror was considered for this very application in its design. This option was rejected:

> It was found that the required field of regard ..., coupled with an aperture diameter of 10 cm, and the required FOV of > 1.75°, resulted in scan mirrors with diameters in excess of 60 cm, with little hope of adequate stray light baffling. Size and mass constraints would also not be met. [43, 284]

It is noteworthy that although the optical engineering for CTEx has not been completed at this point, preliminary estimates are that its optical aperture will be in the range of twice the diameter of CRISM. This may mean a scanning mirror solution to the slewing question will result in a prohibitively large mirror.

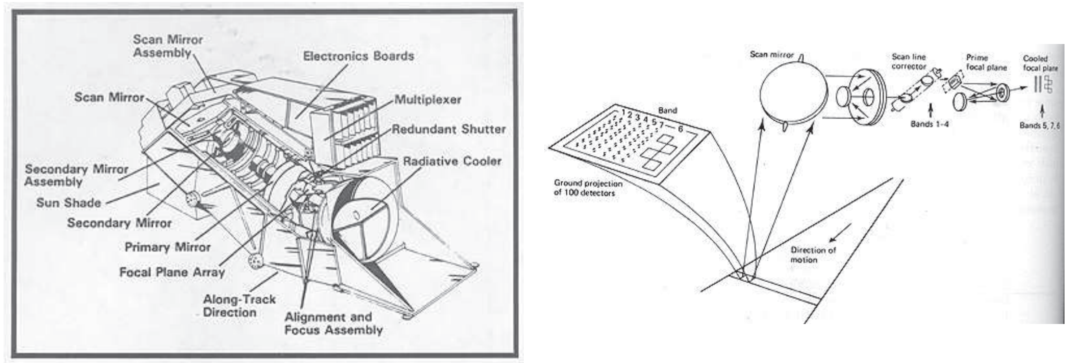

Figure 3.15: Thematic Mapper Scan Mirror Design [41]

Either of the two mechanical slewing options provide CTEx with the capability of meeting the desired collection time per test event of 10 seconds. Against this advantage though, there are considerable disadvantages to be considered. First, both options increase the complexity of the instrument enormously. Mechanical slewing rates must match the angular velocity of the ISS with extremely high precision or smearing of the image will occur. The slewing must take place during data collection. This means vibration and resulting jitter on the focal plane. Both mechanisms, the mirror and the rotation table, require some form of drive motor, leading to more power required, greater mass and greater risk of mechanical failure. Both mechanisms will also increase control, position sensor, and calibration requirements. The mirror option will introduce additional aberration into the optical system and will lower the SNR since no mirror has 100% reflectance efficiency. There are no cost figures available for these options, but it is reasonable to expect adding either to the design will significantly increase the instrument costs monetarily, in design-time, and in build-time.

Overall it would be preferable to rely on the software-driven collection, windowing, over either of the mechanical slewing options. The cost of reduced collection

time per event and/or reduced spatial resolution are outweighed by the numerous disadvantages of slewing listed above.

3.4.1 Cameras. The next issue with the FPA involves the readout speed. As noted, there are several commercially available high speed cameras that easily provide the required number of frames per second (see Appendix 3 for camera specifications). One tradeoff that must be considered here is the signal-to-noise function. At this time the optical engineering for the instrument has not been completed so there are no specific figures. Even when the design is finished, actual hardware testing will be needed to accurately characterize instrument SNR. Nonetheless it is certain that as the fps rate increases the same total signal per unit time is divided into smaller and smaller increments. This means that the SNR will drop as frame rate increases. In fact this may not even be a linear function since electronic shutter produced noise may increase with frame rate as well, resulting in an even greater drop in SNR as a function of frame rate. Factors involved in determining the minimum acceptable SNR include: pixel sensitivity (quantum efficiency), pixel size, minimum acceptable frame rate, total signal produced at the source, total signal transmitted through the atmosphere, and signal loss along the instrument optical path length due to inefficiencies in the optical elements.

Although the requirement for CTEx is set at 1000 fps, since the principle differentiating factor between this instrument and other hyperspectral imagers is speed, it may be that higher frame rates will be a desirable option. Higher frame rate options is actually a no-cost result of the high-speed camera requirement. As is clear from the camera specifications detailed in Appendix C, all of these cameras are capable of frame rates much higher than 1000 fps. The trade-off for going to higher rates, in addition to lower SNR, is poorer resolution. The specifications show that as frame rates are increased, active pixel use goes down. Between the two main choices of camera, the Phantom V12.1 and the Fastcam SA2, both have reduced resolution at higher frame rates. There are some interesting differences between the two which

will require trade-space choices by the end user. The Fastcam model has better pixel pitch, 10μm versus 20μm for the Phantom. This results in the Fastcam having 2048 X 2048 pixels on virtually the same size CMOS versus a maximum of 1280 X 800 for the Phantom. At maximum resolution the Fastcam SA2 can operate at 1080 fps. This is an excellent match for the CTEx requirements. However, as frame rate is increased, the Fastcam resolution drops precipitously, from 2048 X 2048 at 1080 fps to 1024 X 512 at 6250 fps to 384 X 512 at 10800. The Phantom V12.1 offers resolutions of 800 X 1280 at 6242 fps and 512 X 1024 at 11,854. So the Phantom offers better resolution at higher frame rates, but at the required frame rate, 1000 fps, the Fastcam SA2 performs better. If higher rates are considered better for the purposes of the CTEx demonstration, the higher resolution at high frame rates of the Phantom are more advantageous. If this is indeed the case though, then the Fastcam SA5 must be considered. It has the same pixel pitch as the Phantom, but better resolution at higher frame rates: 1024 X 1024 at 7000 fps and 760 X 760 at 12,500 fps.

Other factors that must be considered in the COTS camera choice include ruggedness, and thermal operating regime. All of the cameras are ruggedized to an ability to survive over 30 G in non-operating mode. The Fastcam cameras are rated by their manufacturer at a bit better temperature range than the Phantom, 0 - 40$°C$ versus 10 - 40$°C$. Neither of these meet the requirements for space use at the low end though. So although the Fastcam cameras are marginally better in this arena, it may not matter if any camera chosen will require substantial customization to meet temperature range operating requirements.

Beyond this, there is little to differentiate the choices for high-speed cameras. They all offer remote control that should be adaptable to a hands-off environment, they use silicon-based hybrid CMOS FPAs, solid-state DRAM memory with options up to 32GB, and 12 bit data conversion as a standard. One area that needs to be carefully examined, and may provide a quantifiable measure of merit, is quantum efficiency. Specific test results under strict conditions for specific wavelengths over the instrument spectral range would be invaluable in comparing one camera to another.

This would also help by providing data which could be used to get some idea of the SNR required to acquire usable data.

3.5 Data Handling

The collection of data through hyperspectral imaging is only one step in a process. That data must be stored, downlinked to a ground station and processed for the imagery to have any utility. While CTEx data handling will be similar to other space-borne imagers in some respects, there are aspects to high frame rate chromotomographic imagery that present unique challenges in getting the information to the end users.

3.5.1 Data Generation.

One of the problematic characteristics of the CT scanner is its prodigious rate of data production. Data rate is a function of the camera frame rate, focal plane array size (number of pixels) and digital data encoding. Data rate is calculated by:

Frame rate $\times$ *total number of pixels* $\times$ *pixel encoding per pixel* $\div$ *8bits per byte* $=$ *bytes per second*

If the Photron Fastcam SA2 at full resolution and 1000 fps is used to exemplify, the figures take an alarming turn:

$$1000fps \times 2048^2 pixels \times \frac{12bit}{pixel} \div \frac{1byte}{8bits} = 6.292GB/sec$$

or roughly 63GB for a 10 second data event.

The maximum solid state memory offered for this camera is 32GB. The data production rate calculated above would quickly swamp this amount of memory. Therefore, trade-space analysis of the available options is in order. First, and simplest, the required time of data take can be reduced. The 32GB of available memory would provide a maximum of 5 seconds of operating time. This option has the great advantage of requiring no changes to the instrument at all. The next option is to take data at a reduced resolution. At the same frame rate, 1000 fps, but using 1024X1024

pixels the data rate drops to 1.57GB/sec. Using these parameters the available time delta jumps to over 20 seconds. A third option is to order a custom design adding additional solid state memory to the camera to allow for 10 seconds of data at the full resolution rate. This option is the most costly in terms of design and manufacture time, monetary cost, and added complexity and technical risk.

The first two options offer the tremendous advantage of being implementable on-orbit through software-based control. Frame rate and resolution are both controllable through the camera's standard control selection capability. Therefore, if a particular collection event requires the highest resolution, this can be chosen if the end users are willing to trade-off collection time. Likewise, a test event demanding greater lengths of data collection can be accomplished at the cost of lower resolution. This trade-space then is a dynamic variable that can be adjusted after CTEx is operational to changing customer requirements for different events.

There is no way to move data off the camera fast enough to add storage capacity while it is in operation. Nevertheless, additional on-board storage capacity is desirable in order to: a) provide longer term data storage and redundancy; b) provide the opportunity to clear the camera's intrinsic memory cache so that it is ready to collect again as quickly as possible; and c) serve as a data buffer between the collecting instrument and the downlink communications - that is, the additional storage holds the data and reads it out to communications downlink so the camera memory doesn't have to do that itself. This is an important point since the dedicated downlink channel is only 1Mbps (refer to Appendix H, ISS External Research Capabilities). Assuming an average data collection of only 15GB, it will take over 33 hours to downlink the data from one collection event. Clearly it will be important to be able to hold and downlink data from a secondary storage unit rather than directly from the camera's cache itself. The data hold requirement of 100 - 400 GB can be met fairly easily and given the data assumptions developed here, provide more than adequate storage capacity even in a worst case scenario where data cannot be downloaded for some period of time.

3.5.2 Data Storage. There are a few options to consider with regard to the additional, off-camera, or secondary, data storage. These options resolve to either hard disk drive, flash-based solid state drive, or DRAM (Dynamic Random Access Memory)-based solid state drive. Hard disk drives (HDD) use a magnetic disk and reader which must physically spin and move to operate. Solid state disks (SSD) on the other hand have no moving parts and are inherently more robust for aerospace applications. For reference, open hard disk and solid state drives are pictured in Figure 3.16.

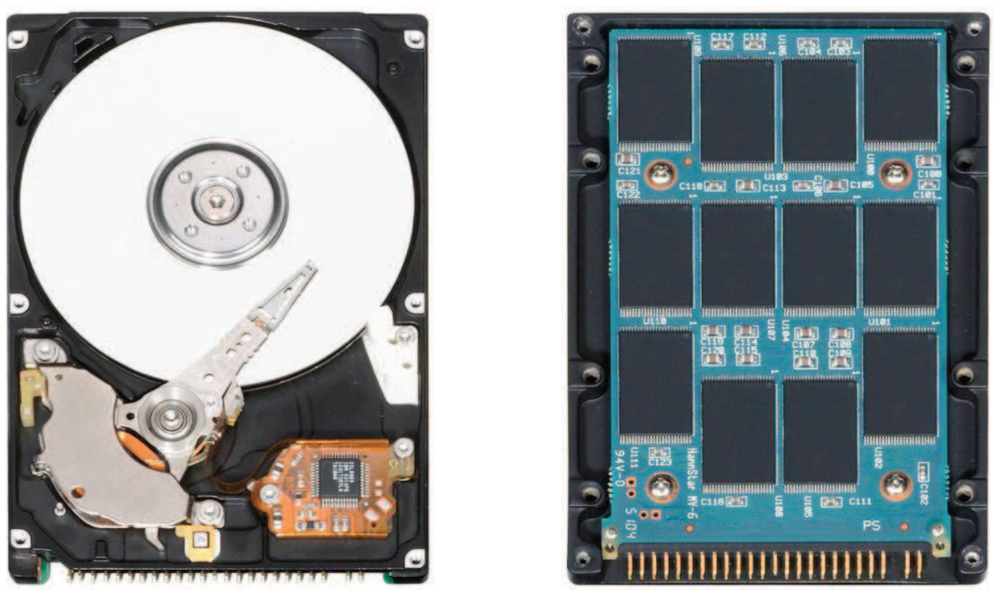

Figure 3.16: Open HDD (left) and SSD (right).

Figure 3.17 provides the results of benchmark average performance capabilities for the three types of data storage devices mentioned. The DRAM-based solid state drive clearly enjoys an immense performance advantage over the other two in all categories of data read and write.

Of these data storage types the SSD offers many advantages, particularly for our application, over traditional HDD.

RANDOM READ BENCHMARK				RANDOM WRITE BENCHMARK			
Block Size	Read IO/s	Read MB/s	Avg Service Time - ms	Block Size	Write IO/s	Write MB/s	Avg Service Time - ms
512B	185	0.09	10.4	512B	290	0.14	6.7
1K	185	0.18	10.5	1K	290	0.29	6.5
2K	182	0.37	10.5	2K	283	0.57	6.9
4K	175	0.70	10.8	4K	280	1.12	6.3
8K	176	1.41	10.9	8K	284	2.27	6.2
16K	172	2.75	11.0	16K	264	4.23	6.3
32K	170	5.44	11.0	32K	237	7.58	6.6
64K	152	9.76	11.0	64K	211	13.51	6,5
128K	132	16.96	11.2	128K	183	23.48	8.0

(a) HDD

RANDOM READ BENCHMARK				RANDOM WRITE BENCHMARK			
Block Size	Read IO/s	Read MB/s	Avg Service Time - ms	Block Size	Write IO/s	Write MB/s	Avg Service Time - ms
512B	1315	0.66	1.4	512B	22	0.01	92.5
1K	1217	1.22	1.5	1K	22	0.02	91.7
2K	1206	2.41	1.5	2K	21	0.04	92.3
4K	1075	4.30	1.7	4K	21	0.09	94.5
8K	906	7.26	2.0	8K	21	0.17	92.5
16K	666	10.66	2.8	16K	21	0.34	93.7
32K	447	14.33	4.2	32K	21	0.68	102.1
64K	322	20.62	5.9	64K	19	1.23	106.7
128K	204	26.16	9.5	128K	18	2.37	113.2

(b) Flash-based SSD

RANDOM READ BENCHMARK				RANDOM WRITE BENCHMARK			
Block Size	Read IO/s	Read MB/s	Avg Service Time - ms	Block Size	Write IO/s	Write MB/s	Avg Service Time - ms
512B	7388	3.69	0.2	512B	7238	3.62	0.2
1K	6794	6.79	0.2	1K	6015	6.01	0.2
2K	5752	11.50	0.2	2K	5353	10.71	0.3
4K	4091	16.36	0.4	4K	4184	16.74	0.4
8K	2959	23.68	0.6	8K	2875	23.00	0.6
16K	1771	28.35	1.0	16K	1773	28.37	1.0
32K	999	31.98	1.8	32K	1004	32.14	1.8
64K	531	34.01	3.5	64K	540	34.57	3.5
128K	277	35.47	6.9	128K	281	36.08	6.8

(c) DRAM-based SSD

Figure 3.17: Memory performance comparison [44]

- Faster start up since there is no spin up time
- Faster random access
- Very fast read times
- Much lower noise and vibration since there are no moving parts
- High mechanical reliability with ability to endure extreme shock, vibration and temperature extremes

Disadvantages are as follows:

- Considerably higher cost per GB of storage, especially with DRAM
- Lower capacity than that offered by HDD
- Limited write cycles for flash-based SSD, although this doesn't apply to DRAM-based
- Slower write speeds for flash-based, but again not for DRAM-based
- Lower storage density
- DRAM-based requires more power and must be supplied with power continuously, even when not operating

For a space-based application it is clear that the reliability and robustness of solid state drive is the option of choice. Furthermore, although cost is an important factor, the additional speed and capability of DRAM-based SSD recommends it over flash-based SSD.

3.5.3 CPU. CTEx will naturally require on-board computing capability for control of the instrument component functions such as prism rotation and camera operation. The computer must be compact, radiation hardened and capable of withstanding the stresses of launch and thermal cycling. In contrast with most of the other instrument components discussed to this point there are commercially available computers which meet all these criteria and have a track record of performance in space.

As a representative sample, BAE Systems of Manassas, Virginia makes several space-rated computers that appear to be well suited for use on CTEx. The full company reported specifications are available in Appendix I. Some of the more significant information on these products is that versions of them are currently in use on the Mars rovers, Spirit and Opportunity, the Mars Reconnaissance Orbiter, and almost 500 other space applications [11]. The small size, low power requirement and high performance of the BAE RAD750 6U single-board computer make this an excellent choice for CTEx. In addition the computer offers 1553 interfaces which make it compatible with the ISS.

Besides the actual on-board strengths of the RAD750, BAE also produces a software package called Virtutech Simics that can simulate the actual computer. This virtual platform allows software to be developed and tested for the on-board computer to ensure proper functioning before operations [11].

3.6 On-orbit Calibration

The capability to calibrate the CTEx instrument remotely in its operating environment is crucial for evaluation of whatever data is taken during the experimental tests. Calibration means taking sample data readings from a well-defined, well known control sample. This allows the development of a baseline against which can be measured the instrument's performance. In this way, any biases or anomalies introduced by the instrument in the produced data can be identified and taken into account when actual test data is analyzed. Calibration from a sample of known size, radiance, position and distance provides surety for the instrument's optical path, prism spin rate, focus on the focal plane array, FPA positioning, number and location of dead pixels in the FPA, data read-out and transfer, and data processing on-instrument or on-ground. It also provides a benchmark against which the instrument controls can be measured, i.e. if a command is uplinked for the prism to spin at 10 Hz, is it actually spinning at that rate and if not, does the issue lie with the rotation stage or the control electronics? A well designed calibration capability is essential to confident

operation of the instrument and confidence in the data returned to the ground. Given that this is an experimental proof-of-concept, calibration is even more crucial to the integrity of the data.

Ground or air-breathing based hyperspectral instruments offer the convenience of hands-on testing. Not so for our space-based application. Since the CTEx instrument will be based on the ISS our calibration control sampling options are going to be limited. With other space-based hyperspectral (or really any imaging) instruments a common method for performing calibration is to rotate the satellite so the imager can take readings off of the sun, specific stars, or less commonly the moon. These methods cannot be used since the space station cannot be turned and the instrument is limited to pointing at the Earth.

There are two general methods that can be considered for calibration specimens. One is to use a particular swath of earth or earth-based targets of will known spectral and illumination signature. Possibilities in this arena include polar regions of flat ice, homogenous desert regions, or placid water regions. This option has the advantage of requiring no additional capabilities for the instrument and thus less cost and complexity. This advantage probably does not outweigh the disadvantages which are that the spectral signature is probably not going to be know to the resolution wanted for instrument calibration. Optimally, the calibration test bed would provide known spectral signature within the bounds of the desired spectral resolution expected in the experiment. This hasn't been completely defined at this time, but a good measure would be no more than two times the FPA's pixel pitch, or approximately 20 μm.

The second method to consider is an on-instrument test bed. This would entail incorporating a light emitting array with elements emitting at well-defined wavelengths over the FPA's designed spectral range onto the instrument. This test array will need to be designed in such a way that when the instrument is being calibrated it is looking only at the test array, with no other noise (stray light) passing through the optical path. Some existing instruments perform this function by using a design

that allows the imposition of a mirror into the normal optical path, changing the source from the normal aperture to the control elements. For the CTEx instrument, a better way to do this might be to incorporate an array of light emitting diodes (LEDs) onto the inner surface (facing into the instrument) of a mechanical aperture shutter. Although this will increase the complexity of the instrument, it also provides the required calibration capability and allows selection of very specific wavelength parameters to test against. The shutter, being closed when calibrating the instrument, eliminates stray light contamination thereby providing a clean sample. Further, since the exact positions of the LEDs relative to the instrument optical axis will be known, this arrangement will also serve to ensure the optical elements in the instrument have maintained correct position (optical collimation is maintained).

LEDs provide the advantages of low power requirements (several miliwatts per LED), small size (3mm or smaller), and the ability to be engineered to specific wavelengths across our spectral band. They also have excellent mean time before failure rates and operate well across a broad temperature range. Figure 3.18 provides a set of performance data for one particular commercial LED series to illustrate these points. Beyond this, a single LED can be engineered to emit in one of several bands at a time if desired.

3.7 Overall Design Space

CTEx design trade-space analysis up to this point has been a component-by-component exercise. In the end, these separate parts will have to work together as a unit and will have to be oriented in a way that allows the instrument to fit into the available space on the ISS JEM-EF platform. Specific component selection has not yet taken place, nor has optical design been completed, much less finalized. That being the case, it is not yet possible to produce an instrument model with any kind of spatial fidelity. Regardless, the analysis performed leads to some conclusions on components that must be included in the instrument. A notional graphic of these components and placement is included in Figure 3.19.

FNL-U300XWCSL Range — 3.0 mm Round High Performance LED Lamp

Features:
- High intensity
- Water clear epoxy
- Range of colours

Available options:
- Flangeless Package

Electro / Optical Characteristics $I_F = 20$ mA $T_a = 25°$ C

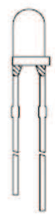

Lamp Package	Part Number	Emitting Colour	Epoxy Type	Die Material	Wavelength		Forward Voltage V_F		Luminous intensity I_V		Viewing ∠ $2\theta½$
					Peak λ_P	Dominant λ_d	typical	max	min	typical	
	FNL-U300R078WCSL	Red	WC	AlGaInP	632	624	2.00	2.40	-	990	35
	FNL-U300R2110WCSL	Red	WC	AlGaInP	632	624	2.10	2.50	-	1280	35
	FNL-U300R2112WCSL	Red	WC	AlGaInP	632	624	2.10	2.50	-	1780	35
	FNL-U300O0813WCSL	Orange	WC	AlGaInP	621	615	2.10	2.40	-	1500	35
	FNL-U300O0310WCSL	Orange	WC	AlGaInP	611	605	2.00	2.40	-	1000	35
	FNL-U300O038WCSL	Orange	WC	AlGaInP	611	605	2.00	2.40	-	720	35
	FNL-U300Y048WCSL	Yellow	WC	AlGaInP	591	589	2.00	2.40	-	980	35
	FNL-U300Y0410WCSL	Yellow	WC	AlGaInP	591	589	2.00	2.40	-	1270	35
	FNL-U300Y1513WCSL	Yellow	WC	AlGaInP	591	589	2.10	2.50	-	2010	35
	FNL-U300G03WCSL	Green	WC	InGaN/SiC	518	525	3.70	4.20	-	950	35
	FNL-U300G16WCSL	Green	WC	InGaN/SiC	518	527	3.85	4.00	-	2130	35
	FNL-U300G282WCSL	Green	WC	InGaN/GaN	-	525 ± 5	3.30	3.50		2970	35
	FNL-U300G06WCSL	Green	WC	InGaN/SiC	502	505	3.70	4.20	-	2130	35
	FNL-U300G11WCSL	Green	WC	InGaN/SiC	502	505	3.80	4.00	-	2130	35
	FNL-U300G273WCSL	Green	WC	InGaN/GaN	-	505 ± 5	3.30	3.50		2700	35
	FNL-U300B07WCSL	Blue	WC	InGaN/SiC	488	490	3.70	4.20	-	790	35
	FNL-U300B03WCSL	Blue	WC	InGaN/SiC	468	470	3.70	4.20	-	380	35
	FNL-U300B12WCSL	Blue	WC	InGaN/SiC	468	470	3.75	4.00	-	740	35
	FNL-U300B17WCSL	Blue	WC	InGaN/SiC	-	470 ±5	3.50	3.80	-	1000	35
	FNL-U300B06WCSL	Blue	WC	InGaN/SiC	458	460	3.70	4.20	-	320	35
	FNL-U300B11WCSL	Blue	WC	InGaN/SiC	458	460	3.75	4.00	-	510	35
	FNL-U300B15WCSL	Blue	WC	InGaN/SiC	-	460 ±5	3.50	3.80	-	640	35
3 mm	Units				nm		V		mcd		deg

FNL-U300XWCSL Range — 3.0 mm Round High Performance LED Lamp

Package Outline

Dimensions in mm
Tol ± 0.25 mm
unless stated

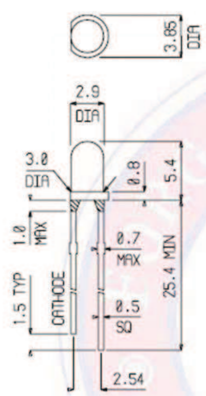

Radiation Diagram

$T_a = 25°C$ $I_F = 20$ mA

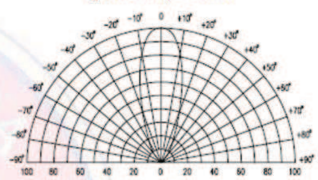

Relative angular intensity

Maximum Ratings $T_a = 25°$ C (Derate above 25° C)

Characteristic	Condition	Die	Symbol	Rating	Units
Pulse Forward Current	0.1 duty cycle @ 1KHz	All types	I_{FP}	100	mA
DC Forward Current		AlGaInP	I_F	50	mA
		InGaN/GaN InGaN/SiC	I_F	30	mA
Reverse Voltage	$I_R = 10\ \mu$A	InGaN/GaN AlGaInP	V_R	10	V
		InGaN/SiC	V_R	5	V
Operating Temperature			T_{opr}	- 20 to + 80	° C
Storage Temperature			T_{stg}	- 20 to + 100	° C
Lead soldering temperature	1.6 mm from body - max. 3 seconds			240	° C

Note:
Industry standard procedures regarding static must be observed when handling product with InGaN die.

WARNING
This range of LEDs is produced with die having a high radiant flux.
Care must be taken when viewing the product at close range as the light may be intense enough to cause damage to the human eye.

Figure 3.18: Forge Europa LED product data sheet.

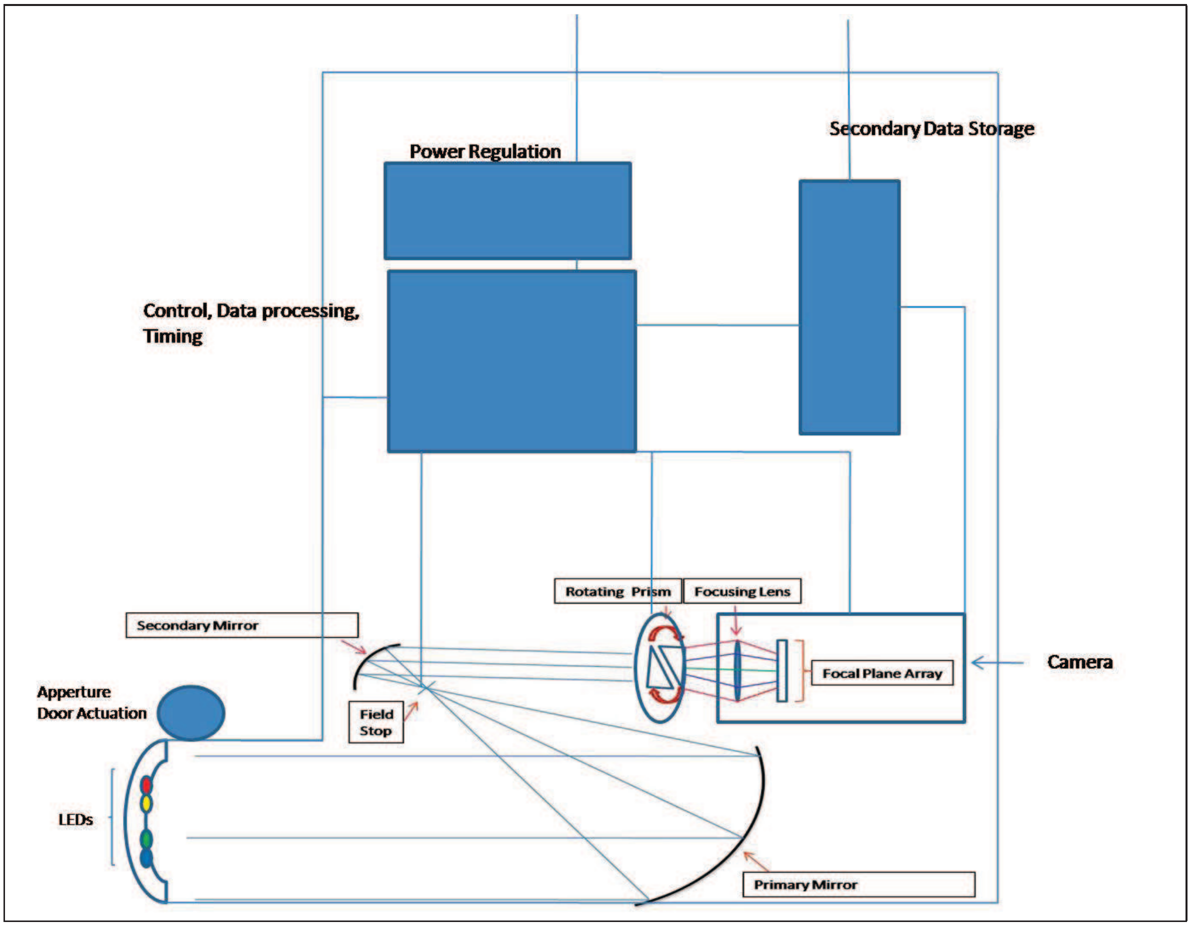

Figure 3.19: Instrument Configuration Space

Referring to the support capabilities on the JEM-EF, or any of the exposed facilities on the ISS (Appendix H), it appears that CTEx will be well within support parameters in power requirements and mass. Size, length in particular, may prove to be a more problematic. This depends a great deal on the final telescope design. A mechanical slewing mechanism, if chosen, will complicate the matter.

3.7.1 Materials and Structure. An issue that has appeared in discussions of several component trade-spaces is that of thermal effects. These effects were particularly troublesome with regard to the direct vision prism and achromatic focusing lens due to asymmetric material expansion rates. Thermal issues must also be considered in design choices for the CTEx instrument as a whole. CTEx on the ISS will be

passing into and out of Earth's shadow about 15 times per sidereal day. It is difficult to estimate the effects this may have on the instrument until the final configuration and positioning are known. Still, it is prudent to take thermal effects into account in a precautionary sense. In the case of the CTEx instrument as a whole, differential heating could pose significant problems with optical collimation and joint tolerances if a slewing mechanism is involved.

When the Hubble Space Telescope (HST) was initially released into orbit in April 1990 a large, unexpected pointing disturbance quickly became apparent. This disturbance was far greater than the tolerances required for the pointing control system and coincided with HST moving into or out of shadow. This coincidence is readily apparent in Figure 3.20.

Investigation by NASA revealed the disturbances were caused primarily by differential heating of the front and back sides of the solar array frames. A temperature gradient of $20°C$ was established after only 30 seconds of exposure to the Sun. The temperature gradient induced a slip/stick condition in joints related to solar array slewing. As it turned out resulting vibrations overwhelmed the pointing control systems ability to compensate [22, 15-21]. The solar arrays were redesigned and replaced during the servicing mission which corrected the HST mirror aberration.

This cautionary tale was related here to emphasize the catastrophic effects that can result from failure to take into account space environment effects. Choice of materials and component placement are essential elements for dealing with rapid heating and cooling effects in space.

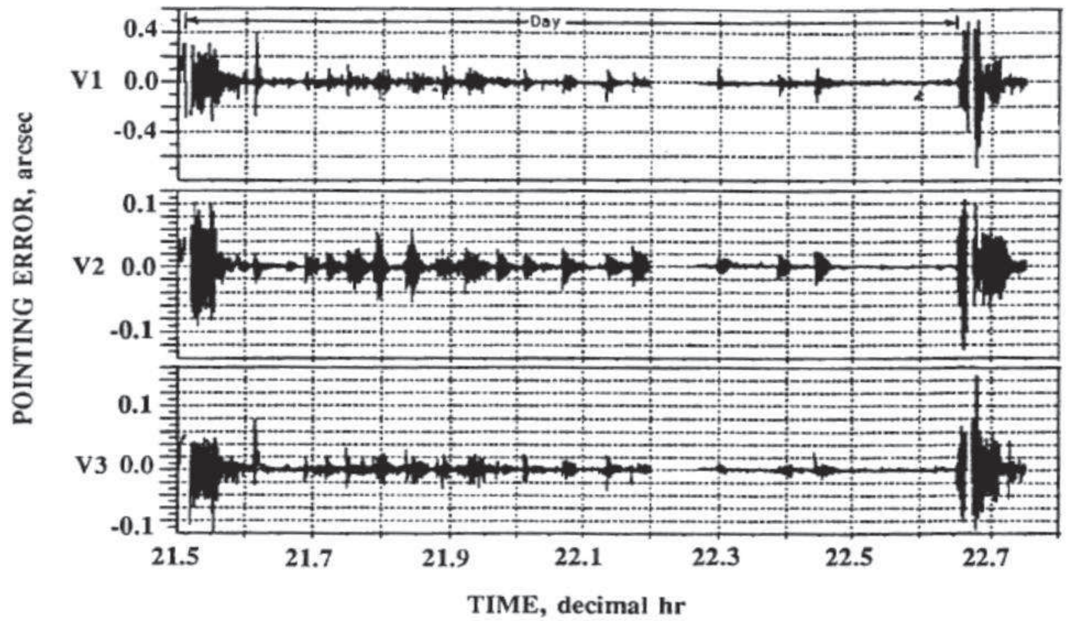

. Orbital day disturbance profile.

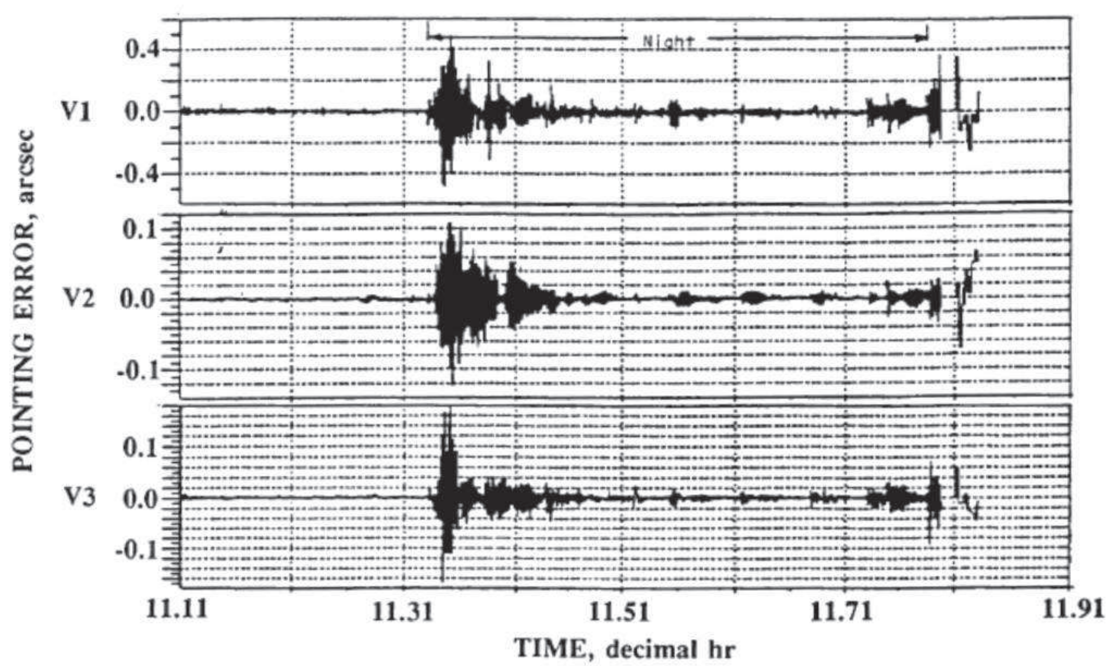

Orbital night disturbance profile.

Figure 3.20: The HST experienced significant pointing disturbances in all three axes coinciding with the instrument moving into or out of sunlight [22]

.

IV. Concept of Operations

4.1 Platform and Orbit

The basic operational assumptions for this experiment are that CTEx will be operated from the ISS Japanese Experimental Module (JEM) Exposed Facility (EF), although there are other options on the ISS as pointed out in Chapter III. This places the CTEx in a low-Earth orbit of about 350 km altitude. Figure H provides a description and graphics of the JEM. Figure 4.2 provides resource data available for operations on the JEM-EF. The maximum mass budget of 550kg should be more than enough to handle CTEx. The same is true for available power, which at 3kW is probably at least six times CTEx demand. The size constraint of $1.5m^3$ is, by far, the biggest concern, but should be manageable. The entire set of ISS orbital ephemeris data can be found in Appendix D.

Since the CTEx is tied to the ISS there is no real trade-space to speak of. The orbit is fixed, as is the space station itself. One of the advantages of having an imager that is the payload of its own satellite bus is the ability to adjust orientation or even orbit to some extent if desired. In the case of CTEx those options are not available. On the other hand, the support functions offered on the ISS are reasonable trade offs for the freedom of movement with a dedicated satellite bus. Power, stability, attitude control, and communications are all essentially free for the CTEx instrument.

As discussed in the previous chapter, the ISS is orbiting at an altitude of approximately 350km, with a velocity of 7.69km/s and an orbital period of about 90 minutes. Using these and the ephemeris data for the ISS, once the CTEx instrument is in place on the JEM-EF and system checks are completed operations can commence.

4.2 System Check

Upon placement onto the JEM-EF there are a series of checkouts that will have to be conducted to ensure it is ready to operate. The assumption being made here is that the control network for the instrument will be designed to include sensors to provide instrument health and status information which can be read and interpreted

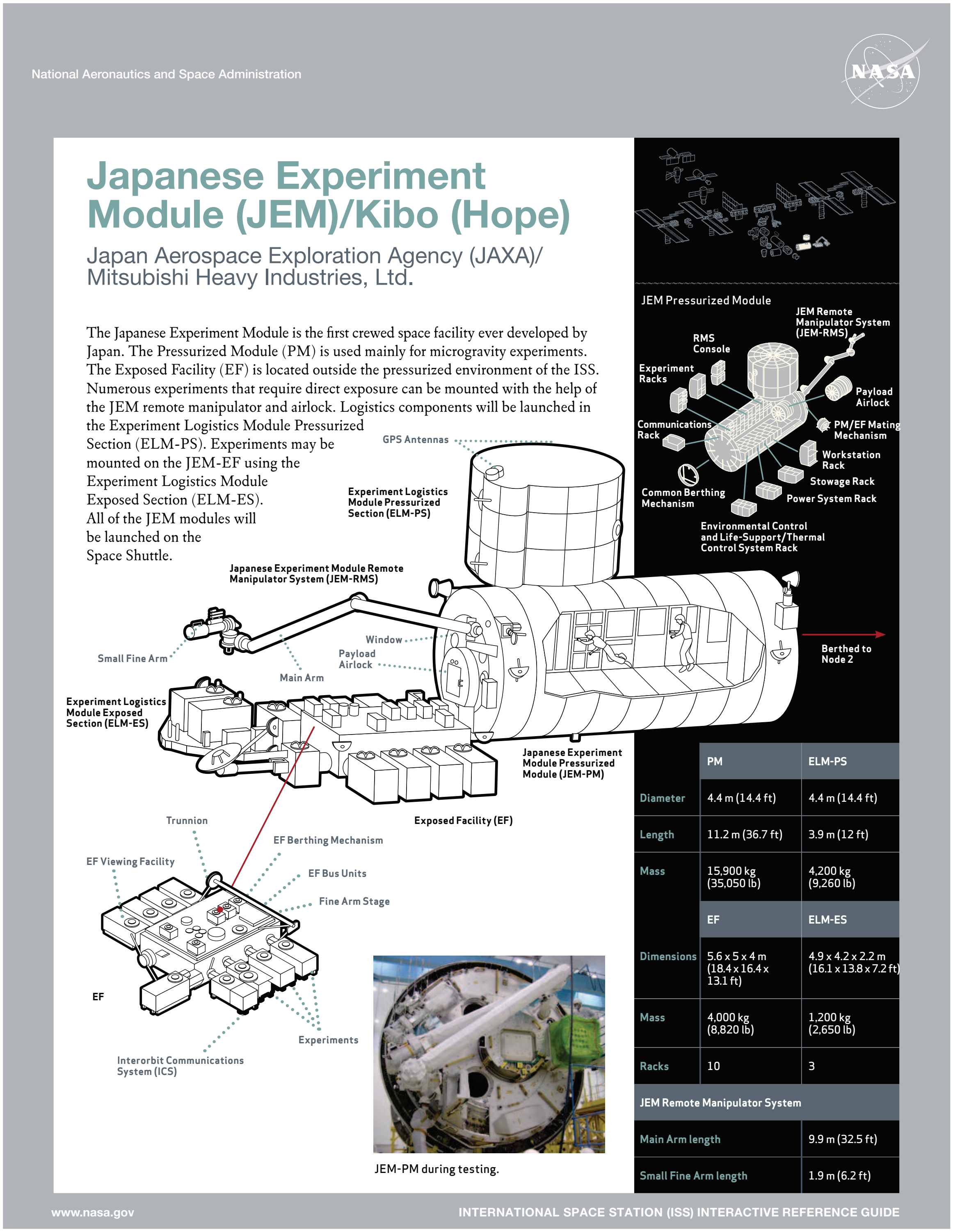

Figure 4.1: The Japanese Experimental Module provides an excellent platform for an experimental space-based instrument [2].

JEM-EF Resources	
Mass capacity	550 kg (1,150 lb) at standard site 2,250 kg (5,550 lb) at large site
Volume	1.5 m^3
Power	3-6 kW, 113-126 VDC
Thermal	3-6 kW cooling
Low-rate data	1 Mbps (MIL-STD-1553)
High-rate data	43 Mbps (shared)

Figure 4.2: The JEM exposed platform provides plenty of power, space, capability to handle mass, and enough communications to accommodate CTEx. [2]

at a ground control station. These checkout actions are listed in Table 4.1. This is not an all inclusive list; there are likely to be additional actions needed during this period.

As noted above, the systems check out table is not exhaustive, and each checkout event listed will require checklists of specific subsets of actions needed to accomplish those checks. If the CTEx instrument follows the average historical path it will probably take between one and two months for full system checkout to be completed and the instrument ready for actual test event collection.

4.3 Collection Event

The orbit of the ISS provides a short orbital period and therefore good opportunities to arrange test events at almost any location between 63°North and South. Running simulations in Satellite Tool Kit provides confidence that data collection opportunities will be available. Selecting Wright Patterson AFB as a hypothetical

Table 4.1: On-orbit Systems Check Items

Check-out Item	**Purpose/Justification**
Data uplink	Ensure ground-to-CTEx communications; command-and-control
Data downlink	Ensure CTEx-to-ground communications; command receipt; proper feedback
Data in-out with ISS	Ensure proper communications between instrument and ISS support/GPS positioning data/timing
Sensors Read	Check health and welfare - power, temperature, timing, position(s)
Command & Control boot up	Start computer processor
Software check	Ensure processes are functioning/responding correctly
Calibration LEDs	Ensure proper functioning, on/off
FPA	Use LEDs to check photons in/voltage out; check pixel health
Secondary Memory	Check on/off; read/write functions
Data routing and storage	Ensure proper data routing to camera memory and to secondary solid-state storage; check camera memory clear capability
Prism rotation table and optical encoder	Check functioning; positioning; control
Camera Electronic Aperture	Test ability to vary frame rate; check read rate
Prism Rotation Table and Camera Electronic Aperture	Check synchronization; data/feedback merge; control
Telescope Aperture	Ensure open/close
Telescope	Check control; component alignment; optical path throughput; nadir pointing
Integrated System	Check ability to capture ground reflected scene information on command and downlink data

test site, and using baseline requirements for the CTEx instrument and a focal length for the primary mirror of 625mm, these simulations indicate acceptable instrument coverage and good probability of a collectable time period (Figure 4.3) during any representative month.

Coverage for ISS-CTEx

	Access	Access Start (UTCG)	Access End (UTCG)	Duration (sec)	Asset Full Name
	1	1 Jul 2009 21:43:52.487	1 Jul 2009 21:43:53.381	0.894	Wright-Patterson
	2	15 Jul 2009 15:54:09.293	15 Jul 2009 15:54:15.669	6.375	Wright-Patterson
Global Statistics					
Min Duration	1	1 Jul 2009 21:43:52.487	1 Jul 2009 21:43:53.381	0.894	Wright-Patterson
Max Duration	2	15 Jul 2009 15:54:09.293	15 Jul 2009 15:54:15.669	6.375	Wright-Patterson
Mean Duration				3.635	
Total Duration				7.269	

Probability of Coverage

Collection Probability for ISS-CTEx

Time From Request (hr)	Probability of Collection
0.000	0.00
9.731	4.19
330.171	96.28
356.096	100.00

Figure 4.3: CTEx coverage times and coverage probability for Wright-Patterson over one month.

4.3.1 Test Plan. A collection event for CTEx will begin with choice of location and target. Knowing the orbital elements for the ISS, the test site can be set many months in advance with good confidence of exactly when the instrument will pass overhead. For each experimental event a detailed test plan will need to be developed. As a first step, an overall test director must be appointed who has the knowledge and authority to deal with all the disparate elements that will be involved.

In conjunction with the location and test event choices, particular considerations must be taken into account. These include the ability of the site to host the desired event and the amount of time needed to apply for authorizations, gather and

arrange logistics, and arrange for needed personnel to include any training (safety, certifications, etc) they may require. If testing is taking place at an actual Air Force or other Service test range, many of these things will be provided as a matter of course. Nevertheless, they will have to be accounted for in planning. Keeping in mind that the purpose of CTEx is to demonstrate the utility and uniqueness of particular Chromotomographic imaging principles, arrangements must also be made to take ground-truth data at the test. Equipment and personnel must be present at the test site to provide baseline measurements of the spectral and spatial information against which the CTEx data can be compared.

4.3.2 CTEx Data Collection. Once a test plan has been implemented and the test site prepared, the data collection event can commence. Prior to the actual test event calibration needs to take place for the reasons set forth in Section 3.6. A specific time period for calibration is hard to estimate at this point. The actual calibration actions on the instrument should be able to be accomplished fairly rapidly. The greater time demand will be in downlinking and analyzing the calibration data. This could be approached in one of two ways. The data from calibration could be downlinked and analyzed prior to the actual test event collection. Due to the limited downlink speed this may take considerable time depending on the data cube size taken for calibration. The other option would be take and hold calibration data in secondary storage and examine it after the test event. Since the closer in time the calibration is taken to the test event the more validity it will have, the second option is probably the better.

After calibration, the telescope aperture doors will be opened and the prism spun up to the desired setting for that particular event. Software driven collection (windowing) will be initiated to coincide with the instrument FOV as the test event enters the scene. Timing is obviously crucial for a successful collection. Fortunately a readily available source of precise timing is GPS. GPS timing is available on the ISS so it can be used for a t_0 common timing mark to synchronize camera operation and

test event. Timing synchronization is more of an issue in a very fast transient event like an explosion rather than a relatively long combustion source such as a rocket engine or flare. Even for these less demanding events though, timing markers will be important since the data taken from the event on the ground will need to match up with the data taken from CTEx to make valid comparisons. The criticality of timing between the event, the ground truth instrumentation and the CTEx raises another issue. Because the data generation rates are so high the CTEx cannot be run for long periods of time. This means that the timing of the command to begin data collection will be very important. This being the case there is a communication latency issue which must also be taken into account. The time it takes between issuing a command, its uplink to the ISS, transfer to the CTEx command computer, and actually executed must be well established and accounted for in the event time line. Again, this is less of an issue for a long duration event like a fire, but it still must be budgeted for to ensure the instrument hasn't partially or fully overflown the test position before data collection actually begins. But if the command is issued too early, the instrument may run low on available memory before the area of interest enters the FOV. Preloading a sequence of commands to be executed at set times will help to mitigate these latency issues. Nevertheless, even under those circumstances the relative times of execution between the CTEx instrument and instrumentation on the ground is necessary. Understanding and management of the sequence of event timing then is imperative to experimental succuss.

To establish good spectral, radiometric and spatial data for each test event there are several pieces of equipment that should be prepared to take data on the ground in conjunction with the CTEx space-borne instrument. Among those already used for these types of events are several spectral-radiometers and imagers. A list of these is provided in Figure 4.4, all of which have been used for fast transient explosive tests as shown in Figure 4.5. At least three instruments should be taking ground-level data during each test to include an FTS (Fourier Transform Spectrometer) with at least one silicon-based FPA to collect data in the visible wavelength band, a terrestrial version of

the CTEx instrument, and a high speed imaging camera. The FTS will provide baseline spectral and radiometric data which will be important for establishing a control for the experiment. The ground-based CT instrument provides a direct comparison data base against which to measure CTEx. This comparison will be important in helping to determine whether anomalous data from CTEx is a factor of the instrument itself or transmission through the atmosphere/space environment effects. The third instrument, the high speed camera, will help by giving a well defined time versus spatial dimension information for the test event. This will ensure reconstruction of the event in time with high precision. Doing this will allow data reconstruction with high confidence that any particular data block is in the right sequence with others. That is an important check since our downlinked data may not arrive in the correct time order. Beyond this, having a precise time-spatial profile of the explosion fireball, for example, is a good control for the spatial data coming from CTEx.

Once the test event has taken place, the CTEx camera and prism rotation will be turned off. The telescope aperture doors will be closed and data transferred from the camera on-board memory to secondary storage. When that has been completed, instrument health sensors will be checked to ensure the CTEx is back in its nominal configuration with camera off, aperture doors shut, and prism in initial position (0° angle or "straight up"). Then a post-event calibration should also be conducted using the on-board calibration set up. All data will need to be partitioned in secondary storage and then downlinked in chunks to the ground station(s) where it will eventually be analyzed. The data taken from the ground instruments will also need to be exported to the analysis site.

Chapter III (Section 3.5.1) makes clear that data downlink is likely to be a lengthy affair, over 30 hours for 15GB of data. Although it will be possible to take data from another test event before the first data set is fully off-loaded, it would be better to do at least a preliminary analysis before starting another run. In the event that there are problems with the first data set, these can be identified and addressed

Spectro-Radiometers

Telops Imaging FTS (Summer 2007)	320x256 (window to 32x8) InSb (1.5-5.5 μm) FPA $\Delta\nu = 0.125\text{-}64\ cm^{-1}$, 0.04-37 Hz 8 Hz @ $\Delta\nu = 5\ cm^{-1}$ & 128x8 pixels IFOV 0.35 mrad, available 4x telescope
ABB/Bomem MR-254 FTS	InSb (1.5-5.5 μm), InGaAs (0.9-1.7 μm) Si (0.63-1.1 μm) $\Delta\nu = 0.5\text{-}64\ cm^{-1}$, 10-100 Hz 82 Hz @ $\Delta\nu = 16\ cm^{-1}$ FOV of 75, 28, or 5 mrad
ABB/Bomem MR-154 FTS	MCT (2-20 μm), InSb (1.5-5.5 μm) $\Delta\nu$ 0.5-64 cm-1, 5-50 Hz 21 Hz @ $\Delta\nu = 8\ cm^{-1}$ FOV of 75, 28, or 5 mrad
Princeton Instruments SP-2500i Spectrometer	Grating 500 mm focal length $\Delta\lambda = 0.05$ nm @ 435.8 nm
Multi-channel radiometer	Si (0.3-1.1 μm), InAs (1-3.8 μm) InSb (1.5-5.5 μm), MCT (2-20 μm) Various filters available 100 kHz, 16-bit A/D, AC or DC modes

Imagers

Phantom v7.1	3-color visible high-speed camera 800x600 RGB CMOS FPA (window to 32x32) 4.8-160 kHz, 12-bit A/D
Phantom v5.1	Monochrome visible high-speed camera 1024x1024 CMOS FPA (window to 64x32) 1.2-95 kHz, 10-bit A/D
XenICs XEVA	InGaAs FPA (0.9-1.7 μm), 320x256, 30 μm pixel 350 Hz, 14-bit A/D
FLIR Systems Alpha NIR	InGaAs FPA (0.9-1.7 micron), 320x256, 30 μm pixel 30 Hz, 12-bit A/D
Santa Barbara	InSb FPA, 640x512 (window to 128x8), 24 μm pixel 87 Hz-10.4 kHz, 14-bit A/D

Figure 4.4: Characteristics of equipment that has been used in characterizing fast transient events in the past [39].

Figure 4.5: Clockwise: (a) Artillery shell on site for a ground explosion test event. Note the measurement equipment on the plateau above.(b) Explosion event from artillery shell test. (c) A longer event is this rocket engine test. [39]

so they are not repeated. Otherwise time and effort may be wasted executing another collection that has the same problems as the first.

Once all data is collected and examined for validity the test director should convene some sort of after action panel to go over the test event, identify problems and issues, and make recommendations for improvement. These then should be implemented for the next round of testing through an upgraded test plan. Testing then continues in an iterative fashion.

4.4 Space Environment Considerations

The ISS orbit is a low-earth orbit. It is well within the Earth's magnetosphere and is even within the ionosphere by most definitions. Therefore there is not a great deal of threat to the CTEx instrument from high energy particles carried by the solar wind, under most circumstances. The orbit is well out of the Van Allen radiation belts, which range from roughly 2.5 to 6 earth radii in altitude. CTEx will still be subject, as all electronics in space are, to the possibility of Single Event Upsets (SEUs). SEUs result in a bit flip caused by an energetic charged particle interacting with processors or other electronic components at the bit level. There is little that can be done to protect against these events, but CMOS based devices are inherently more resistant to them than CCDs. The ISS orbit does not pass through the polar cap areas, where high energy particle flow into lower altitudes is most prevalent, but it does regularly pass through the South Atlantic Anomaly. This region, located off the coast of Argentina, is another region where Earth's magnetic field is weak (see Figures 4.6and 4.7). This weaker geomagnetic field strength results in charged particles flowing down magnetic field lines in that area. Spacecraft passing through the South Atlantic Anomaly have a higher probability of SEUs, some of which may cause electronic malfunctions or data corruption. The bottom graphic in Figure 4.6 dramatically demonstrates the high rate of SEUs in the area. The positioning of more susceptible components, such as the CPU or FPA, can be taken into account to provide some level of shielding, but the risk cannot be totally alleviated. It will

be prudent to limit CTEx active operations as much as possible during periods when the instrument is passing through this area in its orbit.

Another threat from the space environment is the possibility of differential charging between components or areas of the instrument as it orbits. Different materials and/or positioning as the instrument moves from sunlight to shadow can result in the buildup of positive charge on some surface areas and negative on others due to photoelectric effects. If a great enough charge differential is allowed, an arcing discharge may be initiated. This tends to have very deleterious effects on electronics nearby. These electrostatic discharge effects can be minimized through instrument cover design. Another possibility is the addition of a Faraday cage to redistribute surface charge and negate electrostatic buildup. This option will add weight and cost to the instrument.

To summarize, the biggest issues facing CTEx operations once on orbit are primarily organizational and timing. Careful planning and precise coordination between instrument operations and ground-based test events will be critical to producing good data. This is particularly the case for test events, such as explosions, where rapidly changing spatial and spectral signatures are to be captured. The predictability of the ISS orbit and use of GPS-based timing synchronization should help to ameliorate these challenges.

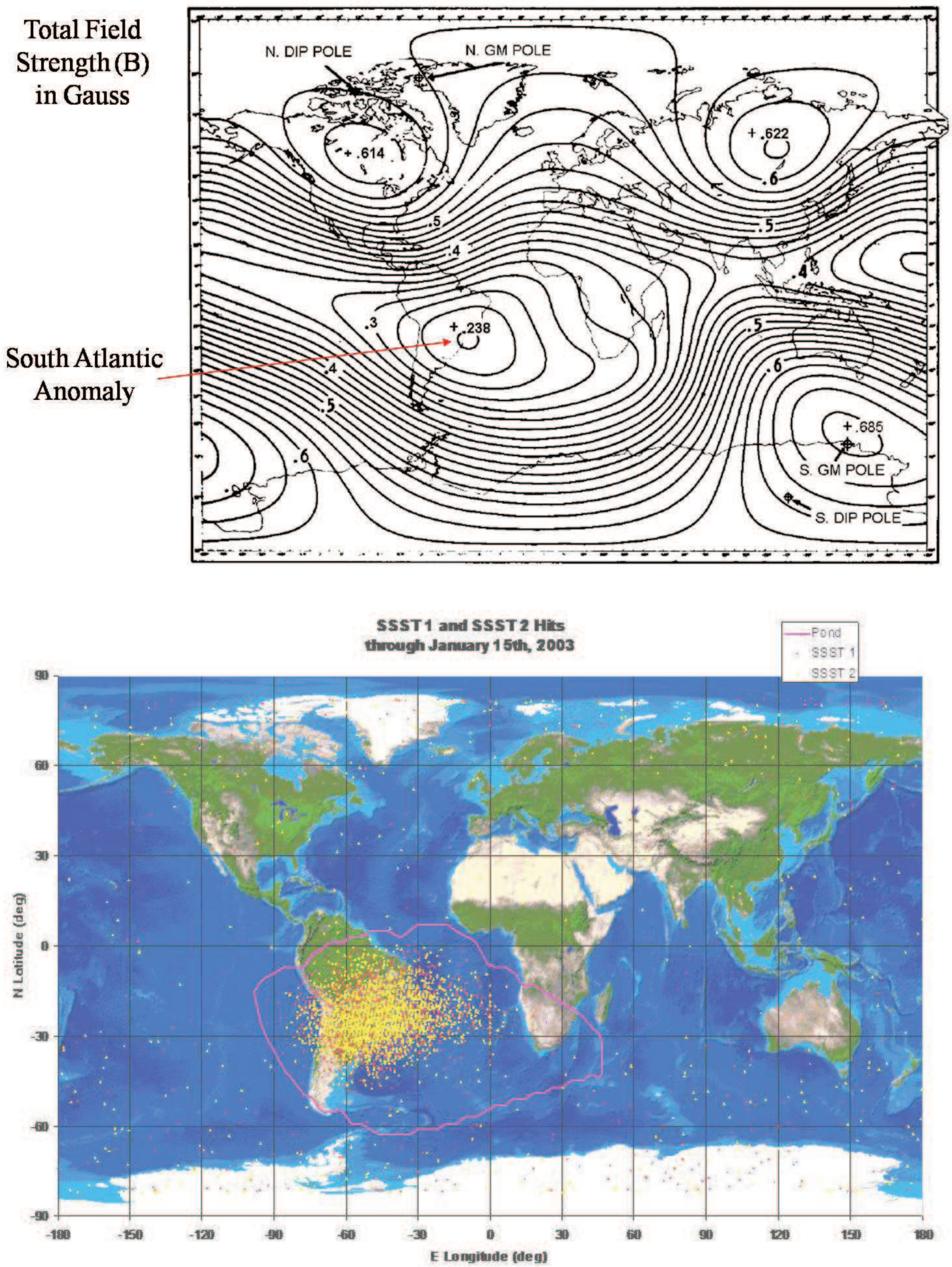

Figure 4.6: (Top) The South Atlantic Anomaly is an area of weak geomagnetic field that allows charged particles to concentrate and penetrate to lower altitudes resulting in higher incidents of SEU. (Bottom) Data from two LEO satellites illustrates the high rate of SEU over the Anomaly. [12, 37]

Figure 4.7: The ISS regularly passes through the South Atlantic Anomaly in its orbit. A higher chance of SEUs results. [12]

V. Conclusions

5.1 Thesis Summary

There are a great many considerations that must be taken into account in translating a lab-based device into a transportable, operating instrument. This is true in just designing a terrestrial instrument much less one that must be operated in space. In producing this thesis the design and key operating principles of the rotating prism chromotomography scanner were examined. The principles and background of spectroscopy in general and hyperspectral imaging in particular were studied. Examples of early and more recent hyperspectral designs were used to both illustrate some of the concepts involved and to provide models from which the CTEx instrument could borrow. Concentrating on space-based instruments helped to frame a lot of issues that had to be addressed in trade space analysis for CTEx. These areas were discussed in Chapters I and II.

Chapter III was dedicated to the trade-space analysis for the planned space-borne instrument. Areas that were specifically studied were the front-end system optics, the prism itself and its rotation component, the focal plane array and issues associated with rapid data capture and reset, data generation and handling to include storage, data downlink and general communications, and system calibration. Beyond straight forward trade-space analysis, instances of possible design problems were also identified.

Chapter IV walked through requirements for actual CTEx data collection. A general time-line of sequences of events was used to introduce and discuss the major considerations for conducting the actual experimental tests. Although the primary focus of this thesis is the instrument itself, the interactions between the space instrument and the ground were explored. Those interactions illustrated the very close dependence of events taking place in space and on the ground which must be coordinated for successful testing. There are three basic criteria defining success for CTEx. These are collecting usable data from test events that include: a single hyperspectral image with no time component (a snapshot), a large, relatively slow changing

transient event, and a rapidly changing transient event. Of these, the fast transient event will demonstrate the capability of CTEx that differentiates it from all other space-borne hyperspectral imagers operating through 2009.

5.2 Issues

This thesis has brought to light several trade-space issues that will need to be decided upon for the design to move forward. Some of these can only be resolved through testing while others will require choices to be made by the end-users of the expected data. One of the most comprehensive issues is that of operating the various components in a space environment. Options for existing hardware for the front-end optics, prism and prism rotation table, camera and FPA, and data storage devices have been presented. The one common factor to all of these components is that none of them have been used in space nor have any been tested for ability to operate in space where near vacuum and thermal considerations must be taken into account. COTS hardware was specifically considered for this project to limit cost and risk, the fact is that some of these components will require significant customization because of the space environment. Customization will partly negate the advantages of choosing COTS components in the first place.

Specific components that will need customization are the telescope, the prism and its associated rotation mechanism, the camera, and possibly the secondary memory. Beyond the capacity to operate in space, all of these components, in their off-the-shelf forms, assume an ability for the operator to access and adjust them by hand if needed. The requirement to be able to remotely operate this instrument and address problems without hands-on intervention is not a trivial one. Just one example is the front-end telescope. It appears at this point that these optics will be engineered and produced by RC Optical Systems. A brief visit to the company's web pages provides a strong indication of the requirements for optical collimation. Technical articles on how to accomplish this collimation with their existing products illustrate the absolute

necessity of collimation and also assume hands-on capability to do so. The article on collimation procedures for Ritchey-Chretien telescopes is included in Appendix E.

Another possible problem that presented itself during the course of this study is that of thermal stresses on the direct vision prism. This also applies to the achromatic focusing lens. Thermal cycling testing will need to be done to determine if there is a real risk of the prism or lens separating due to differences in thermal expansion and contraction between the materials used in these components. The possibility of thermal gradient differences between structural members must also be considered to avoid issues such as that which affected Hubble as related in Section 3.7.1.

A trade-space decision that must be addressed by the data customer is the method used to stare at a test event for data collection. The windowing method described in Chapter III is less costly, probably more precise, and presents less risk of hardware failure. It also only allows for very limited data collection time per event. Mechanical slewing, whether using a rotation bench or a slewing mirror greatly increases the mechanical complexity of the instrument, adds mass, and presents greater risk. It also will allow the instrument to achieve the full 10 second data collection requirement. The end user will have to make an assessment as to whether the short data collection (on the order of 2-3 seconds) is sufficient or it is worth the additional costs of mechanical slewing.

Although there are a number of issues that will need to be resolved in the design and construction of CTEx, this is not unexpected. One of the primary purposes of this thesis was to identify these issues so they can be addressed early in the design process. Proper design study and testing should successfully settle the problems that have been noted.

5.3 Further Study Needed

This thesis is the first study undertaken to identify the major engineering issues and tradeoffs involved with designing the CTEx and using it. However, this is by no

means an exhaustive nor comprehensive analysis. There are a number of areas that have yet to be examined before this instrument can be built, much less launched and operated in space.

Among these areas still to be worked are instrument control, structural design and fit of specific components, and testing and certification for space operations. Control is a very complicated problem. The controls mechanism for CTEx will have to include synchronization between the prism rotation table and optical encoder and the camera. It will require some sort of position feedback data loop for the prism position. It must be able to operate the telescope, the camera, the front-end aperture doors, the calibration LEDs, and, if mechanical slewing is employed, be able to control those movements with extreme precision. Software will have to be written to execute these functions as well as to move data from the camera to secondary storage, perform any pre-downlink processing such as data compression, downlink large masses of data with reliability and some form of data packet encoding to ensure all packets are sent and arrive and are able to be reconstructed in the proper sequence. Electrical power will have to be distributed to various components such as the camera, rotation table and LEDs at the proper voltages, cycles and wattage. There will need to be system health and status sensors that, at a minimum, will report on temperature, power, and instrument component position. Timing will be essential to coordinate operations between CTEx and the ground, and for proper operation of the CMOS FPA, particularly if the windowing data capture method is used since rapid pixel readout and electronic control of specific pixel activation will be paramount. All of this must be taken into account under the heading of "control".

Analysis of major issues trade-offs for various major components for the CTEx instrument has been completed. What has not, and cannot be done until specific components are actually selected is modeling and fitment for the instrument as a whole. As a reminder, as much COTS equipment as possible is being used to hold down costs and lower risk by buying more mature technology. The downside, or trade-space, of this strategy is that the various components, i.e. telescope and prism rotation

table, have never been incorporated into a single design to work together as a whole. This being the case, work will need to be done on exactly how to fabricate CTEx with all the parts working in conjunction with each other. The overall packaging to fit onto the JEM-EM, or other ISS platform, and correctly connect with the supplied power and communications links will also have to be modeled. Part of this design work will need to consider the materials used for structure and housing. As discussed in Sections 3.3 and 3.7.1, care must be taken to account for differences in material properties that could result in problems due to thermal cycling or even differential charging between parts as the ISS orbits and passes through high particle energy portions of the ionosphere.

This trade-space analysis is only an initial step in the design and construction of CTEx. Engineering design and analysis of each of the instrument components, followed by overall instrument design and construction is a natural progression for the project. It is inevitable that as these steps are taken further challenges will present themselves and be resolved in turn.

5.4 Testing

A crucial area of further work on CTEx will be extensive testing. Not only will the instrument need to be tested to ensure it works as designed and produces the data needed, but very stringent requirements for operation in space must be met to satisfy NASA and ESA (European Space Agency) space qualifications. This is the sin quo non of this instrument. If it isn't space rated, it doesn't fly.

The actual regulations are too numerous and beyond the scope of this thesis to go into in any detail. Suffice it to say that safety standards for strength, electrical hazard, overheating, and others will have to be tested for. Each component must be tested and the instrument as a whole must be tested, under all operating regimes.

Therefore, a well designed, planned, and executed test regime must be accomplished. The test program completion will naturally be one of the last steps prior

to launch. This being the case, actual testing must wait not only until specific components are selected and fitted, but produced and delivered. The test planning and design can be accomplished earlier though. Some of the main components a comprehensive test program will have to include are: G-testing (mainly for launch survivability), vibration, noise production by the instrument, thermal cycling effects, operation in a vacuum, and software testing. It cannot be stressed enough that testing will be a major undertaking and require significant time and resources in man hours, lab time, logistics and analysis.

Finally, there is specific instrument information that will be needed that can only be gathered through empirical testing. Besides the vibration and thus jitter data, one of the most important data sets is that of system noise. This can be estimated through modeling to some extent, but one never really knows what the system noise will be until it is actually tested. Once system noise is known, and having data for pixel sensitivity (quantum efficiency), floors for signal-to-noise ratio (SNR) can be derived. Thus minimum signal strength for data capture can be established. One must keep in mind that the faster the prism revolves and the faster the camera frame rate, the less signal per unit time reaches the focal plane array, assuming radiance is constant. Using radiometric data the required radiant power for an event to register with CTEx under various operating conditions will be established. This is important to avoid wasting time and resources trying to collect on a test event if there is no hope of the pixels in the FPA being able to register the incoming photons because there are too few of them.

Testing is going to be a major component in the overall production of CTEx. The safety requirements and the ability of the instrument to perform as expected must be thoroughly vetted to ensure success. This is true though of any space experiment.

5.5 Conclusion

The CTEx instrument is a bold initiative that promises to introduce new capabilities in the field of hyperspectral imaging. There are significant challenges in designing, constructing and operating this HSI. This thesis has investigated these challenges and identified problem areas and design trade-spaces that must be resolved as an initial step towards launching and operating CTEx in space. A summarization of the major instrument component decision areas is presented in Table 5.1. The successful resolution of these issues as CTEx is engineered will, in the end, lead to a successful instrument and successful experiment. Hyperspectral analysis of fast transient events is in its infancy. The successful fielding of CTEx will open up numerous areas of research in Physics, Earth Science, Meteorology and others, as well as proving a technology with direct, immediate applications for the Department of Defense and possibly Homeland Security.

Table 5.1: Summary of Trade-Space Issues

Issue	**Choices**	**Comments**
Front-end Optics	Refractive vs Reflective	Reflective optics offer great advantages in less aberration, better stability, less susceptibility to thermal distortion and better scalability
Telescope Design	Complexity vs Available Space	An off-axis Mersenne design provides a good compromise between compactness and the necessary placement of a field stop and light collimation leading into the prism. A simple Ritchey-Chretian may not fit the available space.
Direct Vision Prism	Bonded materials vs customized, gapped design	Thermal cycling may break bonded layer. A space-gapped DV prism would avoid this. Testing is needed to determine prism susceptibility to thermal failure. The issue may be alleviated through passive thermal protection.
Rotation Table	Rate vs Accuracy	Recommend prism rotation control in increments of 10^N Hz; N = 0, 1, 2, 3. This provides a range of rotation rate while offering precise set points for well defined controllability.
Focal Plane	CCD vs CMOS	Requirements for focal plane throughput strongly indicates in favor of CMOS.
Camera	Frame Rate vs Resolution	User input required: 1000 frames per second requirement favors Photron Fastcam SA2; higher rates favor Phantom v12.1.
Memory	Hard Disk vs Flash-Solid State vs DRAM-Solid State	DRAM-SSD is more expensive but clearly has superior performance and is more robust for space environment.
CPU	Capability	BAE systems RAD750 family of single-board computers is space-rated off-the-shelf, mature, proven and compatible with ISS data architecture.
Scene Staring Technique	Mechanical vs Electronic Slewing	User input required: Mechanical slewing adds complexity and risk but meets time requirements for data collection per test event. Electronic slewing requires no additional components but only provides 25% of requested data collection and may be difficult to accomplish due to demanding precision timing.
Calibration	External vs Internal	LED lights mounted on aperture doors provide good spectral and spatial calibration.

Appendix A. Operational Hyperspectral Imagers [45]

Name	Full Name	Manufacturer Country	Number of Bands	Spectral Range (μm)	Band Width at FWHM (nm)
AAHIS	Advanced Airborne Hyperspectral Imaging System	SETS Technology	288	0.432 – 0.832	6
AHI	Airborne Hyperspectral Imager	Hawaii Institute of Geophysics and Planetology	256	7.5 – 11.7	100
AHS	Airborne Hyperspectral Scanner	Daedalus Enterprise Inc.	48	0.433 – 12.70	
AIP	Airborne Instrument Program	Lockheed USA		2.00 – 6.40	
AIS-1	Airborne Imaging Spectrometer	NASA, JPL USA	128	0.90 – 2.10 1.20 – 2.40	9.3 10.6
AMSS	Airborne Multispectral Scanner MK-II	Geoscan Pty Ltd.	46	0.50 – 12.00	
ARES		USA	75	2.00 – 6.50	
ARIES	Australian Resource Information and Environment Satellite	Australia	128	0.40 – 2.50	
APEX	Airborne Prism Experiment		Programmable to a max of 300	0.38 – 2.50	10
CHRISS	Compact High Resolution Imaging Spectrograph Sensor	Science Applications Int. Corp. (SAIC) USA	40	0.43 – 0.87	
CIS	Chinese Imaging Spectrometer	Shanghai Institute of Technical Physics China	91	0.40 – 12.50	
DAIS 21115	Digital Airborne Imaging Spectrometer	GER Corp. Germany	211	0.40 – 12.00	
DAIS 3715	Digital Airborne Imaging Spectrometer	GER Corp. Germany	37	0.40 – 12.00	
DAIS 7915	Digital Airborne Imaging Spectrometer	GER Corp. Germany	79	0.40 – 12.00	
DAIS 16115	Digital Airborne Imaging Spectrometer	GER Corp. Germany	160	0.40 – 12.00	

Name	Full Name	Manufacturer Country	Number of Bands	Spectral Range (μm)	Band Width at FWHM (nm)
EART EXPLORER		ESA	202 (?)	(3)10 – 1000	
EO-1		USA	7	0.43 – 2.35	
EPS-A	Environmental Probe System	Germany	32	0.40 – 12.00	
EPS-H	Environmental Probe System	Germany	76 * 32 32 12	0.43 – 1.05 * 1.50 – 1.80 2.00 – 2.50 8.00 – 12.00	*Customised according user requirements
FLI/PMI	Fluorescence Line Imager / Programmable Multispectral Imager	Moniteq Ltd.	228	0.43 – 0.805	
FTVFHSI	Fourier Transform Visible Hyperspectral Imager	Kestrel Corp., FIT	256	0.44 – 1.15	
GERIS	Geophysical and Environmental Research Imaging Spectrometer	Germany	63	0.40 – 2.50	
HIRIS	High Resolution Imaging Spectrometer	USA	192	0.40 – 2.50	
HYDICE	Hyperspectral Digital Imagery Collection Experiment	USA	210	0.40 – 2.50	7.6 – 14.9
HYMAP		Integrated Spectronics Australia	126	0.45 – 2.50	15 – 20
HYPERION		TRW	220	0.40 – 2.5	10
IISRB	Infrared Imaging Spectrometer	Bomen	1720	3.50 – 5.00	
IMSS	Image Multispectral Sensing	Pacific Advanced Technology	320	2.00 – 5.00	
IRIS	Infrared Imaging Spectrometer	ERIM USA	256	2.00 – 15.00	
ISM	Imaging Spectroscopic Mapper	DESPA	128	0.80 – 3.20	
LIVTIRS 1	Livermore Imaging Fourier Imaging Spectrometer	Lawrence Livermore USA		3.00 – 5.00	

Name	Full Name	Manufacturer Country	Number of Bands	Spectral Range (μm)	Band Width at FWHM (nm)
LIVTIRS 2	Livermore Imaging Fourier Imaging Spectrometer	Lawrence Livermore USA		8.00 – 12.00	
MAIS	Modular Airborne Imaging System	Shanghai Institute of Technical Physics China	71	0.44 – 11.8	
MAS	Modis Airborne Simulator	Daedalus Enterprise Inc. USA	50	0.53 – 14.50	
MERIS	Medium Resolution Imaging Spectrometer	ESA	15	0.40 – 1.05	
MIDIS	Multiband Identification and Discrimination Imaging Spectroradiometer	Surface Optics Corp., JPL, USA	256	0.40 – 30.00	
MIVIS	Multispectral Infrared and Visible Imaging Spectrometer	Daedalus Enterprise Inc. USA	102	0.43 – 12.70	
MODIS	Moderate Resolution Imaging Spectrometer	NASA USA	36	0.41 – 14.24	
OMIS	Operative Modular Airborne Imaging Spectrometer		128	0.46 – 12.50	
PROBE-1			100 – 200	0.44 – 2.54	11 – 18
ROSIS	Reflective Optics System Imaging Spectrometer	DLR, GKSS, MBB Germany	128	0.45 – 0.85	5
SASI	Shortwave Infrared Airborne Spectrographic Sensor		160	0.85 – 2.45	10
SFSI	SWIR Full Spectrographic Imager	CCRS Canada	122	1.20 – 2.40	10.3
SMIFTS	Spatially modulated Imaging Fourier Transform	Hawaii Institute of Geophysics USA	75	1.00 – 5.00	
SSTI HSI	Small Satellite Technology Initiative Hyperspectral Imager	TRW Inc. USA	384	0.40 – 2.50	
TRWIS III	TRW Imaging Spectrometer	TRW Inc USA.	384	0.30 – 2.50	

Name	Full Name	Manufacturer Country	Number of Bands	Spectral Range (μm)	Band Width at FWHM (nm)
VIFIS	Variable Interference Filter Imaging Spectrometer	University of Dundee	60	0.44 – 0.89	10
VIMS-V	Visible Infrared Mapping Spectrometer	ASI	512	0.30 – 1.05	
WIS	Wedge Imaging Spectrometer	Hughes St. Barbara Research Center USA	170	0.40 – 2.50	
WARFIGHTER (WF-1)		Phillips Laboratory USA	280	0.45 – 5.00	

$n_d = 1.80318$ $\nu_d = 46.38$ $n_F - n_C = 0.017317$
$n_e = 1.80730$ $\nu_e = 46.13$ $n_{F'} - n_{C'} = 0.017499$

LaSF N30 803464

Brechzahlen	λ [nm]	
$n_{2325.4}$	2325.4	1.75970
$n_{1970.1}$	1970.1	1.76700
$n_{1529.6}$	1529.6	1.77487
$n_{1060.0}$	1060.0	1.78352
n_t	1014.0	1.78456
n_s	852.1	1.78903
n_r	706.5	1.79506
n_C	656.3	1.79798
$n_{C'}$	643.8	1.79881
$n_{632.8}$	632.8	1.79958
n_D	589.3	1.80303
n_d	587.6	1.80318
n_e	546.1	1.80730
n_F	486.1	1.81530
$n_{F'}$	480.0	1.81630
n_g	435.8	1.82495
n_h	404.7	1.83308
n_i	365.0	1.84717
$n_{334.1}$	334.1	1.8627_3
$n_{312.6}$	312.6	
$n_{296.7}$	296.7	
$n_{280.4}$	280.4	
$n_{248.3}$	248.3	

Konstanten der Dispersionsformel	
B_1	1.78301085
B_2	$3.88968359 \cdot 10^{-1}$
B_3	1.30150440
C_1	$8.72506277 \cdot 10^{-3}$
C_2	$3.08085023 \cdot 10^{-2}$
C_3	$9.27743824 \cdot 10^{1}$

Konstanten der Formel für dn/dT	
D_0	$3.32 \cdot 10^{-6}$
D_1	$1.12 \cdot 10^{-8}$
D_2	$-8.52 \cdot 10^{-12}$
E_0	$5.88 \cdot 10^{-7}$
E_1	$7.13 \cdot 10^{-10}$
λ_{TK} [μm]	0.209

Reintransmissionsgrad τ_i λ [nm]	τ_i (5 mm)	τ_i (25 mm)
2500.0		
2325.4	0.90	0.61
1970.1	0.985	0.93
1529.6	0.999	0.995
1060.0	0.999	0.996
700	0.999	0.995
660	0.999	0.995
620	0.998	0.994
580	0.998	0.992
546.1	0.997	0.987
500	0.996	0.981
460	0.995	0.975
435.8	0.992	0.960
420	0.988	0.94
404.7	0.981	0.91
400	0.977	0.89
390	0.970	0.86
380	0.950	0.79
370	0.92	0.68
365.0	0.90	0.61
350	0.81	0.35
334.1	0.60	0.08
320	0.39	
310	0.26	
300	0.17	
290		
280		
270		
260		
250		

Farbcode	
λ_{80}/λ_5	40/32

Bemerkungen	

Relative Teildispersionen	
$P_{s,t}$	0.2580
$P_{C,s}$	0.5169
$P_{d,C}$	0.3001
$P_{e,d}$	0.2380
$P_{g,F}$	0.5573
$P_{i,h}$	0.8139
$P'_{s,t}$	0.2553
$P'_{C',s}$	0.5585
$P'_{d,C'}$	0.2500
$P'_{e,d}$	0.2355
$P'_{g,F'}$	0.4942
$P'_{i,h}$	0.8055

Abweichung relativer Teildispersionen ΔP von der „Normalgeraden"	
$\Delta P_{C,t}$	0.0099
$\Delta P_{C,s}$	0.0059
$\Delta P_{F,e}$	−0.0021
$\Delta P_{g,F}$	−0.0084
$\Delta P_{i,g}$	−0.0522

Sonstige Eigenschaften	
$\alpha_{-30/+70°C}$ [10^{-6}/K]	6.2
$\alpha_{20/300°C}$ [10^{-6}/K]	7.3
Tg [°C]	666
$T_{10^{13.0}}$ [°C]	664
$T_{10^{7.6}}$ [°C]	740
c_p [J/(g·K)]	
λ [W/(m·K)]	
ρ [g/cm³]	4.46
E [10^3 N/mm²]	124
μ	0.293
K [10^{-6} mm²/N]	1.41
$HK_{0.1/20}$	770
B	0
CR	1
FR	1
SR	4.3
AR	1.0
PR	1.3

Temperaturkoeffizienten der Lichtbrechung	$\Delta n_{rel}/\Delta T$ [10^{-6}/K]			$\Delta n_{abs}/\Delta T$ [10^{-6}/K]		
[°C]	1060.0	e	g	1060.0	e	g
−40/−20	4.0	5.1	6.1	1.6	2.6	3.6
+20/+40	4.0	5.3	6.5	2.5	3.7	4.9
+60/+80	4.2	5.6	6.9	3.0	4.4	5.7

Nr. 10 000 9/92

SCHOTT Optisches Glas

SF L6 805254

$n_d = 1.80518$ $\nu_d = 25.39$ $n_F - n_C = 0.031708$

$n_e = 1.81265$ $\nu_e = 25.19$ $n_{F'} - n_{C'} = 0.032260$

Brechzahlen	λ [nm]	
$n_{2325.4}$	2325.4	1.74897
$n_{1970.1}$	1970.1	1.75544
$n_{1529.6}$	1529.6	1.76311
$n_{1060.0}$	1060.0	1.77345
n_t	1014.0	1.77489
n_s	852.1	1.78147
n_r	706.5	1.79116
n_C	656.3	1.79609
$n_{C'}$	643.8	1.79751
$n_{632.8}$	632.8	1.79884
n_D	589.3	1.80491
n_d	587.6	1.80518
n_e	546.1	1.81265
n_F	486.1	1.82780
$n_{F'}$	480.0	1.82977
n_g	435.8	1.84733
n_h	404.7	1.86500
n_i	365.0	
$n_{334.1}$	334.1	
$n_{312.6}$	312.6	
$n_{296.7}$	296.7	
$n_{280.4}$	280.4	
$n_{248.3}$	248.3	

Konstanten der Dispersionsformel	
B_1	1.78922056
B_2	$3.28427448 \cdot 10^{-1}$
B_3	2.01639441
C_1	$1.35163537 \cdot 10^{-2}$
C_2	$6.22729599 \cdot 10^{-2}$
C_3	$1.68014713 \cdot 10^{2}$

Konstanten der Formel für dn/dT	
D_0	$-5.26 \cdot 10^{-6}$
D_1	$7.41 \cdot 10^{-9}$
D_2	$-1.89 \cdot 10^{-11}$
E_0	$1.02 \cdot 10^{-6}$
E_1	$1.62 \cdot 10^{-9}$
λ_{TK} [µm]	0.288

Reintransmissionsgrad τ_i		
λ [nm]	τ_i (5 mm)	τ_i (25 mm)
2500.0		
2325.4	0.965	0.84
1970.1	0.989	0.950
1529.6	0.998	0.995
1060.0	0.998	0.988
700	0.998	0.989
660	0.998	0.988
620	0.997	0.983
580	0.996	0.980
546.1	0.994	0.970
500	0.987	0.94
460	0.979	0.90
435.8	0.970	0.86
420	0.956	0.81
404.7	0.93	0.72
400	0.92	0.67
390	0.87	0.52
380	0.76	0.25
370	0.45	0.02
365.0	0.22	
350		
334.1		
320		
310		
300		
290		
280		
270		
260		
250		

Farbcode	
λ_{80}/λ_5	45/37

Bemerkungen	

Relative Teildispersionen	
$P_{s,t}$	0.2075
$P_{C,s}$	0.4611
$P_{d,C}$	0.2867
$P_{e,d}$	0.2355
$P_{g,F}$	0.6159
$P_{i,h}$	
$P'_{s,t}$	0.2040
$P'_{C',s}$	0.4970
$P'_{d,C'}$	0.2380
$P'_{e,d}$	0.2315
$P'_{g,F'}$	0.5444
$P'_{i,h}$	

Abweichung relativer Teildispersionen Δ P von der „Normalgeraden“	
$\Delta P_{C,t}$	0.0032
$\Delta P_{C,s}$	−0.0010
$\Delta P_{F,e}$	0.0027
$\Delta P_{g,F}$	0.0148
$\Delta P_{i,g}$	

Sonstige Eigenschaften	
$\alpha_{-30/+70°C}$ [10^{-6}/K]	9.0
$\alpha_{20/300°C}$ [10^{-6}/K]	10.3
Tg [°C]	605
$T_{10^{13.0}}$ [°C]	592
$T_{10^{7.6}}$ [°C]	
c_p [J/(g·K)]	
λ [W/(m·K)]	
ρ [g/cm³]	3.37
E [10^3 N/mm²]	93
μ	0.260
K [10^{-6} mm²/N]	2.79
$HK_{0.1/20}$	570
B	0
CR	1
FR	0
SR	2
AR	1.0 *
PR	1.0

Temperaturkoeffizienten der Lichtbrechung	$\Delta n_{rel}/\Delta T$ [10^{-6}/K]			$\Delta n_{abs}/\Delta T$ [10^{-6}/K]		
[°C]	1060.0	e	g	1060.0	e	g
−40/−20	−0.8	1.1	3.8	−3.2	−1.4	1.2
+20/+40	−1.0	1.4	4.7	−2.5	−0.1	3.1
+60/+80	−0.9	1.8	5.4	−2.1	0.5	4.2

SCHOTT Optisches Glas

Nr. 10 000 9/92

PHANTOM® V12.1

All specifications subject to change   Rev September 2008

Key Features:

Up to 6242 frames-per-second (fps) at full resolution.
Maximum fps: 680,000 standard, 1,000,000 optional

1280x800 CMOS sensor

Exposure Time (shutter speed): 1μs standard
Sub-microsecond shuttering: 300ns, programmable in 18ns increments (optional)

High-resolution timing system: ...Better than 20ns resolution

Extreme Dynamic Range (EDR): two different exposures within a single frame

Internal Shuttering: session-specific black reference (CSR)

Memory Segmentation: Up to 64 segments

High-Definition, 1280x800, 1 million fps, sub-μs shutter, Phantom CineMag™ compatible

WHEN IT'S TOO FAST TO SEE, AND TOO IMPORTANT NOT TO™

One million fps is the new benchmark in high-speed imaging. Introducing the Phantom V12.1–a megapixel camera capable of taking 1,000,000 pictures-per-second.

With the Phantom V12 camera, Vision Research broke the high-speed digital imaging speed barrier. With the V12.1, the fastest camera now adds remote/automatic black referencing, dual independent HD-SDI outputs, a component viewfinder port, high-speed synchronization and range data input.

Take the wide view with our custom-designed 1280x800 CMOS sensor. The wide aspect ratio of the V12.1 allows you to see more of the event you are recording with a "widescreen" view.

Get 6,242 frames-per-second (fps) at full resolution. At lower resolutions, you will get even higher frame rates, up to 1,000,000 fps (optional).

PHANTOM® V12.1

All specifications subject to change   Rev September 2008

More Key Features:

Non-volatile, hot-swappable Phantom CineMag™ memory magazines (256GB & 512GB)

CineMag™ to CineStation™

Range Data input

Built-in Memory: 8GB, 16GB, 32GB

ISO (ISO-12232 SAT):
6400 Mono
1600 Color

Pixel Bit-depth: 8- and 12-bit

GB ethernet

View recordings immediately via video-out port

With an active pixel size of 20 microns and improved quantum efficiency, the Phantom V12.1 camera has **sensitivity** superior to our acclaimed V7.3. So, even if you are using our sub-microsecond shuttering, you'll get the highest sensitivity with the lowest noise possible.

That's right. You can eliminate blur and see the most minute detail by using our optional **sub-microsecond shuttering**. Down to 300 nanoseconds, programmable in 18ns increments.

Each camera supports **8- and 12-bit pixel depth**. Smaller bit-depth gives you more recording time and smaller files. Greater bit-depth gives you more gray levels and finer detail. With the greater latitude of 12-bits, you can pull more detail out of the image.

The V12.1's **high-resolution timing** system yields a timing resolution of better than 20ns. Frame rate, frame synchronization and exposure accuracy are all improved over previous generations of high-speed cameras. And, a frame synchronization signal is now available via a dedicated BNC for easier cabling and increased signal integrity. This makes the camera perfect for **PIV applications** with a 500 nanosecond straddle time and no image lag.

Of course, the V12.1 offers our unique **Extreme Dynamic Range** (EDR) feature giving you the ability to get two different exposures within a single frame. And, with **auto exposure**, the camera adjusts to changing lighting conditions automatically.

There is an **internal shutter** for shading the lens when doing a session-specific black reference (CSR). You can now do remote CSRs through software control, or set the camera to take a CSR at the end of each shot – automatically applying the reference to the shot!

The V12.1 comes with 8GB of high-speed dynamic RAM standard, but you can order 16GB or 32GB versions. Our **segmented memory** allows you to divide this into up to 64 segments so you can take multiple shots back-to-back without the need to download data from the camera.

Or, record directly to our **Phantom CineMag™** non-volatile, hot-swappable memory magazines (available late 2008.) They mount on the CineMag compatible version of the camera. Continuously record full resolution cines into non-volatile memory at up to 1000 fps. That's up to 256 seconds into the 256GB CineMag or 512 seconds into the 512GB CineMag. Or, record at higher speeds into camera RAM, then manually or automatically move your cine to the CineMag. With CineMag storage you get maximum data protection and an ideal storage medium for secure environments.

PHANTOM® V12.1

All specifications subject to change   Rev September 2008

Resolution/Speed Charts*

H	V	FPS
1280	800	6,242
1280	720	6,933
1024	768	7,921
1024	512	11,854
800	600	11,364
720	576	13,485
640	480	18,769
512	512	20,978
512	384	27,865
512	256	41,483
512	128	81,024
512	64	155,207
512	32	284,171
320	240	54,516
256	256	66,997
256	128	128,998
256	64	240,096
256	32	423,190
256	16	683,994
256	8	980,392
128	128	183,250
128	96	236,239
128	64	330,469
128	32	560,224
128	16	852,514
128	8	1,000,000

	18	256	512	768	1024	1280
8	1,000,0085	980,392	763,941	632,511	534,759	463,177
16	2,514	683,994	490,196	381,970	312,891	264,970
32	560,224	423,190	284,171	214,684	172,503	143,472
64	330,469	240,096	155,207	114,220	90,637	74,934
96	236,239	168,067	106,371	77,911	61,402	50,709
128	183,250	128,998	81,024	59,059	46,464	38,296
256	96,749	66,997	41,483	30,042	23,548	19,362
512	49,724	34,140	20,978	15,156	11,854	9,735
768	33,479	22,906	14,042	10,134	7,921	6,501
800	32,161	22,006	13,485	9,730	7,605	6,242

Move the CineMag from the camera to a **CineStation™** connected to a PC and view, edit, and save your cines using the Phantom Software supplied with the camera. Keep them in their original cine raw format, or convert them to TIFF, QuickTime, AVI, or a number of other formats. Move the files from the CineStation to a disk or tape deck via GB Ethernet, dual HD-SDI, or Component Video outputs. (A 10GB Ethernet interface will be available as an option in late 2008.)

When used on a tracking mount, elevation and azimuth data can be transfered to the camera and associated with image frames through our unique **Range Data** input.

A video-out port on the camera allows you to connect to a component video monitor and **view your recordings immediately** in a variety of formats including NTSC, PAL, SDI and high-definition 720p. And, there are **two HD-SDI** ports that can be used together for 4:4:4 video out, or used independently (giving you one for playback while the other is used for live preview.) A component video viewfinder port has been added so any viewfinder compatible with our Phantom HD camera can now be used
with the V12.1.

The V12.1 is controlled by the feature-rich Phantom Software. If you've used any Phantom camera before, you will know how to run the V12.1. And, we'll ship you a trial version of Image System's TEMA Starter for Phantom for motion analysis applications.

The V12.1 comes in two base models, either with or without a CineMag interface. The base models operate at up to 680,000 fps and 1us exposure. An option is available to enable 1,000,000 fps and 300ns exposure. All models come in either color or monochrome configurations.

3

* Assumes optional 1,000,000 fps, 300nsec upgrade is installed.

PHANTOM® V12.1

All specifications subject to change Rev September 2008

Additional Features:

Analog video out: PAL, NTSC & HD Component (720p)

HD-SDI: 720p

Lensing: F-mount, C-mount, PL-mount

Size (without lens): 12.25 x 5.5 x 5.0 in.
(L,W,H) 31.1 x 14 x 12.7 cm

Weight (without lens): 12 lbs (5.4 Kg)

Power: 90 Watts @ 24 VDC, without CineMag

Operating Temperature: 10°C to 40°C @ 8% to 80% RH

Storage Temperature: -10°C to 55°C

Non-Operational Shock: 33G, half sine wave, 11ms, all axes

Operational Shock: 5.56G, half sine wave, 11ms, all axes

Operational Vibration: 0.25G, 5-500 Hz, all axes

Focused

Since 1950, Vision Research has been shooting, designing, and manufacturing **high-speed cameras**. Our single focus is to invent, build, and support the most advanced cameras possible.

VISION RESEARCH

Vision Research
100 Dey Road
Wayne, NJ 07470 USA
+1.973.696.4500
phantom@visionresearch.com
www.visionresearch.com

An AMETEK® Company

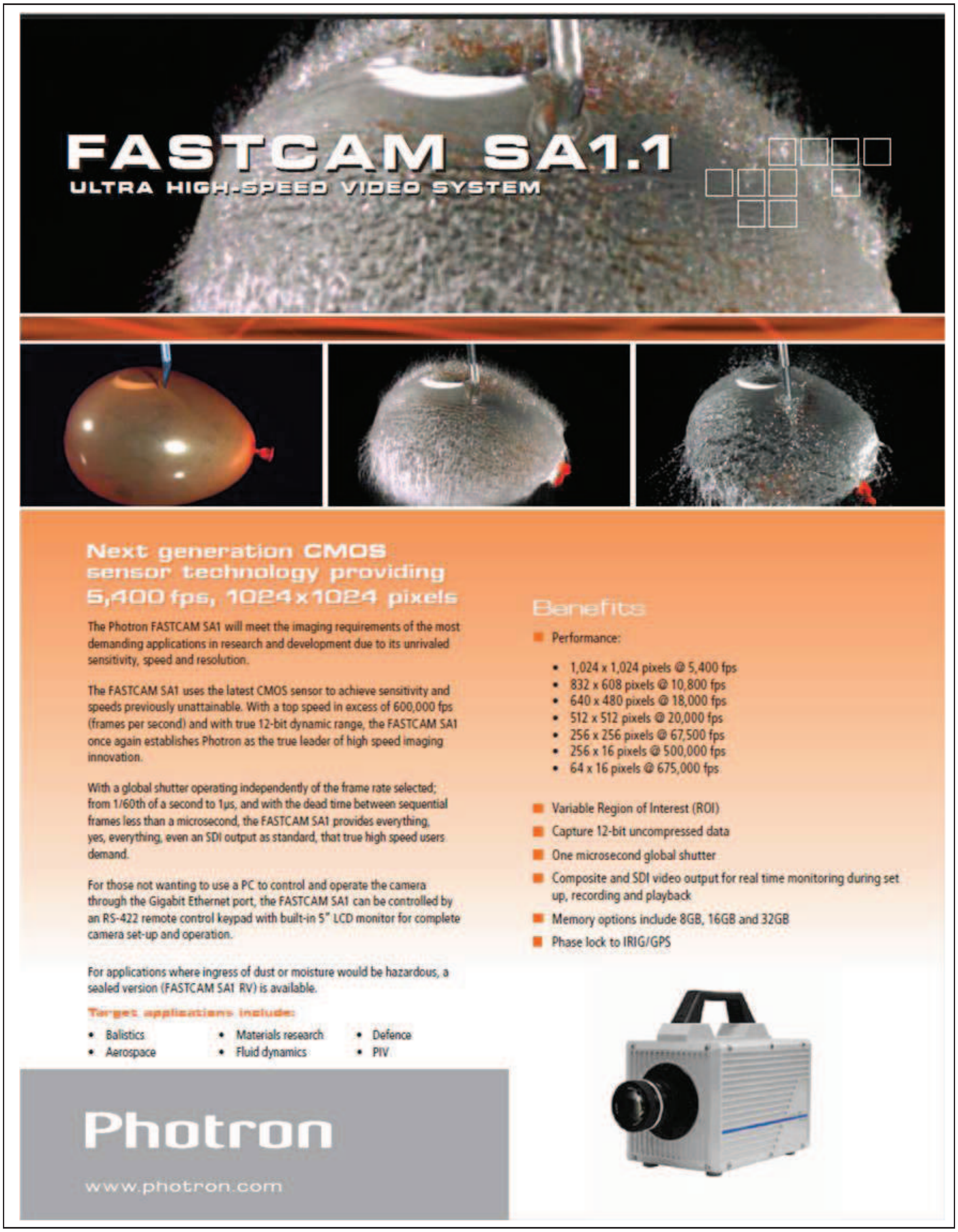
FASTCAM SA1.1
ULTRA HIGH-SPEED VIDEO SYSTEM
Next generation CMOS sensor technology providing 5,400 fps, 1024×1024 pixels
The Photron FASTCAM SA1 will meet the imaging requirements of the most demanding applications in research and development due to its unrivaled sensitivity, speed and resolution.
The FASTCAM SA1 uses the latest CMOS sensor to achieve sensitivity and speeds previously unattainable. With a top speed in excess of 600,000 fps (frames per second) and with true 12-bit dynamic range, the FASTCAM SA1 once again establishes Photron as the true leader of high speed imaging innovation.
With a global shutter operating independently of the frame rate selected; from 1/60th of a second to 1µs, and with the dead time between sequential frames less than a microsecond, the FASTCAM SA1 provides everything, yes, everything, even an SDI output as standard, that true high speed users demand.
For those not wanting to use a PC to control and operate the camera through the Gigabit Ethernet port, the FASTCAM SA1 can be controlled by an RS-422 remote control keypad with built-in 5" LCD monitor for complete camera set-up and operation.
For applications where ingress of dust or moisture would be hazardous, a sealed version (FASTCAM SA1 RV) is available.
Target applications include:
• Balistics • Materials research • Defence
• Aerospace • Fluid dynamics • PIV
Photron
www.photron.com
Benefits
Performance:
• 1,024 x 1,024 pixels @ 5,400 fps
• 832 x 608 pixels @ 10,800 fps
• 640 x 480 pixels @ 18,000 fps
• 512 x 512 pixels @ 20,000 fps
• 256 x 256 pixels @ 67,500 fps
• 256 x 16 pixels @ 500,000 fps
• 64 x 16 pixels @ 675,000 fps
Variable Region of Interest (ROI)
Capture 12-bit uncompressed data
One microsecond global shutter
Composite and SDI video output for real time monitoring during set up, recording and playback
Memory options include 8GB, 16GB and 32GB
Phase lock to IRIG/GPS

Specifcations: Frame Rate / Recording Duration Table

FRAME RATE (fps)	MAXIMUM RESOLUTION Horizontal	MAXIMUM RESOLUTION Vertical	SHUTTER EXPOSURE TIME	RECORD DURATION (12-BIT) TIME (SEC.) 8GB	TIME (SEC.) 16GB	TIME (SEC.) 32GB	FRAMES 8GB	FRAMES 16GB	FRAMES 32GB
1,000	1,024	1,024	1/Frame Rate to 1µs	5.46	10.92	21.84	5,457	10,918	21,841
2,000	1,024	1,024		2.73	5.46	10.92	5,457	10,918	21,841
3,000	1,024	1,024		1.82	3.64	7.28	5,457	10,918	21,841
5,000	1,024	1,024		1.09	2.18	4.37	5,457	10,918	21,841
5,400	1,024	1,024		1.01	2.02	4.04	5,457	10,918	21,841
10,000	768	768		0.97	1.94	3.88	9,701	19,410	38,829
15,000	768	512		0.97	1.94	3.88	14,552	29,116	58,243
20,000	512	512		1.09	2.18	4.37	21,829	43,674	87,365
30,000	512	352		1.06	2.12	4.24	31,751	63,526	127,076
75,000	512	128		1.16	2.33	4.66	87,317	174,698	349,461
100,000	320	128		1.40	2.80	5.59	139,707	279,517	559,138
125,000	256	128		1.40	2.80	5.59	174,634	349,397	698,922
180,000	128	128		1.94	3.88	7.77	349,269	698,794	1,397,845
250,000	128	80		2.24	4.47	8.95	558,830	1,118,071	2,236,552
300,000	128	64		2.33	4.66	9.32	698,538	1,397,589	2,795,690
500,000	64	32		5.59	5.59	22.37	2,794,354	2,795,178	11,182762
675,000	64	16		8.28	16.56	33.13	5,588,309	11,180,714	22,365,525

Sensor	12-bit ADC (Bayer system color, single sensor) with 20µm pixel
Shutter	Global electronic shutter from 16.7ms to 1µs independent of frame rate is standard
Lens Mount	Interchangeable F-mount and C-mount using supplied adapters
Extended Dynamic Range	Selectable in twenty steps (0 to 95% in 5% increments) to prevent pixel over-exposure
Memory	8GB (standard), 5457 frames, 1.01 sec @ 5400fps 16GB (option), 10918 frames, 2,02 sec @5400fps 32GB (option), 21841 frames, 4.04 sec @5400fps
Video Output 1	NTSC/PAL composite VBS (BNC). Ability to zoom, pan and scroll within image via keypad. Live video during recording.
Video Output 2	SDI:D1 digital component 1 channel (BNC) industry standard digital output NTSC and PAL
Camera Control	Available Gigabit Ethernet and RS-422 keypad with built in 5" LCD viewfinder
User Preset Switches	Four user selectable camera function control mounted on the cameras rear panel
Low Light Mode	Low light mode drops the frame rate and shutter time to their maximum values, while maintaining other set parameters, to enable users to position and focus the camera
Triggering	Selectable positive or negative TTL 5Vp-p or switch closure
Trigger Delay	Programmable delay on selected input and output triggers, 100ns resolution
Timing	Internal clock or external source such as IRIG or GPS
Phase Lock	Enables cameras to be precisely synchronized together, or to an external source, such as IRIG or GPS time codes
Event Markers	Ten user –entered event markers mark specific events within the image sequence in real time. Immediately accessible through software
Dual Speed Recording™	Enables the recording speed to be changed up or down by a factor of 2,4 or 8 during a recording
Recording Modes	Start, End, Center, Manual, Random, Random Reset, Random Center, Random Manual and Dual Speed Recording
Saved Image Formats	JPEG, AVI, TIFF, BMP, RAW, RAWW, PNG and FTIF. Images can be saved with or without timing and comment data
Data Display	Frame Rate, Shutter Speed, Trigger Mode, Date or Time (can be switched), Status (Playback/Record), Real Time, Frame Count and Resolution
Partitioning	Up to 64 memory segments for multiple recordings in memory
Data Acquisition	Supports Photron MCDL and DAQ
Cooling	Actively cooled
Operating Temp.	0-40 degrees C (Range version increases upper limit to 45C)
Mounting	1x ¼-20 UNC, 1x 3/8-16 UNC, 6x M6
Dimensions and Weight	160mm (6.30")H x 153mm (6.02")W x 242.5mm (9.55")D *excluding protrusions Weight 13 lbs (5.9 kg)
Power Requirements	100V - 240V AC ~ 1.5A, 50-60Hz optional DC operation 20 to 36V DC. AC adaptor provided

PHOTRON USA, INC.
9520 Padgett Street, Suite 110
San Diego, CA 92126-4446
USA
Tel: 858.684.3555 or 800.585.2129
Fax: 858.684.3558
Email: image@photron.com
www.photron.com

PHOTRON (EUROPE) LIMITED
The Barn, Bottom Road
West Wycombe, Bucks, HP14 4BS
United Kingdom
Tel: +44 (0) 1494 481011
Fax: +44 (0) 1494 487011
Email: image@photron.com
www.photron.com

PHOTRON LIMITED
Fujimi 1-1-8
Chiyoda-Ku, Tokyo 102-0071
Japan
Tel: +81 (0) 3 3238-2106
Fax: +81 (0) 3 3238-2109
Email: image@photron.co.jp
www.photron.co.jp

Photron

SLOW MOTION IMAGING SOLUTIONS

FASTCAM SA-2

FASTCAM SA-2: High-Speed Video System

2,048 x 2,048 (4MEGA pixel) resolution, developed for a broad range of applications including automotive safety testing, defenc fluid dynamics and materials research

The FASTCAM SA-2 has been engineered to permit detailed observation and analysis of large spatial areas in the fields of automotive safety testing, fluid dynamics and solid mechanics. With full HD (1920 x 1080 pixels) resolution at up to 2,000fps this system has also the potential to be applied to broadcast applications in Sports, Advertising and Entertainment.

- A light sensitive CMOS imaging sensor allowing images to be captured in the field with little or no additional lighting
- 12-bit A-D yields excellent dynamic range
- Simple to operate via the intuitive Photron Fastcam Viewer (PFV) software
- Integration with existing motion analysis, PIV or DIC systems is achieved through use of the supplied SDK
- Optional RS422 remote keypad control offers added versatility with built-in 5-inch LCD color display
- Gig-E interface to user networks

FEATURES

- 2,048 x 2,048 pixels @ 1,000fps
- 1,920 x 1,080 pixels @ 2,000fps (Full HD 1080i)
- 12-bit A-D
- Monochrome or colour sensor
- 8,16 or 32GB memory options
- Gigabit Ethernet (1000BASE-T) interface
- Optional handheld remote controller with integrated video monitor for simple control of all functions and viewing of live and recorded images.
- Low-light mode for initial set up of camera position and focus
- Rugged design for use in industrial environments
- Intuitive Photron Fastcam Viewer (PFV) software with comprehensive range of functions for camera set-up, image acquisition, replay and storage.

Photron

Specifications *FASTCAM SA2* **Photron**

Partial frame rate / resolution table:

(for clarity some options have been omitted)

Horizontal

Vertical

PIXELS	2048	1792	1536	1280	1024	768	512	256
2048	1,080	1,125	1,250	1,440	1,500	1,800	2,160	2,500
1920	1,125	1,250	1,350	1,500	1,500	1,875	2,250	2,700
1792	1,200	1,350	1,440	1,600	1,800	2,000	2,400	2,880
1664	1,250	1,440	1,500	1,500	2,000	2,250	2,500	3,000
1536	1,440	1,500	1,600	1,875	2,160	2,400	2,880	3,375
1408	1,500	1,600	1,875	2,000	2,250	2,700	3,000	3,750
1280	1,600	1,875	2,000	2,250	2,500	2,880	3,375	4,000
1152	1,875	2,000	2,250	2,500	2,880	3,200	3,750	4,500
1088	2,000	2,160	2,400	2,700	3,000	3,375	4,000	4,800
1024	2,160	2,250	2,500	2,880	3,200	3,600	4,000	5,000
896	2,400	2,700	2,880	3,200	3,600	4,000	4,800	5,400
768	2,880	3,000	3,375	3,750	4000	4,800	5,400	6750
640	3,375	3,750	4,000	4,500	5,000	5,400	6,750	8,000
576	3,750	4,000	4,500	5,000	5,400	6,250	7,500	8,000
512	4,000	4,500	5,000	5,400	6,250	7,200	8,000	9,600
384	5,400	6,000	6,750	7,500	8,000	9,000	10,800	12,500
256	8,000	9,000	9,600	10,800	12,000	13,500	16,000	18,000
128	16,000	16,000	18,000	20,000	22,500	25,000	28,800	30,000
32	50,000	54,000	54,000	62,500	64,000	72,000	80,000	86,400

Sensor	12-bit CMOS (Bayer system color, single sensor) with 10µm pixel
Shutter	Global electronic shutter from 16.7ms to 2.7µs independent of frame rate
Lens Mount	Interchangeable F-mount and C-mount using supplied adapters, optional PL and B4 lens mounts
Extended dynamic range	Twenty presets prevent pixel over-exposure
Memory	8GB (standard) 16GB (option) 32GB (option)
Video Output # 1	HD SDI Ability to zoom, pan and tilt within image via keypad. Live video during recording.
Camera Control	Through optional keypad with integrated viewfinder and Gigabit Ethernet or RS-422A
User preset switches	4 camera mounted user defined function buttons
Low light mode	Low light mode selection for simple camera adjustment when working in low ambient light, high frame rate or short exposure modes
Triggering	Selectable positive or negative TTL 5Vp-p or switch closure
Trigger delay	Programmable delay on selected input and output triggers, 100ns resolution
Timing	Internal
Phase Lock	Enables cameras to be synchronized precisely together to a master camera or external source
Event markers	Ten user -entered event markers mark specific events within the image sequence in real time. Immediately accessible through software
Dual Speed Recording	TBA
Recording Modes	Start, End, Center, Manual, Random, Random Center, Random Manual
Saved Image Formats	JPEG, AVI, TIFF, BMP, RAW (compressed or uncompressed) PNG and FTIF. Images can be saved with or without image or comment data
Data Display	Frame Rate, Shutter Speed, Trigger Mode, Date or Time, Status (Playback/Record), Real Time, Frame Count and Resolution
Partitioning	TBA
Data Acquisition	TBA
Cooling	Actively cooled
Operating Temperature	0-40 degrees C
Mounting	1x ¼-20 UNC, 1x 3/8-16 UNC, 6x M6
Dimensions and Weight	286mm L x 156mm W x 191mm H, weight 5.9kg
Power requirements	100V - 240V AC ~ 1.5A, 50-60Hz optional DC operation 18-36 VDC, 100VA

Specifications subject to change without notice.

FASTCAM-SA5

FASTCAM-SA5: High-Speed Video System
Next generation CMOS sensor technology
providing 7,000fps, 1024 x 1024 pixels

The Photron FASTCAM-SA5 will meet the requirements of the most demanding applications in research and development due to its unrivaled sensitivity, frame rate and resolution.

This high specification will permit the SA5 to be applied to areas of research once dismissed as unsuitable for digital high-speed video.

Building on the success of the Ultima APX range of systems our sensor design improves sensitivity, image quality and color reproduction.

The Fastcam SA5 delivers mega-pixel resolution at 7,500fps, an impressive maximum frame rate of 1,000,000fps and a 1 microsecond exposure time.

Target applications include:

- Materials research
- Combustion
- Inkjet
- Cavitation
- Aerospace
- Fluid dynamics
- PIV

FEATURES

- Performance examples:

  1,024 X 1,000 pixels @ 7,500fps
  512 x 512 pixels @ 25,000fps
  256 x 256 pixels @ 87,500fps
  128 x 128 pixels @ 262,500fps

  Up to 1,000,000 fps at reduced resolution
- Variable Region of Interest (ROI)
- Capture 12-bit uncompressed data
- 20μm pixels ensure best light sensitivity for demanding high-speed or low light applications
- 1μs global shutter can be set independent of selected frame rate.
- Composite and SDI video output for real time monitoring during set up, recording and playback
- Optional remote keypad control with integrated viewfinder
- 8GB, 16GB or 32GB memory options
- Gigabit Ethernet interface

Specifications *FASTCAM-SA5*

Photron

Partial frame rate / resolution table:

Variable frame rate steps 64 x 8
Some options omitted for clarity

Horizontal resolution

Vertical resolution

PIXELS	1024	896	768	640	512	384	256	128	64
1024	7,000	7,500	9,300	10,000	12,500	18,800	21,000	37,500	54,250
896	7,500	9,300	10,000	12,500	15,000	18,800	25,000	42,000	62,000
768	9,300	10,000	12,500	14,000	17,500	21,000	31,000	50,000	70,000
640	10,000	12,500	15,000	17,500	21,000	25,000	37,500	60,000	84,000
512	14,000	15,000	18,800	21,000	25,000	31,000	46,500	70,000	105,000
384	18,800	21,000	25,000	28,000	35,000	42,000	62,000	93,000	131,250
256	28,000	31,000	37,500	42,000	50,000	65,100	87,500	140,000	168,000
128	54,250	62,000	70,000	84,000	100000	124,000	162750	262,500	350,000
112	62,000	70,000	75,000	93,000	105,000	140,000	168,000	262,500	372,000
96	75,000	84,000	93,000	105,000	131,250	162,750	210,000	325,500	420,000
64	105,000	105,000	140,000	162,750	168,000	232,500	300,000	420,000	581,250
32	168,000	210,000	232,500	262,500	325,500	372,000	525,000	700,000	
16	350,000	372,000	420,000	465,000	525,000	620,000	775,000		
8	581,250	620,000	700,000	700,000					

Sensor	12-bit CMOS (Bayer system color, single sensor) with 20μm pixel
Shutter	Global electronic shutter from 16.7ms to 1μs independent of frame rate
Lens Mount	Interchangeable F-mount and C-mount using supplied adapters
Extended dynamic range	Twenty presets prevent pixel over-exposure
Memory	8GB (standard), 5457 frames (1024 x 1024 x 12-bits), 0.78 seconds 16GB (option), 10,913 frames (1024 x 1024 x 12 bits), 1.56 seconds 32GB (option), 21,841 frames (1024 x 1024 x 12 bits), 3.12 seconds
Video Output # 1	NTSC/ PAL composite VBS (BNC). Ability to zoom, pan and tilt within image via keypad. Live video during recording.
Video Output # 2	SDI D1 digital component 1 channel (BNC) Industry standard digital output, 720 x 576 PAL, 720 x 480 NTSC
Camera Control	Through optional keypad with integrated viewfinder and Gigabit Ethernet or RS-422A
User preset switches	4 camera mounted user defined function buttons
Low light mode	Low light mode selection for simple camera adjustment when working in low ambient light, high frame rate or short exposure modes
Triggering	Selectable positive or negative TTL 5Vp-p or switch closure
Trigger delay	Programmable delay on selected input and output triggers, 100ns resolution
Timing	Internal clock or external source such as IRIG or GPS (requires optional software module)
Phase Lock	Enables cameras to be synchronized precisely together to a master camera or external source
Event markers	Ten user-entered event markers mark specific events within the image sequence in real time. Immediately accessible through software
Dual Speed Recording	Enables the recording speed to be changed up or down by a factor of 2,4 or 8 during a recording
Recording Modes	Start, End, Center, Manual, Random, Random Reset, Random Center, Random Manual and Dual Speed Recording
Saved Image Formats	JPEG, AVI, TIFF, BMP, RAW, PNG (12bit) and FTIF (8 bit). Images can be saved with or without image or comment data
Data Display	Frame Rate, Shutter Speed, Trigger Mode, Date or Time, Status (Playback/Record), Real Time, Frame Count and Resolution
Partitioning	Up to 64 memory segments for multiple recordings in memory
Data Acquisition	Supports Photron MCDL
Cooling	Actively cooled
Operating Temperature	0-40 degrees C
Mounting	1x ¼-20 UNC, 1x 3/8-16 UNC, 6x M6
Dimensions and Weight	286mm L x 156mm W x 191mm H, weight 8.2kg
Power requirements	100V - 240V AC ~ 1.5A, 50-60Hz optional DC operation 18-36 VDC, 100VA

Specifications subject to change without notice.

ISS TRAJECTORY DATA

```
   Lift off time (UTC)  :  N/A
   Area (sq ft)  :  9902.8
   Drag Coefficient (Cd)  :   2.00
   Monthly MSFC 50% solar flux (F10.7-jansky)  :   72.1
   Monthly MSFC 50% earth geomagnetic index (Kp)  :   2.19
   ET - UTC  (sec) :   66.18
   UT1 - UTC (sec) :    0.00

Vector Time (GMT): 2009/019/12:30:00.000
    Vector Time (MET): N/A
    Weight (LBS)     : 639525.7

              M50 Cartesian                         M50 Keplerian
    -----------------------------------      --------------------------------
     X    =        -859769.88                A    =        6730277.74  meter
     Y    =       -4099237.52  meter         E    =          .0007386
     Z    =       -5274263.00                I    =          51.54805
     XDOT =       7514.656335                Wp   =          73.91166
     YDOT =      -1633.687561  meter/sec     RA   =         347.45781  deg
     ZDOT =         46.809239                TA   =         196.52163
                                             MA   =         196.54571
                                             Ha   =           194.186  n.mi
                                             Hp   =           192.517

              M50 Cartesian                         J2K Cartesian
    -----------------------------------      --------------------------------
     X    =       -2820767.31                X    =        -788246.44
     Y    =      -13448942.00  feet          Y    =       -4108451.62  meter
     Z    =      -17304012.48                Z    =       -5278266.34
     XDOT =      24654.384302                XDOT =       7532.138605
     YDOT =      -5359.867325  feet/sec      YDOT =      -1549.556570  meter/sec
     ZDOT =        153.573620                ZDOT =         83.357444

              TDR Cartesian                         TDR Cartesian
    -----------------------------------      --------------------------------
     X    =        9320903.81                X    =        2841011.48
     Y    =      -10069934.11  feet          Y    =       -3069315.92  meter
     Z    =      -17319838.23                Z    =       -5279086.69
     XDOT =      18026.440118                XDOT =       5494.458948
     YDOT =      16188.538540  feet/sec      YDOT =       4934.266547  meter/sec
     ZDOT =        295.751854                ZDOT =         90.145165


    The mean element set is posted at the UTC for which position is
    just north of the next ascending node relative to the above
    vector time


    TWO LINE MEAN ELEMENT SET

    ISS
    1 25544U 98067A   09019.53659256  .00010596  00000-0  82463-4 0  9000
    2 25544  51.6402 347.8788 0008205 285.4453  74.5802 15.70436401 22574


    Satellite: ISS
    Catalog Number: 25544
    Epoch time:      09019.53659256   =   yrday.fracday
    Element set:     900
    Inclination:       51.6402  deg
    RA of node:       347.8788  deg
    Eccentricity:     .0008205
    Arg of perigee:   285.4453  deg
    Mean anomaly:      74.5802  deg
    Mean motion:   15.70436401  rev/day
    Decay rate:    1.05960E-04  rev/day^2
    Epoch rev:            2257
```

RC OPTICAL SYSTEMS TECH SHEET

Ritchey-Chrétien Alignment & Collimation

Authored by John Smith exclusively for RC Optical Systems

Introduction

In order to obtain optimum performance from a Ritchey-Chrétien design, the primary and secondary mirrors must have their optical axes aligned with each other such that the optical axis of one mirror lies along that of the other. This is called collimation. Additionally, some optics sets require a rotational alignment (indexing) between the primary and secondary mirrors. Stan Moore has developed an excellent collimation methodology using the Takahashi collimation telescope in concert with a dot in the center of the secondary mirror that is highly recommended and quite successful. It is summarized on the RC Optical Systems web site at: http://www.rcopticalsystems.com/collimation.html. Stan's method is incorporated into this alignment procedure.

Tools

The following tools are needed to perform this alignment:

- Takahashi Collimating Telescope
- Tak-2-AP adapter or T-2-AP adapter from RCOS
- Allen wrenches (T-handle preferred)
- Small flashlight
- Laser collimator (optional)

Note that T-handle Allen wrenches provide more precise control and allow a screw to be tightened securely without introducing a bending or twisting force on the assembly being tightened.

Indexing (if required)

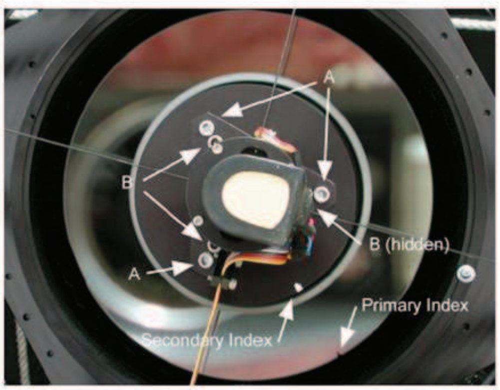

Figure 1: Front View

RC Optical Systems • 4025 E. Huntington Drive, Suite 105 • Flagstaff, Arizona 86004 • Phone 928-526-5380 • Email - info@rcopticalsystems.com

Refer to Figure 1, above. Looking in the scope from front, you should see a white dot on the back of the secondary mirror assembly. This is the secondary index. Looking at the primary, you should see a black mark on the edge of the mirror. This is the primary index. (If you do not have these index marks, then your optics do not require indexing.) How locate your eye approximately in the center of the telescope from the secondary end. Keeping your eye close to the center, move closer to or further from the scope until you can see the primary mirror mark close to the secondary mirror mark. When the perceived size of the secondary is close to the size of the primary, you will see the two marks very close to each other and can best judge the primary alignment.

If the mirrors are not rotationally aligned, you need to rotate the primary mirror so that the two index marks are very close to each other rotationally. The primary is held in position by a locking collar, which secures the mirror snugly. You can rotate the mirror without excessive force. The object is to get the primary index and secondary index rotationally aligned by rotating the primary. For the truss model, you can reach in and rotate the primary and review the alignment. For the closed tube model, you need to remove the back plate, rotate the primary, secure the back plate and review the alignment. Do not touch the front surface of the mirror as finger oils can damage the coatings. After you have rotated the primary mirror, check the indexing again as described above. You should try to get this as close as you can.

Collimation

Collimation is done in two parts - in daylight and then with a star test. The more precise the daylight alignment, the easier the star test adjustments will be, if needed at all. The star test is always a good check on collimation to see if anything has changed significantly.

The secondary mirror has a dot in the center. This dot is very precisely located to define the mirror center. To distinguish it from other reference marks, it is called a "blot" (contraction of "black dot"). It is not completely black but has an appearance as if drawn by a felt pen (it was!) This blot is the key to successful alignment. Before proceeding, look at the secondary through the back of the telescope to see this blot and note its appearance. It is important to identify its texture, as this will be a good visual cue later in the collimation process

1. Daylight Alignment

Collimation is best done with a Takahashi Collimating Telescope and an adapter, which mates this scope to the 2.7" extension tubes. Additionally a suitable measuring tool is useful for checking the spider centering. Using the long end of an Allen wrench of the appropriate size as a feeler gauge can work equally well. The Optical Tube Assembly (OTA) should be horizontal to minimize the possibility of dropping tools on the primary. Also, the OTA should be pointed at a flat illumination. This can be the sky, a sheet hung up a short distance away, or any relatively uniform illumination source. Also, before beginning, be sure the secondary mirror position is set as close to the spider assembly as possible, i.e., as far from the primary mirror as possible. This is the home position on the Telescope Command Center (TCC) or, if you have the RoboFocus set up properly, it should be close to the zero position.

1.1 Spider Centering

At each of the four spider mounting points, note that there is a gap between the secondary support ring and the spider rib. The spider is under tension by the four screws that mount it to the secondary support ring. The four gaps should be as equal as possible, say within an Allen wrench size (.016"). To adjust these gaps if necessary, tighten one screw and loosen the opposite one until they are equal. See what Allen wrench fits snugly into a gap and adjust the others similarly. Check the pair at right angles to the first pair and adjust them if necessary. Check all four gaps after adjustment and repeat if necessary. This is a reasonably precise way to achieve secondary centering with the camera axis.

RC Optical Systems • 4025 E. Huntington Drive, Suite 105 • Flagstaff, Arizona 86004 • Phone 928-526-5380 • Email - info@rcopticalsystems.com

Another and perhaps better way to do this adjustment is to insert a laser collimator in the 2" eyepiece adapter. It is important to insure the laser is bore sighted accurately by rotating the laser in the 2" holder, locking it down every 90 degrees or so and noting the position of the laser dot on the secondary mirror. Observe all laser cautions if you try this. If the position of the laser relative to the blot is consistent as you rotate the laser collimator in the holder, then it may be used to center the secondary mirror. If not, then you must determine an "average center position" for the laser and adjust the secondary spider to that position. Once the laser collimator bore sight accuracy is established, you should see an image as shown below.

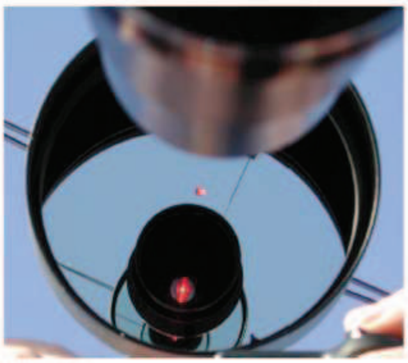

Figure 2

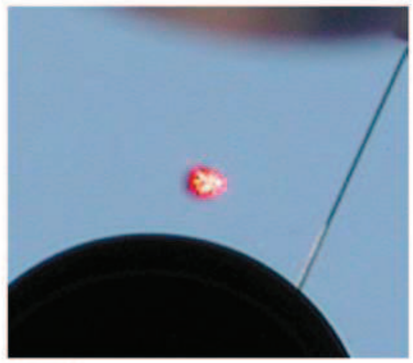

Figure 3

Figure 2 is a photo of the front of the scope. The red light towards the bottom is the laser light emanating from the back of the scope and through the primary baffle. The small red dot at the center is the laser beam landing on the secondary mirror. Figure 3 is a close-up of the red laser dot landing on the secondary blot. The laser is very slightly to the right of the center of the blot. This represents very good alignment and was achieved by the gap measurement method. Again, a laser collimator is not necessary. However, if you happen to have a laser collimator with good centration, it can be used effectively.

1.2 Secondary Mirror Tip-Tilt

This step adjusts secondary de-centering to the viewing axis more precisely, albeit via tip/tilt adjustments. Again refer to Figure 1. Looking at the secondary assembly, you will note three sets of two screws spaced 120 degrees around the assembly. The outer three are labeled "A" in Figure 1 and are the "pull adjustments" - they pull the secondary toward the mounting plate. The inner three, labeled "B" in Figure 1 are "push adjustments" - they push against the secondary mounting plate to the degree the pull adjustments allow and lock the secondary mounting plate. The push adjustments are essentially locking screws.

If the telescope has been shipped uncollimated (14.5" and larger), the pull adjusters are fully clockwise. You need to loosen these to get some adjustment range. After mounting the mirror, unscrew each of the three adjusters equally around 1.5 to 2 turns. The push adjusters will now be loose and no longer contacting the mirror mounting plate.

Screw all the 2.7" extension tubes that came with your telescope together and screw them into the Fixed Instrument Adapter (FIA) plate. (If you do not have the Fixed Instrument Adapter, extend the draw tube all the way out and add any 2.7" extension tubes you may have. If the Takahashi collimating scope is not extended far enough from the back plate, you may not see the light annulus, as shown in Figure 5.) Look through the back plate and observe the blot in the center of the secondary mirror. This blot should be close

to the center of the extension tube. If not, adjust the pull adjusters until it is. This step roughly aligns the optical axis of the secondary to the extension tube/instrument axis.

Now, thread in the Tak-2-AP adapter and then the Takahashi collimation telescope into the adapter. Note that the Takahashi scope has a white frosted area partway down the scope. This is a diffuser that can be illuminated with a flashlight to make the secondary dot more distinct.

Note that the Takahashi scope uses a sliding action for focusing. Start with the sliding all the way in. While looking in the Takahashi scope, slowly slide to tube out while keeping a flashlight on the diffuser. Eventually you will see the blot come into sharp focus. It may or may not be in the center of the illuminated area. Continue to slide the tube out and then another dot will come into sharp focus. This is the outline of the end of the Takahashi collimating scope. Slide the tube back in to refocus the blot. Ignore any other light and dark patterns for the moment. The goal of adjusting the secondary is to get the blot centered on the Takahashi collimating scope dot. Do not be concerned with the centering of the blot in the light area. The goal is to get the blot and the dot on top of each other.

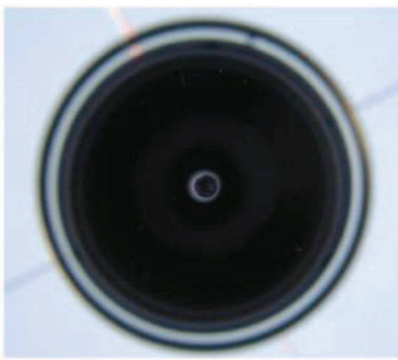

Figure

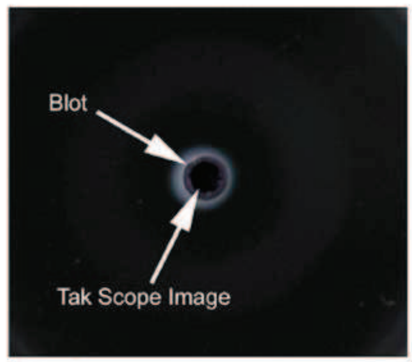

Figure 5

Figure 4 is an image taken through the Takahashi scope. Figure 5 is a blow-up of that image. Note the blot (secondary dot) is less dark than the image of the Takahashi scope, the latter being better defined. This image shows the blot and the dot being very well centered. When you begin, the blot will most likely be well off the center.

This adjustment is done by trial and error adjustment of the pull screws to center the secondary dot. As you get close, it is helpful to focus the Takahashi scope alternately on the dot and the ring to fine-tune your centering. Once this is close, snug up the push screws but do not over tighten them. Check centering after doing this and make smaller adjustments if necessary by loosening the push screw and tightening the pull screws.

RC Optical Systems • 4025 E. Huntington Drive, Suite 105 • Flagstaff, Arizona 86004 • Phone 928-526-5380 • Email - info@rcopticalsystems.com

1.3 Primary Mirror Tip-Tilt

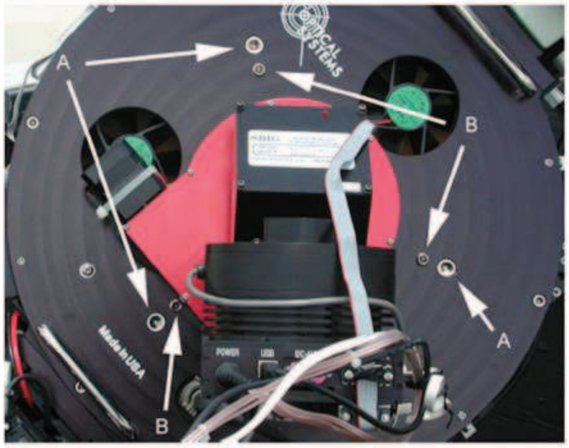

Figure 6: Back view

Now that the secondary mirror optical axis is aligned with the viewing axis, this step adjusts the primary tip/tilt to line up with the secondary. Look at the back plate of the OTA as shown in Figure 6. Again you will note three sets of two screws spaced 120 degrees around the back plate. The outer three, labeled "A" in Figure 6, are "pull adjustments" - they pull the primary mounting plate toward the back plate. The inner three, labeled "B" in Figure 6, are "push adjustments" - they push the primary mounting plate away from the back plate to the degree the pull adjustments allow. The push adjustments are essentially locking screws.

If the telescope has been shipped uncollimated (14.5" and larger), the pull adjusters are fully clockwise. You need to loosen these to get some adjustment range. Unscrew each of the three adjusters equally around 1.5 turns. The push adjusters will now be loose and no longer contacting the mirror mounting plate.

Again look in the Takahashi scope. Moving radially out from the secondary dot, you will see a light area, the image of the end of the Takahashi scope and another much larger dark area, which is comprised of the primary baffle and primary mirror locking collar. Next, a small annulus of light should be visible and finally an outer dark ring, which is the secondary baffle. The object of the primary tip/tilt adjustment is to have this annulus of light as symmetrical (equal width around the circumference) as you can possibly make it.

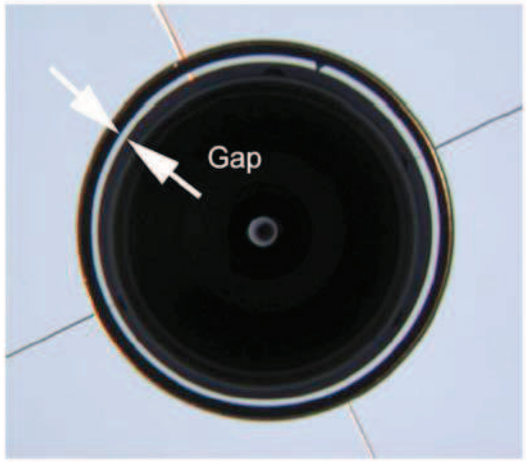

Figure 7

Figure 7 identifies the gap that is to be made symmetrical. (As an aside, note the mark in the gap at 1 o'clock. This is the secondary indexing mark that is applied on the mirror itself. The white secondary index mark shown in Figure 1 refers this mark to the back of the secondary mounting plate for alignment ease.)

This symmetry adjustment is achieved by adjusting the pull screws while looking in the Takahashi scope. Adjust these screws in small increments to get this annulus of light as symmetrical as possible. Once you are satisfied with this adjustment, snug up the push screws. As before, again check the symmetry of the annulus and adjust if necessary by loosening the appropriate push screw and tightening the corresponding pull screw.

Now recheck the secondary dot and Takahashi scope dot for symmetry. If it is no longer symmetrical, repeat the secondary tip/tilt adjustment, followed by the primary tip/tilt adjustment. Repeat as necessary until the symmetry is as good as you can make it.

As you are doing these final steps, you may find it useful to walk away from the OTA once you have it done as well as you can for a few minutes. When you return, you may see some asymmetry that you didn't see before. Adjust as needed and be sure the push screws are all snug before you are done.

When you are satisfied with the symmetrical appearance of the blot, dot and annulus ring, you can proceed to the star test. Do not make any further adjustments to the secondary focuser during the star test. You will rapidly go away from the correct secondary alignment and must return to the daylight collimation to re-establish the correct the secondary alignment.

2. Star Test

A star test consists of looking at a moderately bright star with good seeing conditions after the scope has come to thermal equilibrium. With your telescope mounted and tracking, you are ready to begin final collimation using a star. Locate a bright star near the zenith and center it visually in the eyepiece field of view. Use a moderate to high power. Slightly defocus the star and look for asymmetry in the rings surrounding the star. Slightly adjust the primary tip-tilt adjustments to minimize the asymmetry. Move the star back to the center of the field of view after any adjustment. The adjustments should be very small, 1/6 of a turn or less, if you were successful on the daylight collimation. Don't be surprised if no further adjustment is needed on the star test. If you were very exacting in the daylight test, this could be the case.

If the seeing is exceptionally good, you may begin to see the Airy disk and the first ring. Critically focus the star and look carefully for the first ring. If it is continuous and unbroken, you are perfectly adjusted; if not, you may make very small adjustments to the primary tip/tilt.

There is an excellent web page on Collimation written by Thierry Legault at http://perso.club-internet.fr/legault/collim.html. This site is highly recommended for the fine points of star testing and some examples of collimated and uncollimated stars, both in focus and out of focus.

RC Optical Systems • 4025 E. Huntington Drive, Suite 105 • Flagstaff, Arizona 86004 • Phone 928-526-5380 • Email - info@rcopticalsystems.com

RGV100BL

High-Speed Precision Rotation Stage

- Brushless direct-drive provides faster rotating speeds, high torque, superior reliability, and enhanced position sensitivity
- Ultra-compact footprint – only 115 mm x 115 mm
- Precision glass scale encoder ensures 0.0003° repeatability
- 30 mm diameter through-hole for convenient cable routing

The RGV100BL is a very compact direct-drive rotation stage that provides ultra-fast rotation with very high resolution and outstanding positioning performance. Applications include semiconductor wafer inspection, micro-robotics, and precision metrology.

The direct-drive technology of the RGV100BL eliminates the worm gear of traditional rotation stages. The advantages are higher speeds, superior reliability, and enhanced position sensitivity. Speed, resolution, and repeatability are increased by a factor of up to ten times compared to worm-driven rotation stages of the same size.

A high efficiency brushless DC torque motor with rare earth magnets supplies an optimum ratio of torque per inertia for high acceleration, with minimal stage heating. At maximum continuous torque, the temperature of the motor increases by only 30°C. This is significantly less than other stage designs and guarantees high performance and high reliability for the most demanding applications.

Precision is ensured by a high-resolution glass scale with 15,000 line pairs per revolution that directly measures the position of the rotating platen. The flat encoder is mounted on a precision ground reference surface and is perfectly aligned with the stage's rotation axis to minimize position errors induced by eccentricity, wobble, or axial runout. The encoder signals are interpolated by the XPS motion controller with less than 0.1 arcsec resolution for outstanding position sensitivity and stability.

The RGV100BL features a proprietary 4-point contact ball bearing. This unique, 2-piece design takes advantage of Newport's excellent and proven capabilities in the design, manufacturing and assembly of precision mechanics and integrates multiple functions, like the bearing ways and the direct drive motor, minimizing the number of parts. The result is a more compact rotation stage with superior stiffness, high reliability and outstanding wobble and eccentricity specifications.

A 30 mm diameter through-hole allows convenient routing of cables and vacuum lines through the stage. A once-per revolution index pulse permits precision homing to a unique home position. The RGV100BL also features two limit switches that can be enabled or disabled by an external switch.

Design Details

Base Material	Aluminum
Bearings	Large diameter steel ball bearings
Motor	High-torque brushless DC motor with rare earth magnets
Motor Initialization	Done by the XPS controller by a patented process that avoids major motion during initialization and that does not require Hall effect sensors
Motor Commutation	Done by the XPS controller on encoder signals
Feedback	Glass scale encoder with 15,000 line pairs per revolution, 1 Vpp, 32768-fold signal subdivision when used with XPS controller
Limit Switches	Two optical limit switches at approx. +/- 168°, Disabled by external switch
Origin	Optical, fixed at position 0°, including mechanical zero signal
Cable Length (m)	5

Specifications

Travel Range (°)	360 continuous
Resolution (°)	0.00001*
Uni-directional Repeatability, guaranteed (°)	0.0003
Reversal Value (Hysteresis), typical (°)	0.0001
Accuracy, guaranteed (°)	0.01
Maximum Speed (no load) (°/s)	720
Maximum Acceleration (°/s2)	1000
Maximum Torque (Nm)	0.42 @ 0°/s
Inertia (no load) (kg.m²)	0.00116
Wobble, guaranteed (µrad)	20
Eccentricity, guaranteed (µm)	3
MTBF (h)	20,000 with 5 kg load, 720°/s speed and a duty cycle of 30%
Weight [lb (kg)]	4.84 (2.6)

* The resolution used internally by the XPS is below 0.01 arcsec.

Newport

Phone: 1-800-222-6440 • Fax: 1-949-253-1680

Load Characteristics and Stiffness

Cz, Normal centered load capacity	100 N
Kα, Transversal compliance	15 µrad/Nm
Mz, Maximum torque	0.42 Nm @ 0°/s
Jz, Maximum Inertia	0.032 kgm^2
Q, Off-center load	$Q \leq Cz/(1+D/35)$ and $Q \leq (Jz-Jq)/D_2$
Where: D = Cantilever distance in mm; Jq = Inertia of payload	

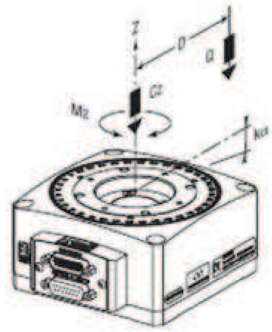

Ordering Information

Model	Description
RGV100BL	RGV100BL Rotation stage

Recommended Motion Controller: XPS see page 844

CAD *See our website for CAD files*

Dimensions

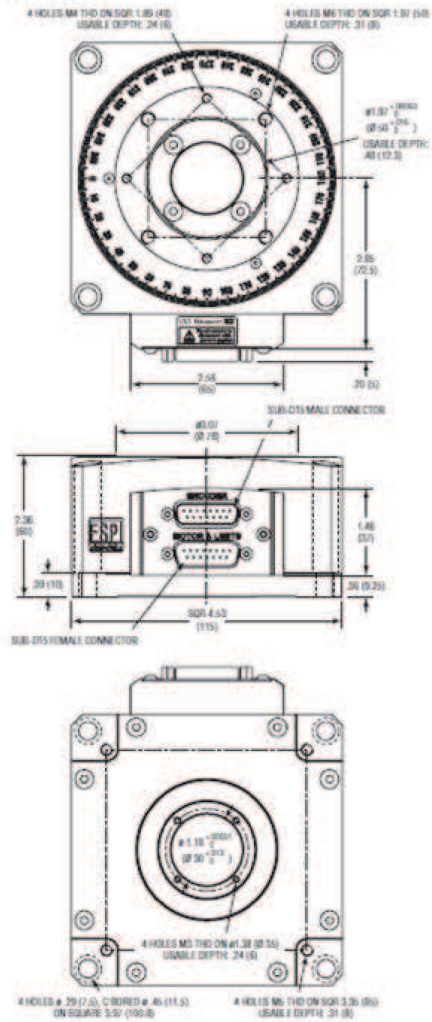

Hollow shaft motor/encoder

CM-5000 series, 5" brushless DC , 2.0" ID through shaft — 1

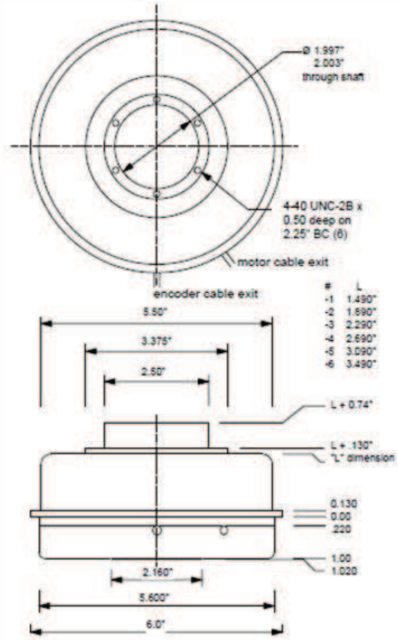

Description:

The CM-5000 is a high performance brushless DC motor with integral optical encoder characterized by a very high toque to inertia ratio. Six different sizes are available with peak torques from 1010 oz.in through 6654 oz.in @ 100 V. For different motor windings, please contact the factory.
The motor was specifically designed for high speed, high resolution positioning applications and is available with the following encoder configurations:

- ultra low distortion incremental sine/cosine, specifically designed for use with interpolators, yielding up to 144 million measuring steps
- digital incremental up to 36,000 c/r (144,000 measuring steps)
- high resiotion digital incremental from 50,000 c/r (200,000 measuring steps) to 2,250,000 c/r (9 million measuring steps)
- 18/20 bit absolute in parallel format (external electronics necessary)

Applications include semiconductor robots, turret scanners, capstan drives, spinners etc.

Ordering information:

CM-5000-(1)-(2): sine/cosine output encoder.
(1) motor size, see specsheet
(2) standard linecounts: 2,000 c/r, 9,000 c/r

CM-5050-(1)-(2): digital output encoder.
(1) motor size, see specsheet
(2)standard linecounts: 2,000, 4,000, 9,000, 18,000 & 36,000 c/r

CM-5050-HHC-(1)-(2): digital output, high resolution
(1) motor size, see specsheet
(2)standard linecounts: 50,000, 62,500, 100,000, 125,000, 200,000, 225,000, 250,000, 281,000, 400,000, 450,000, 500,000, 562,500, 900,000, 1,125,000, 1,800,000 & 2,250,000 c/r.

For absolute output, please consult factory.

Mechanical Data:

shaft ID:	1.997"- 2.003"
shaft loading:	40 lbs axial, 35 lbs radial
shaft runout:	.0002" T.I.R.
starting torque:	4.5 oz.in max @20°C
shaft rotation:	continuous,reversible
shaft speed:	1,500 RPM max
shaft material:	416 stainless
housing material:	aluminum (stainless optional)
bearing life:	manufacturer's specs
moment of inertia:	0.07 oz.in.sec^2
weight:	approx.5 lbs
temperature:	operating: -20°C to+90°C
shock:	50 G's @ 11 ms
vibration:	5-2,000 Hz @ 20 G's
humidity:	98% without condensation

Allied Motion Technologies Corporation/Computer Optical Products, Inc.•(800)340-0404 • sales@opticalencoder.com•www.opticalencoder.com
96-0048 Rev - 06/29/05 (Specifications Subject to Change)

Hollow shaft motor/encoder

CM-5000 series, 5" brushless DC , 2.0" ID through shaft

2

Motor specifications **size constants @ 25°C ambient:**

parameter	symbol	unit	-1	-2	-3	-4	-5	-6
maximum rated torque @ temperature rise of 80°C	Tr	in-oz Nm	1313 9.2	3019 21.3	4405 31.1	5760 40.6	7156 50.5	8651 61.0
maximum continuous stall torque @ temperature rise of 80°C	Tc	in-oz Nm	201 1.41	419 2.96	623 4.40	790 5.57	997 7.04	1192 8.41
Max. continuous power output	Pout	Watt	271	360	464	468	591	665
motor constant	Km	in-oz/ W Nm/W	30.2 0.21	61.2 0.43	86.9 0.61	108.6 0.78	128.0 0.90	146.2 1.03
electrical time constant	Te	ms	1.56	3.00	4.14	5.05	5.93	6.87
mechanical time constant	Tm	ms	4.5	2.4	1.8	1.6	1.4	1.3
thermal resistance*	TPR	°C/Watt	1.3	1.2	1.1	1.0	0.9	0.8
maximum cogging torque	Tf	in-oz Nm	5.5 0.04	13.4 0.09	18.1 0.14	23.7 0.17	29.6 0.2	36.2 0.26
viscous damping	Fi	in-oz/rpm Nm/rpm	3.6E-3 2.6E-5	7.5E-3 5.3E-5	0.01 8.0E-5	0.015 1.0E-4	0.018 1.3E-4	0.021 1.5E-4
hysteresis drag torque	Th	in-oz Nm	4.8 0.03	10.3 0.07	15.6 0.11	20.9 0.45	25.5 0.18	29.8 0.21
rotor inertia	Jm	$oz.in.s^2$ $Kg.m^2$	2.9E-2 2.0E-4	6.3E-2 4.5E-4	9.7E-2 6.8E-4	1.3E-1 9.2E-4	1.6E-1 1.1E-3	2.0E-1 1.4E-3
number of poles	P		12	12	12	12	12	12
weight		lbs kg	3.9 1.8	5.7 2.6	7.5 3.4	9.2 4.2	11 5	12.8 5.8

Winding constants @ design voltage Vp = 100 V, 25° ambient

peak torque, ± 25%	Tp	in-oz Nm	1010 7.13	2323 16.4	3389 23.93	4431 31.29	5505 38.87	6654 47.0
peak current, ±15%	Ip	Ampere	11.1	14.4	15.2	16.6	18.5	20.7
torque sensitivity, ±10%	Kt	in-oz/A Nm/A	90.6 0.64	181.1 1.14	223.3 1.58	266.5 1.88	297.7 2.10	321.1 2.27
no-load speed	Snl	rpm rad/s	1477 156	833 87	602 63	504 53	451 47	418 44
voltage constant	Kb	V/krpm V/rad/s	67.0 0.64	119.2 1.14	165.1 1.58	197.1 1.88	220.1 2.10	237.6 2.27
terminal resistance, ± 12%	Rm	Ohm	6.97	6.94	6.59	6.02	5.41	4.83
terminal inductance, ±30%	Lm	mH	14.0	20.8	27.3	30.4	32.1	33.2

Allied Motion Technologies Corporation/Computer Optical Products, Inc.•(800)340-0404 • sales@opticalencoder.com•www.opticalencoder.com

86-0048 Rev - 06/29/05 (Specifications Subject to Change)

Hollow shaft motor/encoder

CM-5000 series, 5" brushless DC , 2.0" ID through shaft

3

Encoder specifications

sine/cosine output

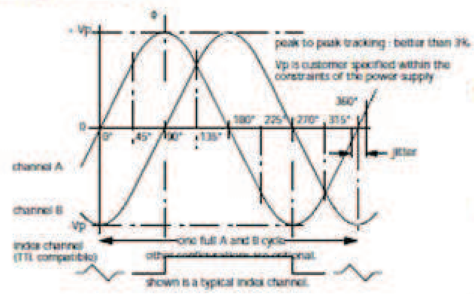

digital, incremental or HHC output

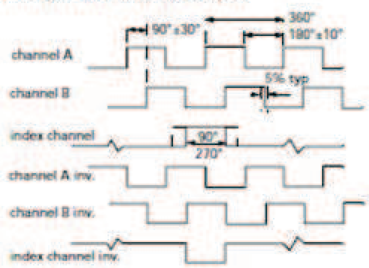

sine/cosine:	**CM-5000 Model**
power supply:	± 5 Vdc @ 60 mA max.
output format:	A/B sine/cosine, incremental
output:	default Vout = ± 0.5 V , zero-centered
frequency response:	flat up to 100 kHz
distortion:	less than 5% (Rmax/Rmin)
digital, incremental:	**CM-5050 Model**
power supply:	+ 5Vdc ± 10% @ 100 mA max (no load)
output format:	A/B quadrature, incremental, digital
freqency response:	150 kHz min. @ 85 °C
output:	linedriver 26LS31,EIA std. RS 422 & DIN 66259 compatible
HHC (interpolated):	**CM-5050-HHC Model**
power supply:	+ 5Vdc ± 10% @ 250 mA max (no load)
output format:	A/B quadrature, incremental, digital
freqency response:	2.0 MHz min. @ 85°C
output:	linedriver 26LS31,EIA std. RS 422 & DIN 66259 compatible
digital, absolute:	18, 20 & 22 bits Consult factory

Motor excitation sequence and "Hall" switch output

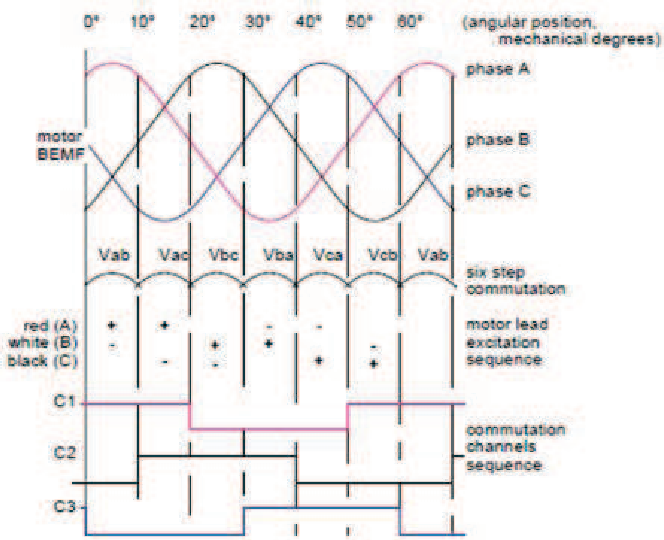

Motor wire color code:

red	phase A
white	phase B
black	phase C

"Hall" switch color code:

brown	C1
orange	C2
yellow	C3
blue	+ 5V to + 24V
green	ground

External Research Accommodations

Many locations are available for the mounting of payloads or experiments on the outside of the Station: on the U.S. Truss, on the Russian elements, and additional accommodations will be provided when the Japanese Experiment Module (JEM) Exposed Facility (EF) and Columbus modules are attached.

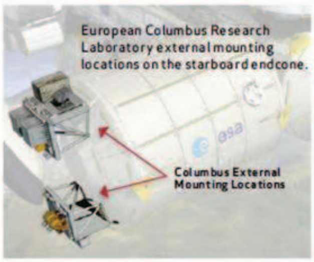

JEM-EF in preparation for launch.

External Research Locations

EXTERNAL UNPRESSURIZED ATTACHMENT SITES	STATION-WIDE	U.S. SHARED
U.S. Truss	10	10
Japanese Exposed Facility	10	5
European Columbus Research Laboratory	4	0
Total	24	15

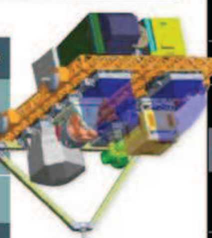

External Payload Accommodations

External payloads may be accommodated at several locations on the U.S. S3 and P3 Truss segments. External payloads are accommodated on an Expedite the Processing of Experiments to the Space Station racks (EXPRESS) Logistics Carrier (ELC). Mounting spaces are provided, and interfaces for power and data are standardized to provide quick and straightforward payload integration. Payloads can be mounted using the Special Purpose Dexterous Manipulator (SPDM), Dextre, on the Station's robotic arm.

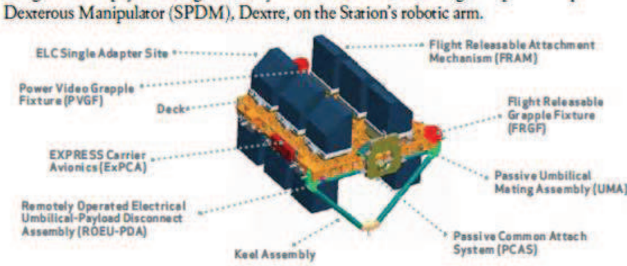

Express Logistics Carrier (ELC) Resources	
Mass capacity	4,445 kg (9,800 lb)
Volume	30 m^3
Power	3 kW maximum, 113-126 VDC
Low-rate data	1 Mbps (MIL-STD-1553)
High-rate data	95 Mbps (shared)
Local area network	6 Mbps (802.3 Ethernet)
ELC Single Adapter Resources	
Mass capacity	227 kg (500 lb)
Volume	1 m^3
Power	750 W, 113-126 VDC 500 W at 28 VDC per adapter
Thermal	Active heating, passive cooling
Low-rate data	1 Mbps (MIL-STD-1553)
Medium-rate data	6 Mbps (shared)
JEM-EF Resources	
Mass capacity	550 kg (1,150 lb) at standard site 2,250 kg (5,550 lb) at large site
Volume	1.5 m^3
Power	3-6 kW, 113-126 VDC
Thermal	3-6 kW cooling
Low-rate data	1 Mbps (MIL-STD-1553)
High-rate data	43 Mbps (shared)
European Columbus Research Laboratory Resources	
Mass capacity	230 kg (500 lb)
Volume	1 m^3
Power	2.5 kW total to carrier (shared)
Thermal	Passive
Low-rate data	1 Mbps (MIL-STD-1553)
Medium-rate data	2 Mbps (shared)

Japanese Experiment Module (JEM)/Kibo (Hope)

Japan Aerospace Exploration Agency (JAXA)/ Mitsubishi Heavy Industries, Ltd.

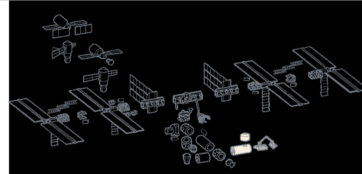

The Japanese Experiment Module is the first crewed space facility ever developed by Japan. The Pressurized Module (PM) is used mainly for microgravity experiments. The Exposed Facility (EF) is located outside the pressurized environment of the ISS. Numerous experiments that require direct exposure can be mounted with the help of the JEM remote manipulator and airlock. Logistics components will be launched in the Experiment Logistics Module Pressurized Section (ELM-PS). Experiments may be mounted on the JEM-EF using the Experiment Logistics Module Exposed Section (ELM-ES). All of the JEM modules will be launched on the Space Shuttle.

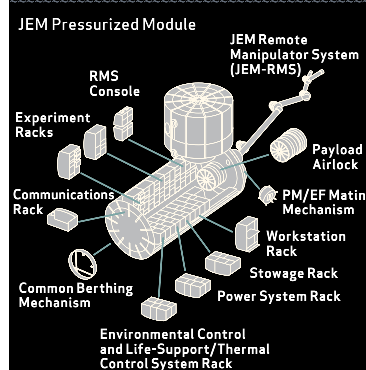

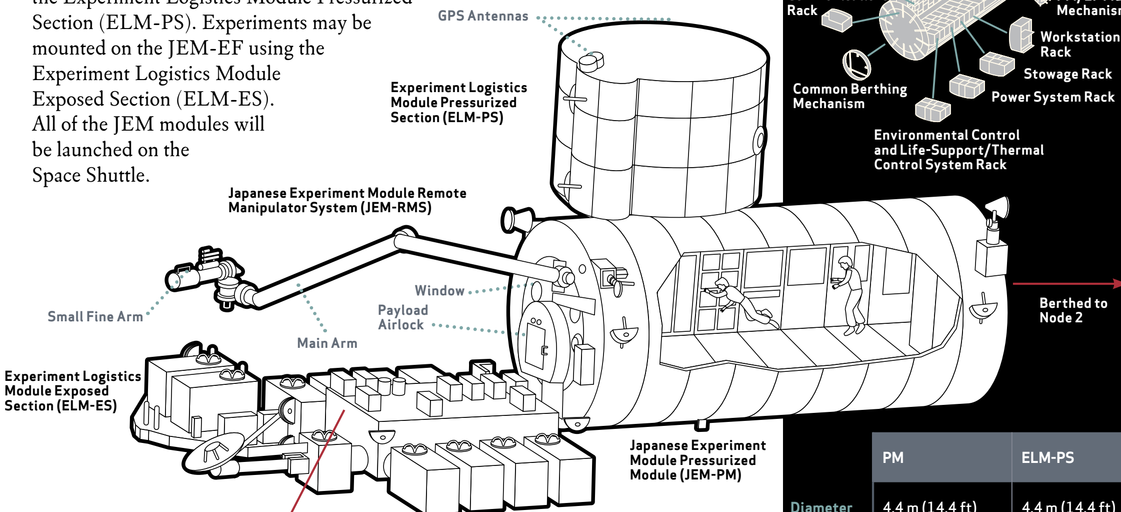

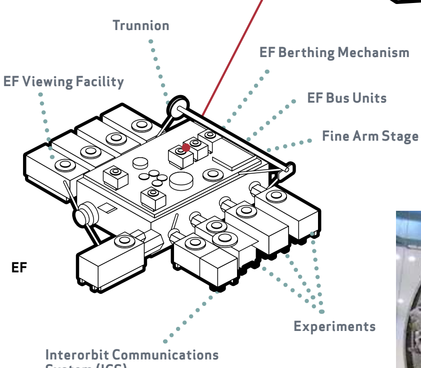

JEM-PM during testing.

	PM	ELM-PS
Diameter	4.4 m (14.4 ft)	4.4 m (14.4 ft)
Length	11.2 m (36.7 ft)	3.9 m (12 ft)
Mass	15,900 kg (35,050 lb)	4,200 kg (9,260 lb)
	EF	**ELM-ES**
Dimensions	5.6 x 5 x 4 m (18.4 x 16.4 x 13.1 ft)	4.9 x 4.2 x 2.2 m (16.1 x 13.8 x 7.2 ft)
Mass	4,000 kg (8,820 lb)	1,200 kg (2,650 lb)
Racks	10	3
JEM Remote Manipulator System		
Main Arm length		9.9 m (32.5 ft)
Small Fine Arm length		1.9 m (6.2 ft)

RAD750® 3U CompactPCI single-board computer

FEATURES AND CAPABILITIES

The 3U CompactPCI standard single-board computer, available in flight and prototype versions, employs the PowerPC RAD750 microprocessor, the radiation-hardened version of the IBM PowerPC750. The companion PowerPC bridge ASIC provides access to the memory and the PCI version 2.2 backplane bus.

Software features
- Example startup ROM and VxWorks board support package provided for all hardware configurations.
- Green Hills Software's INTEGRITY real-time operating system can serve as an alternate board-support package.
- Hardware reference manuals and software users guide provided.
- Software developed for the RAD6000® processor is easily ported to the RAD750.
- All compilers currently available for the commercial PowerPC 750 are fully compatible with the RAD750 processor.
- Operating systems for PowerPC 750-based computers are easily ported to RAD750 computers. VxWorks and INTEGRITY are both currently available.
- Virtutech offers a RAD750 simulator.

Form factor
- CompactPCI 3U (100 mm x 160 mm)
- Weight: 549 grams

Memory
- 128 MB SDRAM, 256 kB SUROM

Radiation-hardness
- Total dose: >100 Krad (Si)
- SEU: 1.9 E-4 errors/card-day (90% W. C. GEO) varies with orbit
- Latchup-immune

Performance
- >260 Dhrystone 2.1 MIPS @ 132 MHz
- 4.3 SPECint95 4.6 SPECfp95 at 132 MHz

Power supply
- 3.3V ± 10%
- (2.5V generated via on-board regulator)

Power dissipation
- <10.8W

Rail temperature range
- -55°C to +70°C

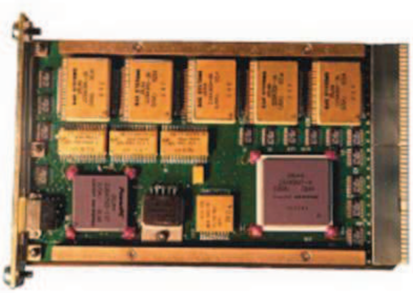

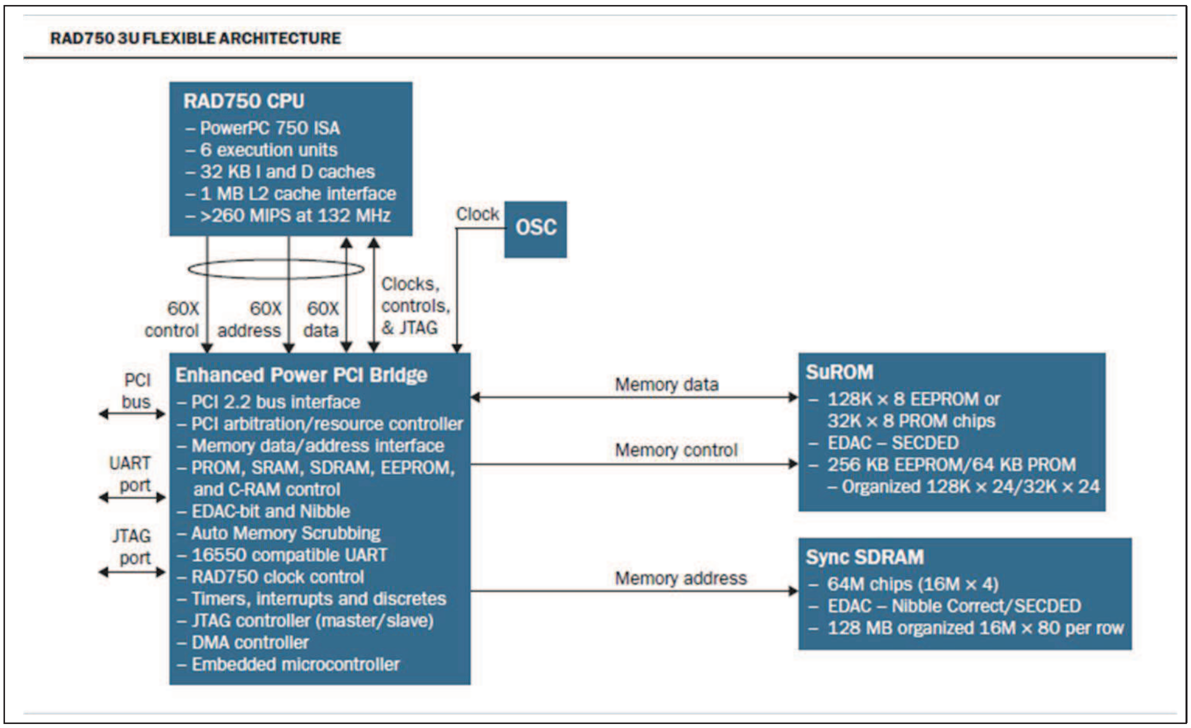
RAD750 3U FLEXIBLE ARCHITECTURE
RAD750 CPU
– PowerPC 750 ISA
– 6 execution units
– 32 KB I and D caches
– 1 MB L2 cache interface
– >260 MIPS at 132 MHz
Clock
OSC
60X control
60X address
60X data
Clocks, controls, & JTAG
PCI bus
UART port
JTAG port
Enhanced Power PCI Bridge
– PCI 2.2 bus interface
– PCI arbitration/resource controller
– Memory data/address interface
– PROM, SRAM, SDRAM, EEPROM, and C-RAM control
– EDAC-bit and Nibble
– Auto Memory Scrubbing
– 16550 compatible UART
– RAD750 clock control
– Timers, interrupts and discretes
– JTAG controller (master/slave)
– DMA controller
– Embedded microcontroller
Memory data
Memory control
Memory address
SuROM
– 128K × 8 EEPROM or 32K × 8 PROM chips
– EDAC – SECDED
– 256 KB EEPROM/64 KB PROM
– Organized 128K × 24/32K × 24
Sync SDRAM
– 64M chips (16M × 4)
– EDAC – Nibble Correct/SECDED
– 128 MB organized 16M × 80 per row

Bibliography

1. *CRISM: Compact Reconnaissance Imaging Spectrometer for Mars*. Technical report, Johns Hopkins University/Applied Physics Laboratory, 11/17/2008. URL http://crism.jhuapl.edu/instrument/innoDesign.php.

2. *Japanese Experiment Module (JEM)/Kibo (Hope)*. Technical report, National Aeronautics and Space Administration, 7 November 2008. URL http://www.nasa.gov/externalflash/ISSRG/.

3. *Optical Glass Data Book*. Corporate publication, Sumita New Glass and Fiber Optics, 2002. URL http://www.sumita-opti.co.jp.

4. *Hyperspectral Imaging*. Technical report, Global Security.org, 2006. URL http://www.globalsecurity.org/intell/library/imint/hyper.htm.

5. *AVIRIS Concept*. Technical report, NASA/Jet Propulsion Laboratory, 2007. URL http://aviris.jpl.nasa.gov/html/aviris.concept.html.

6. *AVIRIS Instrument*. Technical report, NASA/Jet Propulsion Laboratory, 2007. URL http://aviris.jpl.nasa.gov/html/aviris.instrument.html.

7. *AVIRIS Moffett Field Image Cube*. Technical report, NASA/Jet Propulsion Laboratory, 2007. URL http://aviris.jpl.nasa.gov/html/aviris.cube.html.

8. *Spectra*. Technical report, NASA/Jet Propulsion Laboratory, 2007. URL http://aviris.jpl.nasa.gov/html/aviris.spectrum.html.

9. *AP Series CCD Imaging Systems*. Technical report, NCU, 2008. URL http://www.lulin.ncu.edu.tw/lot/ApogeeCCD.htm#QECurves.

10. *The Landsat Program*. Technical report, National Aeronautics and Space Administration, 2008. URL http://landsat.gsfc.nasa.gov/about/.

11. *RAD750 Family of Products*. Technical report, BAE Systems, 2008. URL http://www.baesystems.com/ProductsServices/bae_prod_s2_rad750.html. BAE Systems product descriptions for the RAD 750 space-rated microprocessors and computers.

12. Acebal, Ariel O. "Geomagnetism: Slide 4-16", 2008. Class notes from Physics 519, presented by Maj Ariel Acebal at the Air Force Institute of Technology, Fall quarter, 2008.

13. Bai, Yibin, Steve G. Bernd, Joseph R. Hosack, Mark C. Farris, John T. Montroy, and Jagmohan Bajaj. "Hybrid CMOS focal plane array with extended UV and NIR response for space applications". volume 5167, 83–93. SPIE, January 12, 2004 2004. URL http://link.aip.org/link/?PSI/5167/83/1.

14. Bogaerts, Jan, Gerald Lepage, and Didier Dantes. *High-End CMOS Active Pixel Sensors for Space-Borne Imaging Instruments*. Conference paper ADA445549, FillFactory Cypress Mechelen, 2005. URL `http://handle.dtic.mil/100.2/ADA445549`.

15. Bostick, Randall. *Characterization and Optimization of a Rotating Prism Chromotomographic Imaging System*. Powerpoint presentation to dissertation committee, Air Force Institute of Technology, 2008.

16. Bostick, Randall. "Development, Characterization and Application of a Rotating Prism Imaging Spectrometer", 2008.

17. Chowdhury, A. Roy and K. R. Murali. "Compact hyperspectral imager with selectable bands". volume 6405, 64050U. SPIE, December 1, 2006. URL `http://link.aip.org/link/?PSI/6405/64050U/1`.

18. Corson, Michael R. and Curtiss O. Davis. *HICO Science Mission Overview*. Presentation, Naval Research Laboratory, 2008. URL `http://www.ioccg.org/sensors`.

19. Dearinger, Anthony J. "Simulating A Chromotomographic Sensor for Hyperspectral Imaging in the Infrared", 2004. Masters Thesis presented by Anthony Dearinger in fullfillment of degree requirements for the MS in Applied Physics, Air Force Institute of Technology.

20. Dib, Sami and Jean Surdej. *The CCD Detector*. Technical report, Max-Planck-Institute for Astronomy, 2006. URL `www.mpia.de/AO/INSTRUMENTS/FPRAKT/CCD_online/CCD_onlineSep2006.ppt_files/CCD_online`

21. Fisher, John, Mark M. Baumback, Jeffrey H. Bowles, John M. Grossmann, and John A. Antoniades. "Comparison of low-cost hyperspectral sensors". volume 3438, 23–30. SPIE, October 16, 1998. URL `http://link.aip.org/link/?PSI/3438/23/1`.

22. Foster, C. L., M. L. Tinker, G. S. Nurre, and W. A. Till. *The Solar Array-Induced Disturbance of the Hubble Space Telescope Pointing System*. NASA Technical Paper 3556, NASA, 1995. URL `http://ntrs.nasa.gov/archive/nasa/casi.ntrs.nasa.gov/19950021793_1995121793.pdf`.

23. Gould, Malcolm G. "Reconstruction of Chromotomographic Imaging System Infrared Hyperspectral Scenes", 2005. Master of Science Thesis presented in fullfilment of requirements for the degree in Applied Physics, Air Force Institute of Technology.

24. de Groh, Kim K. and Morgana Martin. *The Effect of Heating on the Degradation of Ground Laboratory and Space Irradiated Teflon FEP*. Technical Memorandum NASA TM2002-211704, National Aeronautics and Space Administration, John H. Glenn Research Center, July 2002. URL `http://gltrs.grc.nasa.gov/reports/2002/TM-2002-211704.pdf`. Prepared

for the Sixth International Conference on Protection of Materials and Structures From Space Environment cosponsored by the ITL, UTIAS, MMO, AFOSR/NL, CRESTECH, EMS Technologies, and MDRobotics Toronto, Canada, May 13, 2002.

25. Hawks, Michael R. "CTEx Optical Design Notes", 2009. Unpublished work of Lt Col Michael Hawks while working in the Engineering Physics department, Air Force Institute of Technology.

26. Henson, Tammy, Steve Bender, Don Byrd, William Rapporport, and Gon-Yen Shen. "Optical Assembly of a Visible Through Thermal Infrared Multispectral Imaging System". 31 July 1998.

27. Hoffman, Alan, Markus Loose, and Vyshnavi Suntharalingam. "CMOS Detector Technology". *Experimental Astronomy*, 19:111–134, 2005.

28. Holtgrave, Jeremy. "Class Notes: Physics 640, Optics, Fall, 2008", 2008. Class notes of Lt Col Jeremy Holtgrave from lectures in Physics 640: Optics, presented Fall quarter, 2008 at the Air Force Institute of Technology.

29. Janesick, James R. "Charge-coupled CMOS and hybrid detector arrays". volume 5167, 1–18. SPIE, January 12, 2004. URL `http://link.aip.org/link/?PSI/5167/1/1`.

30. Ji, Yiqun and Weimin Shen. "Compact hyperspectral imaging system with a convex grating". volume 6834, 68340Y. SPIE, November 29, 2007. URL `http://link.aip.org/link/?PSI/6834/68340Y/1`.

31. Johnson, Scott D., Augustyn Waczynski, Paul W. Marshall, Elizabeth J. Polidan, Cheryl J. Marshall, Robert A. Reed, Randy A. Kimble, Gregory Delo, David Schlossberg, Anne Marie Russell, Terry Beck, Yiting Wen, John Yagelowich, Robert J. Hill, Edward Wassell, and Edward S. Cheng. "Radiation effects in WFC3 IR detectors". volume 5167, 243–257. SPIE, January 12, 2004. URL `http://link.aip.org/link/?PSI/5167/243/1`.

32. Johnson, William R., Daniel W. Wilson, Gregory H. Bearman, and Johan Backlund. "An all-reflective computed tomography imaging spectrometer". volume 5660, 88–97. SPIE, December 30, 2004. URL `http://link.aip.org/link/?PSI/5660/88/1`.

33. Kaiser, Stefan, Bernhard Sang, Josef Schubert, Stefan Hofer, and Timo Stuffler. "Compact prism spectrometer of pushbroom type for hyperspectral imaging". volume 7100, 710014. SPIE, September 19, 2008. URL `http://link.aip.org/link/?PSI/7100/710014/1`.

34. Leon, Nancy J. *Earth Observing 3-GIFTS: Technology*. Technical report, National Aeronautics and Space Administration, 3 November 2008. URL `http://nmp.nasa.gov/eo3/TECHNOLOGY/instrument.html`.

35. Murchie, Scott L., Raymond E. Arvidson, Peter Bedini, K. Beisser, Jean-Pierre Bibring, J. Bishop, John D. Boldt, Tech H. Choo, R. Todd Clancy, Edward H. Darlington, D. Des Marais, R. Espiritu, Melissa J. Fasold, Dennis Fort, Richard N. Green, E. Guinness, John R. Hayes, C. Hash, Kevin J. Heffernan, J. Hemmler, Gene A. Heyler, David C. Humm, J. Hutchison, Noam R. Izenberg, Robert E. Lee, Jeffrey J. Lees, David A. Lohr, Erick R. Malaret, T. Martin, Richard V. Morris, John F. Mustard, Edgar A. Rhodes, Mark S. Robinson, Ted L. Roush, Edward D. Schaefer, Gordon G. Seagrave, Peter R. Silverglate, S. Slavney, Mark F. Smith, Kim Strohbehn, Howard W. Taylor, Patrick L. Thompson, and Barry E. Tossman. "CRISM (Compact Reconnaissance Imaging Spectrometer for Mars) on MRO (Mars Reconnaissance Orbiter)". volume 5660, 66–77. SPIE, December 30, 2004. URL `http://link.aip.org/link/?PSI/5660/66/1`.

36. Murguia, James E., Toby D. Reeves, Jonathan M. Mooney, William S. Ewing, Freeman D. Shepherd, and Andrzej K. Brodzik. "Compact visible/near-infrared hyperspectral imager". volume 4028, 457–468. SPIE, July 17, 2000. URL `http://link.aip.org/link/?PSI/4028/457/1`.

37. Nichitiu, Florian. "Space Weather: The Case of MOPITT on Board of TERRA Spacecraft, Slide 25", 2004. URL `www.lnf.infn.it/seminars/nichitiu.ppt`. Seminar presentation made by Florian Nichitiu at the University of Toronto, Canada.

38. Pearlman, Jay S. *Hyperion Validation Report*. Boeing Report 03-ANCOS-001, NASA Goddard Space Flight Center, July 16, 2003.

39. Perram, Glen. "Class Notes: Physics 521, Space Surveillance, Winter, 2008", 2008. Lecture presentation for Physics 521 at the Air Force Institute of Technology, Winter quarter, 2008.

40. Puschell, Jeffery J. "Hyperspectral imagers for current and future missions". volume 4041, 121–132. SPIE, June 29, 2000. URL `http://link.aip.org/link/?PSI/4041/121/1`.

41. Short, Nicholas M. Sr. *History of Remote Sensing: Landsat's Thematic Mapper (TM)*. Technical report, NASA, 2007. URL `http://rst.gsfc.nasa.gov/Intro/Part2_20.html`.

42. Silverglate, Peter R. and Dennis E. Fort. "System design of the CRISM (compact reconnaissance imaging spectrometer for Mars) hyperspectral imager". volume 5159, 283–290. SPIE, December 29, 2003. URL `http://link.aip.org/link/?PSI/5159/283/1`.

43. Silverglate, Peter R., Kevin J. Heffernan, Peter D. Bedini, John D. Boldt, Peter J. Cavender, Tech H. Choo, Edward H. Darlington, Erik T. Donald, Melissa J. Fasold, Dennis E. Fort, Reid S. Gurnee, Allen T. Hayes, John R. Hayes, James B. Hemler, David C. Humm, Noam R. Izenberg, Robert E. Lee, William J. Lees, David A. Lohr, Scott L. Murchie, Graham A. Murphy, Ralph A. Reiter, Edigio

Rossano, Gordon G. Seagrave, Edward D. Schaefer, Kim Strohbehn, Howard W. Taylor, Patrick L. Thompson, Barry E. Tossman, Paul Wilson IV, Mark S. Robinson, Robert Green, and Steven E. Mitchell. "Compact reconnaissance imaging spectrometer for Mars (CRISM): characterization results for instrument and focal plane subsystems". volume 5563, 98–110. SPIE, October 21, 2004. URL http://link.aip.org/link/?PSI/5563/98/1.

44. Tuma, Wade. *Comparison of Drive Technologies for High-Transaction Databases*. Technical report, Solid Data Corp., 2007. URL http://www.soliddata.com/pdf/WP_Drive_Comparison_v2.pdf.

45. Vagni, Fabrizio. *Survey of Hyperspectral and Multispectral Imaging Technologies*. Technical Repoort ADA473675, NATO RESEARCH AND TECHNOLOGY ORGANIZATION, MAY 2007. URL http://handle.dtic.mil/100.2/ADA473675.

46. Weber, Marvin J. *Handbook of Optical Materials*. CRC Press, LLC, Boca Raton, Florida, 2003.

REPORT DOCUMENTATION PAGE					*Form Approved* *OMB No. 0704–0188*
The public reporting burden for this collection of information is estimated to average 1 hour per response, including the time for reviewing instructions, searching existing data sources, gathering and maintaining the data needed, and completing and reviewing the collection of information. Send comments regarding this burden estimate or any other aspect of this collection of information, including suggestions for reducing this burden to Department of Defense, Washington Headquarters Services, Directorate for Information Operations and Reports (0704–0188), 1215 Jefferson Davis Highway, Suite 1204, Arlington, VA 22202–4302. Respondents should be aware that notwithstanding any other provision of law, no person shall be subject to any penalty for failing to comply with a collection of information if it does not display a currently valid OMB control number. PLEASE DO NOT RETURN YOUR FORM TO THE ABOVE ADDRESS.					
1. REPORT DATE (DD–MM–YYYY) 26-03-2009			2. REPORT TYPE Master's Thesis		3. DATES COVERED *(From — To)* 1 Jan 08 – 26 Mar 09
4. TITLE AND SUBTITLE An Engineering Trade Space Analysis for a Space-Based Hyperspectral Chromotomographic Scanner					5a. CONTRACT NUMBER
					5b. GRANT NUMBER
					5c. PROGRAM ELEMENT NUMBER
6. AUTHOR(S) Major Phillip Sheirich					5d. PROJECT NUMBER
					5e. TASK NUMBER
					5f. WORK UNIT NUMBER
7. PERFORMING ORGANIZATION NAME(S) AND ADDRESS(ES) Air Force Institute of Technology Graduate School of Engineering and Management (AFIT/ENY) 2950 Hobson Way WPAFB OH 45433-7765					8. PERFORMING ORGANIZATION REPORT NUMBER AFIT/GA/ENY/09-M08
9. SPONSORING / MONITORING AGENCY NAME(S) AND ADDRESS(ES) Intentionally left blank					10. SPONSOR/MONITOR'S ACRONYM(S) Intentionally left blank
					11. SPONSOR/MONITOR'S REPORT NUMBER(S)
12. DISTRIBUTION / AVAILABILITY STATEMENT APPROVED FOR PUBLIC RELEASE; DISTRIBUTION UNLIMITED					
13. SUPPLEMENTARY NOTES					
14. ABSTRACT Hyperspectroscopy for fast transient events such as battlefield explosions is an undeveloped area of spectral imaging. This thesis is a discussion of issues involved with taking a laboratory design for a rotating prism hyperspectral chromotomographic (CT) instrument and producing a first approximation satellite payload design, operating scheme and trade space analysis to support demonstration of this technology in low-earth orbit. This instrument promises the capability of adding a time dimension to the normal spatial and spectral data produced by most hyperspectral imagers. The ultimate goal is to conduct experiments demonstrating the ultimate viability of spectral definition of transient combustion events on the ground from space. The experiment will be designed to use the CT scanner to collect, store and transmit data from any suitable target on the earth's surface in the orbit footprint.					
15. SUBJECT TERMS hyperspectral, chromotomography, spectroscopy, space					
16. SECURITY CLASSIFICATION OF:			17. LIMITATION OF ABSTRACT	18. NUMBER OF PAGES	19a. NAME OF RESPONSIBLE PERSON Dr. Jonathan Black
a. REPORT U	b. ABSTRACT U	c. THIS PAGE U	UU	161	19b. TELEPHONE NUMBER (Include Area Code) 937-785-3636 x4578 jonathan.black@afit.edu

Standard Form 298 (Rev. 8–98)
Prescribed by ANSI Std. Z39.18